中 國 醫 藥 大 學

基礎醫學研究所

碩士學位論文

間葉幹細胞在奈米金材料上之機制探討

The molecular mechanisms of mesenchymal stem cells on gold nanocomposites

指 導 教 授 ：洪慧珊　博 士

共同指導教授：黃志揚　博 士

研 究 生：林建勳

中華民國 100 年 7 月

第一部分

奈米金複合機材與血管生長因子促進間葉幹細胞與內皮前驅細胞內皮化之機制探討

Part I

Gold nanocomposites with angiogenic factors promote endothelialization in mesenchymal stem cells and endothelial progenitor cells

中文摘要

先前的研究指出，將聚氨酯 (polyurethane, PU) 與奈米金粒子 (gold nanoparticle) (～43.5 ppm) 製備成聚氨酯奈米金複合基材 (polyurethane-gold nanocomposites, PU-Au) 對於內皮細胞有較好的生物相容性。此研究中將以聚氨酯奈米金複合基材為研究模式，探討間葉幹細胞 (Wharton's jelly mesenchymal stem cells, WJCs) 於此奈米基材之移動 (migration) 以及增生 (proliferation) 之能力。此外，同時比較從周邊血單核球細胞 (peripheral blood mononuclear cells, PBMNCs) 中分離出內皮前驅細胞 (endothelial progenitor cells, EPCs)，培養於此奈米金基材，更進一步以體內動物實驗驗證其促進血管內皮化 (endothelialization) 之修復效果。研究發現，將 WJCs 培養於奈米金基材上，予以血管內皮生長因子 (vascular endothelial growth factor, VEGF) 以及基質衍生因子 (stromal cell derived factor-1, SDF-1) 的刺激活化，可以顯著促進 WJCs 於奈米金基材上之移動以及增生之能力。此外，奈米金基材亦可以藉由活化 focal adhesion kinase (FAK)/Rho-GTPase 及 PI3K/Akt/eNOS 以及 matrix metalloproteinase-9 (MMP-9) 之訊息調控機轉促進 WJCs 之移動能力，同時，亦可顯著誘導 α5β3 integrin 與 CXCR4 integrin 之表現。同時亦發現將 EPCs 培養於基材上並移植入動物受損血管內一個月

後可以有效增進血管組織內皮化及抑制血栓之形成。結果顯示奈米金基材可以增加血液幹細胞的分化成內皮細胞之能力，進而促進受損血管內皮化。

Abstract

Stem cell therapy and the hope for myocardium and vascular regeneration has become the focus of many basic and clinical investigations for more than a decade. Wharton's jelly stem cells (WJCs) has self-renew, multipotent differentiation potential and represents an attractive cell source for regeneration of damaged tissues. The implantation of artificial blood vessels and repair damaged tissue has an important capacity. The nanocomposites from polyurethane (PU) containing small amount (43.5 ppm) of gold (Au) nanoparticles was prepared. Previous studies showed that the nanocomposites (PU-Au) exhibited greater proliferation and biological performance of endothelial cells. In this study, we focus on the novel gold nanocomposites whether they can promote the migration and proliferation of WJCs. On the other hand, we collected the endothelial progenitor cells (EPCs) from peripheral blood mononuclear cells (PBMNCs) and cultured on PU-Au can effectively improve the response capacity of vascular tissue damage in vivo. Vascular endothelial growth factor (VEGF) and stromal cell-derived factor-1 (SDF-1, CXCR4 specific ligand) enhanced WJCs migration and proliferation has been observed in this study. Indeed, PU-Au can be modulated signal through the activation of focal adhesion kinase (FAK)/Rho-GTPase, PI3K/Akt/eNOS and matrix metalloproteinase-9 (MMP-9) molecular mechanism to promote the migration effect of WJCs. The higher level of integrins ($\alpha 5\beta 3$ and CXCR4) was also induced by PU-Au after VEGF and SDF-1 stimulation. In addition, the EPCs with PU-Au were reduced thrombosis effectively

and enhanced the differentiation of EPCs to endothelial cells. These results demonstrate that PU-Au might enhance cell proliferation and migration, and differentiate into endothelial cells contribute to neovascularization in the vascular lesion.

Content

Abbreviations

PU: polyurethane

PU-Au: polyurethane-gold nanocomposite

WJCs: Wharton's jelly stem cells

PBMNCs: peripheral blood mononuclear cells

EPCs: endothelial progenitor cells

VEGF: vascular endothelial growth factor

SDF-1: stromal cell derived factor-1

FAK: focal adhesion kinase

MMP: matrix metalloproteinase

ECs: endothelial cells

MSCs: mesenchymal stem cells

BM: bone marrow

ECM: extracellular matrix

eNOS: endothelial nitric oxide synthase

TCPS: tissue culture plates

FN: fibronectin

FN-Au: fibronectin-gold nanocomposite

AFM: atomic force microscope

FTIR: fourier transform infrared spectrometer

SEM: scanning electron microscope

NO: nitric oxide

Introduction

1. Atherosclerosis

Atherosclerosis is a condition in which an artery wall thickens as the result of a build-up of multiple plaques within the arteries, such as fatty materials [1]. It is a syndrome affecting arterial blood vessels, a chronic inflammatory response in the walls of arteries, in large part due to the accumulation of macrophage white blood cells and promoted by low-density lipoproteins (LDL) without adequate removal of fats and cholesterol from the macrophages by functional high density lipoproteins (HDL) [2]. These complications of advanced atherosclerosis are chronic, slowly progressive and cumulative. Most commonly, soft plaque suddenly ruptures, causing the formation of a thrombus that will rapidly slow or stop blood flow, leading to death of the tissues fed by the artery in approximately 5 min [3]. This catastrophic event is called an infraction. One of the most common recognized scenarios is called coronary thrombosis of a coronary artery, causing myocardial infarction (a heart attack) [4]. The same process in an artery to the brain is commonly called stroke [5]. Another common scenario in very advanced disease is claudication from insufficient blood supply to the legs, typically due to a combination of both stenosis and aneurysmal segments narrowed with clots. Since atherosclerosis is a body-wide process, similar events occur also in the arteries to the brain, intestines, kidneys, legs, *etc* [5-6].

In general, the group of medications referred to as statins has been the most popular and is widely prescribed for treating atherosclerosis [7].

On the other hand, stents are also used in a variety of vessels aside from the coronary arteries [7]. The most common techniques in current practice are angioplasty with stenting, and CABG surgery (for patients with multivessel disease) [8]. Balloon angioplasty and stenting in fact manage the form of the plaque, and does not create a significant problem of plaque residue flowing from the site. Once a role for elective stent implantation was established, the next goal was to overcome the complications of subacute stent thrombosis (drug-eluting stents) and neointimal hyperplasia (bare-metal stents) through pharmacologic and physical means [9-10]. Among unresolved issues the investigators can describe restrictions in patients with stenosis of an unprotected left main coronary artery, multivessel disease, diabetes mellitus, still rather high rate of in-stent restenosis, and as a solution of the problem with a foreign body in vessel, the development of biodegradable stents [11-12]. Recently, atificial graft with cell-based therapy and the hope for myocardium and vascular regeneration has become the focus of many basic and clinical investigations.

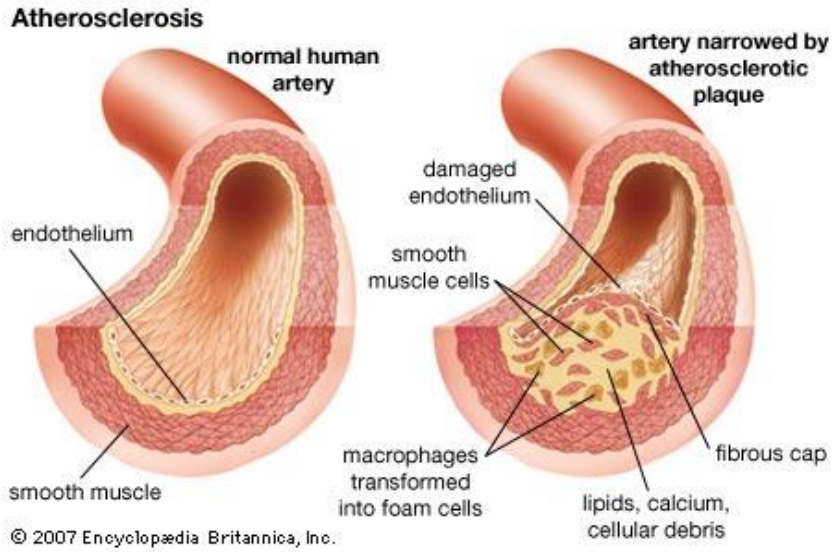

2. Endothelialization

Endothelialization of vessel grafts is considered a protective mechanism where the endothelial cells (ECs) a range of favorable responses, including antithrombotic, noninflammatory responses and inhibition of intimal hyperplasia [13]. The most exciting strategy exploration in ECs sourcing is the seeding of endothelial progenitor cells (EPCs). EPCs are considered as a promising alternative to primary endothelial cells for the development of vascular grafts [14]. These cells meet important requirements for tissue engineering applications, namely, they have therapeutic potential, a highly proliferative and antithrombogenic behavior, and can be obtained easily from peripheral blood and human cord blood. In 1997, Asahara *et al*. characterized EPCs in human peripheral blood using magnetic bead selection [15]. Since EPCs can give rise to ECs and are known to facilitate the neovascularization of an implanted site, EPCs may be used to facilitate collateral vessel growth into ischemic tissues through delivery of anti- or proangiogenic agents [16]. EPCs have been implanted into various ischemic tissue models, for example, ischemic hindlimbs [17] and areas of myocardial infarction [18]. Recently, EPCs have also been used to engineer blood vessels. It has been shown that an intramyocardial injection of autologous EPCs or intravenous administration of EPCs can increase vasculogenesis and improve cardiac function after myocardial infarction in animal experiments and clinical trials [19]. However, abundant evidence suggests that EPCs contribute to vascular repair, remodeling, and lesion formation under physiological and pathological conditions. Systemic administration of EPCs also improves functions of ischemic tissues after stroke [20] or myocardial infarction [21]. Thus, it is hypothesized that homing and differentiation of EPCs largely depend on

their signaling cascade that occurs upon artificial vascular graft. Coating of biomaterials by EPCs attracting compounds such as PU-Au may be used to achieve the settlement of synthetic surfaces by endothelial cells. However, EPCs could proliferate in vitro but gradually lost their proliferative potential and specific functions, which limited their clinical applications [22]. To replace EPCs, mesenchymal stem cells (MSCs) are a promising source of stem cells for regenerative therapy [23].

3. Stem cells

Stem cells from many sources have been used to induce angiogenesis, neovascularization and endothelialization, associated with local proliferation, differentiation and angiogenic cytokine production of implanted cells within ischemic tissues [24-26]. Stem cells are biological cells found in all multicellular organisms, that can divide through mitosis and differentiate into diverse specialized cell types and can self renew to produce more stem cells. In mammals, there are two broad types of stem cells: embryonic stem cells that are isolated from the inner cell mass of blastocysts, and adult stem cells that are found in various tissues. In adult organisms, stem cells and progenitor cells act as a repair system for the body, replenished in adult tissues. In a developing embryo, stem cells can differentiate into all the specialized cells, but also maintain the normal turnover of regenerative organs, such as blood, skin, or intestinal tissues. Stem cells can be taken from a variety of sources, including bone marrow, umbilical cord and umbilical cord blood. The MSCs are one of the most interesting of the adult stem cell types [27]. MSCs are multipotent stem

cells that can differentiate into a variety of cell types, including osteoblasts, chondrocytes, and adipocytes [28-32].

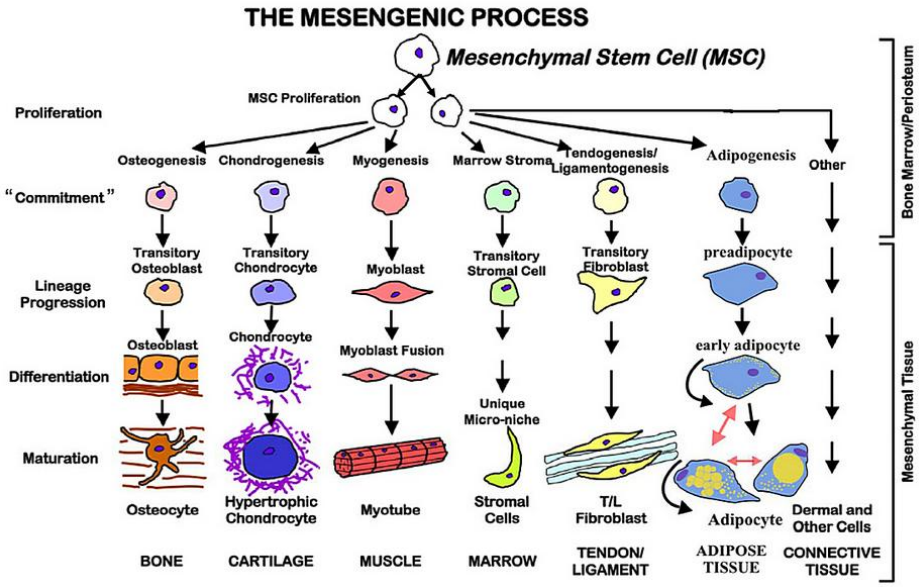

Discov Med 2010; 9(47):337-45.

These cells are easily isolated, cultured, and manipulated ex vivo. MSCs exhibit great plasticity and harbor the potential for therapeutic applications. In 2006, the International Society for Cellular Therapy (ISCT) convened a working group to discuss immunophenotypic analysis MSCs [28]. This group defined bone marrow-derived MSCs, in a clear, minimalist fashion, as a plastic adherent cell population isolated from the bone marrow cavity with the following surface markers: CD13, CD44, CD90, CD73, $CD105^{+}$, CD14, CD11b, CD79, CD 34, CD45 and $HLA\text{-}DR^{-}$[33]. Bone marrow is the main source of multipotent MSCs. Human bone marrow–derived MSCs (BM-MSCs) can differentiate into endothelial like cells [34]. However, BM harvesting is a highly invasive procedure to the donors, and proliferation efficiency, multipotent

differentiation potential, and maximal lifespan of BM-MSCs decline with aging [35-38]. Alternative sources for MSC isolation have been pursued. MSCs can also be isolated from umbilical cord Wharton's jelly. Wharton's jelly (WJ) from the umbilical cord is a novel source of MSCs, called Wharton's jelly stem cells (WJCs) [39]. The WJCs self-renew and can be induced to differentiate into various cell types. Previous studies showed that WJ-derived MSCs were induced to differentiate into endothelial-like cells and had highly endothelial differentiation potential compared with BM-MSCs [40]. WJCs display MSCs surface markers, suggesting that they are of the MSC family [40].

4. Polyurethane

Nanatechnology creates new platforms that might enable novel tissue-engineering technologies [41]. Current methods for synthesis of nano-composites allow for manipulation of their unique properties. Examples of nanomaterials include nanotubes, nanofiber, nanoparticles, polymeric micelles, nanogels and dendrimers [43]. Polyurethane (PU) is one of the most interesting synthetic elastomers [45]. Because of its unique properties, more attention has been paid to the synthesis, morphology, chemical, and mechanical properties of the polymer. PU is also widely used in biomedical applications because of its good biocompatibility and mechanical properties [43]. Gold (Au) is regarded as one of the noble metals with high biocompatibility. Au nanoparticles were used for immobilization of biomolecules such as proteins, enzymes, and antibodies [44]. This combination has been recently used as a

biomimetic interface to construct a cellular biosensor [44]. The response of ECs to a PU characteristic of surface micelles (~89 nm in diameter) and a novel nanocomposites (PU-Au) containing smaller surfaces micelles (~14-22 nm in diameter) was investigated [43, 45, 59-60]. The advantage of the nanocomposites as a model system is that the chemical composition of the model polymers is essentially uniform because of the limited amount of Au in each composite. The better improvement of in vitro and in vivo biocompatibility of this PU at such low Au concentrations (43.5 ppm) is believed to be a result of the altered surface morphology as well as associative effects in the presence of Au [43, 45, 59-60].

5. Stem cells migration and homing

As in development, stem cell homing and migration are critical for the ongoing replacement of mature cells and regeneration of damaged cells in many adult tissues [46]. This process requiring a interplay of adhesion molecules, cytokines and chemokines, and extracellular matrix degrading proteases [47-48]. Stem cell function in adult tissue repair and replacement often recapitulates the processes that gave rise to these cells and enabled their dissemination during development. Stem cells within the bone marrow reside in close contact with surrounding stromal cells and are released upon activation by physical or chemical stimuli [49]. Several of these factors can further enhance stem cells proliferation, migration and homing to damage tissues and subsequently induce differentiation of mobilized stem cells into matured cells [50]. One of the

most prominent chemokines that initiate stem cell migration is the stromal cell-derived factor-1 (SDF-1) [50]. It provides a gradient toward which stem cells migrate, and in which they are retained in the bone marrow microenvironment. SDF-1 is a member of the CXC chemokine family, and has been shown to be essential for chemotaxis of both stem and progenitor cells, and is involved in B lymphopoiesis and myelopoiesis [51]. It binds to the CXCR4 receptor, also known as CD184, which belongs to the class of G-protein coupled receptors, whereby chemokine binding will initiate the migration of lymphocytes, hematopoietic stem cells [52], and tumor cells [53-55]. The interaction between CXCR4 and its' ligand SDF-1 plays a pivotal role in regulating the retention, migration, and mobilization of stem cells during steady state homeostasis and injury [56].

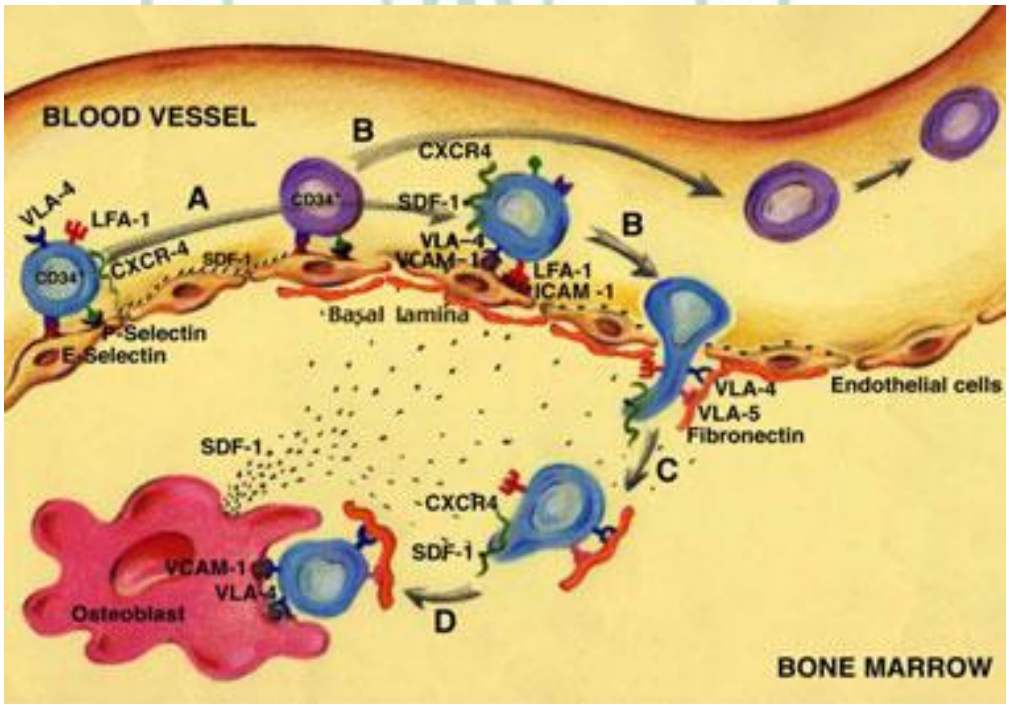

Blood 2000; 95(11):3289-96.

Several studies showed that cell homing were linked with CXCR4 and through the focal adhesion kinase (FAK) to activate the Rho GTPase protein, resulting in the matrix metalloproteinases (MMP-2 and MMP-9) activation, which stimulates cell adhesion, and migration [57-58]. On the other hand, recently, found that the response of ECs to different surface morphology of PU-Au involved PI3K/Akt/eNOS activation and FAK signaling [59, 66]. Therefore, the PI3K/Akt/eNOS pathway also plays a pivotal role in the process of stem cell mobilization, migration and homing.

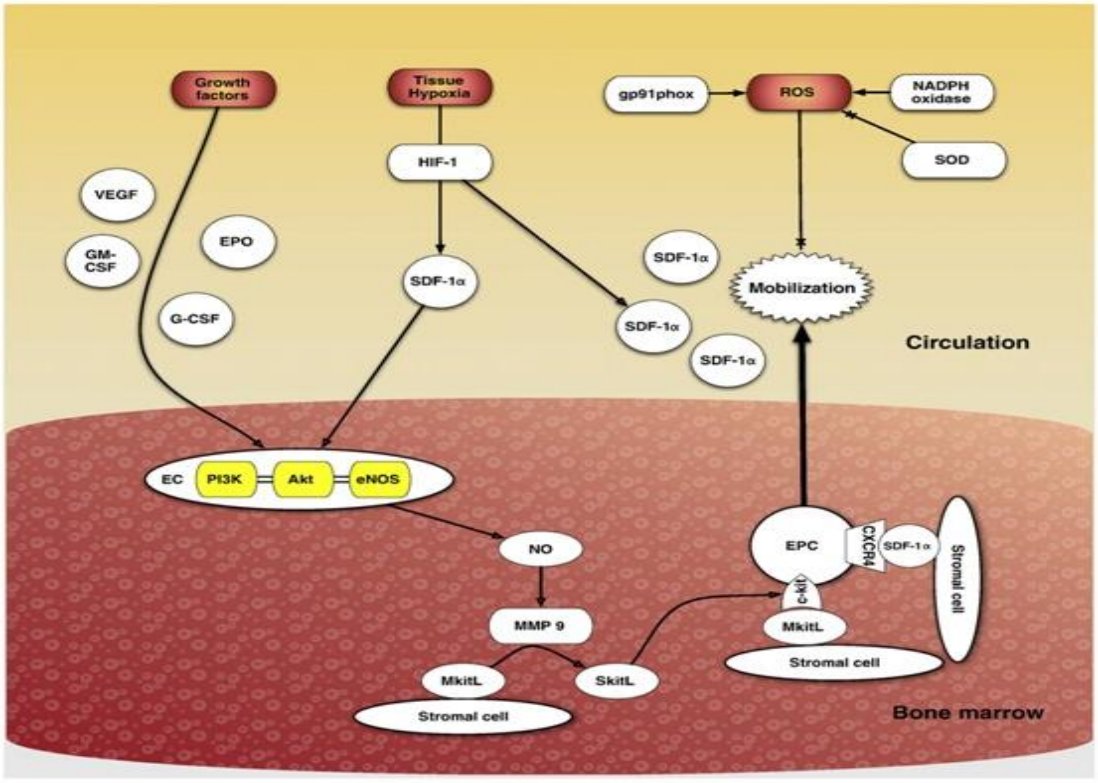

Int J Cardiol 2010; 144(3):350-66.

Materials and Methods

1. Synthesis of polyurethane

PU dispersion and the diisocyanate salt were supplied by Great Eastern Resins Industrial Co., Taiwan. The PU dispersion (50% solid content in distilled water) was synthesized based on a molecular ratio 3:1 from hexamethylene diisocyanate (HDI) and the macrodiol poly(butadiene adipate), and further chain-extended by ethylene diamine sulfonate sodium salt and ethylene diamine. The diisocyanate salt was a mixture of isocyanurate trimer of hexamethylene diisocyanate (HDI trimer) and 6% Bayer hardener (made from HDI trimer and polyethylene glycol). The final polymer had a hard segment weight fraction of about 34.6% [60]. Au nanoparticles were supplied as a suspension (50 ppm/ml in distilled water). The diameter of the Au nanoparticles was uniform in the range of 4~7 nm (average 5 nm), as determined by transmission electron microscopy [59].

2. Preparation of polyurethane-gold (PU-Au) nanocomposite films

The PU dispersion was diluted by distilled water or Au suspension to 10 wt% solid content. The diisocyanate salt was added to the PU dispersion (concentration of the diisocyanate salt at 1 wt%), and the mixture was stirred for 30 min to obtain the suspension of plain PU or PU-Au nanocomposites. The PU-Au suspensions were prepared to contain 43.5 ppm of Au in the final nanocomposites after water removal. Thin films (~0.02 mm) were cast from the PU or PU-Au suspension on

15-mm or 32-mm round glass coverslips by a spin coater. They were dried at 60^{o}C for 48 hrs and further dried in a vacuum oven at 60^{o}C for 72 hrs to remove any residual solvent. The surface morphology and microphase separation were confirmed by atomic force microscopy [66].

3. Characterization and immunophenotyping of Wharton's jelly stem cells (WJCs)

The collected human umbilical cord tissues were washed three times with Ca^{2+} and Mg^{2+}-free PBS. They were mechanically cut by scissors in a midline direction and the vessels of the umbilical artery, vein and outlining membrane were dissociated from the Wharton's jelly (WJ). The jelly was then extensively cut into pieces smaller than 0.5 cm^3, treated with collagenase type 1 (Sigma, St Louis, USA) and incubated in DMEM containing 10% fetal calf serum (FCS) for 14 to 18 hrs at 37℃ in a 95% air/5% CO_2 humidified atmosphere. The cellular morphology became homogenously spindle shaped in cultures after 4~8 passages, and the specific surface molecules of cells from the WJ were characterized by flow cytometric analysis [40]. The cells were detached with 2 mM EDTA in PBS, washed with PBS containing 2% BSA and 0.1% sodium azide and incubated with the respective antibody conjugated with fluorescein isothiocyanate (FITC) or phycoerythrin (PE) against the indicated markers: CD14-FITC, CD29-PE, CD34-FITC, CD44-FITC, CD45-PE, CD73-PE, CD90-FITC and CD105-PE. PE-conjugated IgG1 and FITC-conjugated IgG1 were used as isotype controls. Thereafter, the cells were analyzed by a FACS calibur flow cytometry.

4. Matrix metalloproteinase (MMPs) activity

WJCs (2×10^5 cells per well) were seeded in 6-well plates with material-coated coverslips and cultured for 48 hours. After 48 hrs the conditioned medium was collected, centrifuged and assayed for gelatin zymography as previously described [66]. The gels were stained with 0.5% Coomassie brilliant blue R-250 in 10% acetic acid and 45% methanol and destained with 10% acetic acid and 45% methanol. Bands of gelatinase activity appeared as transparent areas against a blue background. MMP-2 and MMP-9 gelatinase activity was then evaluated by quantitative densitometry. Data were normalized on the protein amount measured in cell supernatant.

5. Western blotting

WJCs (2×10^5 cells) were seeded into each well of a 6-well tissue culture plate containing 32-mm material-coated coverslips cultured with 50 ng/ml VEGF and 50 ng/ml SDF-1 treatment. After 48 hrs of incubation, cells were washed three times with the ice-cold PBS, lysed in the RIPA lysis buffer [50 mM Tris, pH 7.4, 1 mM EDTA, 1 mM phenylmethyl sulfonyl fluoride (PMSF), 25 mg/ml leupeptin, 0.1 mg/ml aprotinin, 1 mM dithiothreitol, 1 mM NaF, and 1% NP-40]; scraped from the dish, rotated for 1 hr at 4 ^{o}C, and centrifuged for 15 min at 14000×g. The protein concentration in the supernatant was quantified by using a protein assay kit, and 30 μg proteins of each sample were subjected to SDS-PAGE. For immunoblotting, separated proteins were transferred onto a nitrocellulose membrane by a semi-dry blotting technique. The membrane was blocked with 5% non-fat dry milk in PBS for 1 hr at room

temperature before overnight incubation at 4℃ with the primary antibodies [anti-phospho-eNOS antibody (1:500 dilution), anti-phospho-Rho (Ser188) antibody (1:500 dilution), anti-phospho-Rac/Cdc42 (Ser71) antibody (1:500 dilution), anti-phospho-Akt (Ser473) antibody (1:500 dilution), anti-phospho-FAK (Tyr576/577) antibody (1:500 dilution)] and controls [anti-actin antibody (1:5000 dilution), total anti-Akt antibody (1:1000 dilution), total anti-FAK antibody (1:500 dilution), total anti-Rho antibody (1:500 dilution), total anti-Cdc42 antibody (1:500 dilution), total anti-Rac antibody (1:500 dilution)] to ensure uniformity of loading. After incubation with the primary antibodies, the membrane was washed, incubated for 1 hr with peroxidase-conjugated secondary antibodies, and then treated with the ECL Western blotting detection system, according to the manufacturer's instructions. Quantification was performed by densitiometric analysis with the LabWork Image Acquisition and Analysis software. The tests were performed three times and the representative data are shown.

6. Immunofluorescence staining of CXCR4 and α5β3 integrin expressions

WJCs (2×10^4 cells per well) were seeded in 24-well plates with PU and PU-Au material-coated coverslips and cultured with VEGF (50 ng/ml) and SDF-1(50 ng/ml) treatment on PU-Au nanocomposites for 8 hrs and 48 hrs. After 8 hrs and 48 hrs in culture, they were fixed with 4% paraformaldehyde and permeabilized with 0.5% (v/v) Triton X-100 in PBS for 10 min prior to staining. Following fixation and permeabilization, non-specific binding was blocked by adding 1% (w/v) bovine serum albumin (BSA) for 30 min at room temperature. Cells were incubated

with primary anti-CXCR4 antibody solution (1:100 dilution), and anti-α5β3 antibody solution (1:100 dilution) overnight, washed extensively and then incubated with the appropriate secondary Cy5.5-conjugated immunoglobulin (red color fluorescence: anti-α5β3 antibody) (1:100 dilution) or FITC-conjugated antibody (green color fluorescence: anti-CXCR4 antibody) (1:100 dilution) for 60 min. Following further extensive washing, the nuclei were stained with 4', 6'-diamidino-2-phenylindole (DAPI) (1:500 dilution) for 30 min. After two further washes, coverslips were mounted on microscope slides with the storage solution (glycerol/PBS) and sealed with a synthetic mount. Images were collected on fluorescence microscope.

7. Flow cytometry of CXCR4 and α5β3 integrin analysis

The expression of cellular α5β3 integrin and CXCR4 was detected by flow cytometry. WJCs (2×10^5 cells) were seeded into each well of the 6-well tissue culture plate containing material-coated coverslips as described. WJCs were cultured with 50 ng/ml VEGF or 50 ng/ml SDF-1 for 48 hrs. After 48 hrs of incubation, the cells were collected by trypinization. Cells were treated with labeled α5β3 integrin and CXCR4 at the concentration of 10 μg/ml for 1 hr. Cells were then treated with PE or FITC-goat anti-mouse immunoglobulin antibody, washed three times in PBS and then analyzed by a FACS calibur flow cytometer. Fluorescein-positive cells were processed using the FCS software. The expression of α5β3 integrin and CXCR4 were also determined by immunofluorescence staining as described earlier.

8. Human blood samples collection

EPCs were cultured according to a previously described technique. Briefly, peripheral blood mononuclear cells (PBMNCs) were isolated from healthy volunteers by density gradient centrifugation with Percoll separating solution.

9. Buffy coat cell preparation

Human peripheral mononuclear cells (PBMNCs) were obtained as previously described [18], with minor modifications. Blood (20~100 ml) was diluted 1:1 with Hanks balanced salt solution (HBSS) and was overlaid onto an equivalent volume of Histopaque. Cells were centrifuged for 30 min at room temperature at 740 g. PBMNCs were isolated and washed 3 times with M199 medium supplemented with 10% fetal bovine serum (FBS), 2% penicillin/streptomycin, 2 mM glutamine and 50 ng/ml VEGF.

10. Purification and selection of $CD34^+$ endothelial progenitor cells

PBMNCs were prepared from fresh or cryopreserved whole adult human peripheral blood sample. The PBMNCs layer was collected using the ficoll-Histopaque centrifugation method, and washed twice with 1mM EDTA in PBS. The $CD34^+$ PBMNCs were separated from 2×10^8 PBMNCs by a magnetic bead separation method (MACS) according to the manufacturer's instructions. In brief, PBMNCs were suspended in 300 μl PBS and 5 mM EDTA. These cells were labeled with a hapten-conjugated mAb against CD34, followed by an anti-hapten Ab coupled with microbeads, and were incubated with beads at ratios of 100 μl beads per 10^8 cells for 15 min at 4 ^oC. The bead-positive cells ($CD34^+$

PBMNCs) were enriched on positive selection columns set in a magnetic field. FACS analysis using anti-CD34 antibodies labeled with PE of MACS-sorted cells showed that 90% ± 3% of the selected cells were positive for both CD34 and CD133, and cultured with VEGF (50 ng/ml) for 72 hrs in medium at 37^{o}C in a humidified atmosphere of 5% CO_2 / 95% air and antibiotics, and prepared for transplantation.

11. Culture of $CD34^{+}$ endothelial progenitor cells

EPCs were resuspended in M199 medium. Cells were seeded onto 3 separate wells of a 6-well tissue culture plate precoated with Fibronectin at 37℃, 5% CO_2, in a humidified incubator. After 24 hrs of culture, non adherent cells and debris were aspirated, adherent cells were washed once with complete medium, and complete medium was added to each well. After 3 days in culture, non-adherent cells were removed by washing with PBS, new medium was applied, and culture was maintained through 1 to 21 days of incubation. Endothelial cell colonies were enumerated by visual inspection using an inverted microscope under 40 × magnification.

12. Characterization of endothelial progenitor cells

EPCs (2×10^4 cells on each 15 mm material-coated coverslip glass placed in a 24-well plate) were incubated in the complete medium. After 48 hrs in culture, they were fixed with 4% paraformaldehyde and permeabilized with 0.5% (v/v) Triton X-100 in phosphate buffered saline (PBS) for 10 min prior to staining. Following fixation and permeabilization, non-specific binding was blocked by adding 1% (w/v) bovine serum albumin for 30 min at room temperature. Cells were incubated in the primary anti-eNOS antibody solution (1:300 dilution)

and anti-vWF antibody solution (1:300 dilution) for 60 min, washed extensively and then incubated with the appropriate secondary anti-FITC-conjugated antibody (1:300 dilution) for 60 min. Following further extensive washing, the nuclei were stained with 4', 6'-diamidino-2-phenylindole (DAPI) (1:500 dilution) for 20 min. After two further washes, the coverslip was mounted on microscope slides with the storage solution (glycerol/PBS) and sealed with a synthetic mount. In each case a primary antibody free control was produced. Images were collected on a fluorescence microscope.

13. Surface grafting of PU-Au

Gold (Au) nanoparticles (180 ppm pure 5 nm Au fine particles in water) were mixed with the filtered PU solution. The final nano gold concentration in the polymer was 43.5 ppm [45]. The plasma surface of catheter coated with PU-Au was grafted by air plasma equipment. The plasma equipment used was an open air plasma system developed by Plasmatreat. The apparatus included a power generator, a transformer of high voltage power supply and a rotating nozzle. The operating platform was designed and assembled by the San Fan Machinery Company. The plasma source was compressed dried air (21% oxygen and 79% nitrogen). Air plasma was ejected from a rotating nozzle. The temperature of the plasma at the exit of nozzle was 65 ^{o}C. The pressure and power of the air plasma as well as the distance and scan speed of the plasma nozzle were among the parameters that could be adjusted. For the current experiment, parameters were optimized as follows. The air pressure was 2.5 kg cm^{-2}. The plasma power was set at 1000 W. The substrate was placed at a distance of 10 mm from the nozzle. The scan speed of the nozzle was 15 m min^{-1}. Immediately after the plasma treatment, the substrates were

immersed in PU solution containing an extra 43.5 ppm of Au at 37 ^{o}C for 1 hr. The substrates were then rinsed with distilled water, washed extensively in an ultrasonic bath for 30 min, air-dried and stored in a desiccator.

14. Cell seeding and maintenance of materials in vitro

First, cells (1×10^{6} cells/ml) were suspended in 1 ml culture medium and label with Quantum Dot (10nM), a fluorescent dye that bind the cell membrane, at a concentration of 10 nM. PU-Au materials with cells were rolled into catheter with the 3D shaker at 20 rpm/min speed for 48 hrs. After rolling, materials were checked for their attachment ability under fluorescence microscopy before implantation. Before implantation, the cells-seeded materials were cultured in medium supplemented with 10% FBS, human VEGF (10 ng/ml) for 1 week in humidified air with 5% CO_2 at 37 ^{o}C.

15. Implantation of cell-seeded materials

Female New Zealand White rabbits (2.5 to 3 kg) were used in all experiments. All materials (1×10^{6} cells per material) were implanted into the femoral artery of rabbit. Three experimental groups were studied for cells implantation with: (i) treatment with catheter (ii) PU-Au coated with catheter, (iii) PU-Au plus cells coated with catheter. Cells-seeded vascular catheters were implanted into the femoral arteries of rabbit. All tissue constructs were harvested at 4 weeks after implantation for analyses. The adult rabbit were anesthetized with intramuscular injection of ketamine (30 mg/kg) and intravenous injection of pentobarbital (30 mg/kg) and ventilated with a mixture of O_2, N_2 and isoflurane during the operation.

The femoral artery was exposed and the surrounding tissues were dissected from the artery. After heparin (100 unit/kg) was given intravenously, the proximal and distal portions of the femoral artery were clamped. The femoral artery was clamped and ligated, and the graft was placed end to-end and sutured with 10-0 interrupted stitches. A 40 mm length of the femoral artery was dissected, and the vessel was washed with a heparin solution and transplanted with the vascular grafts (catheter) using a 22 GA1. No anti-coagulants or anti-platelets were administered post-operatively. All animals received humane care in compliance with the ‘‘Guide for the Care and Use of Laboratory Animals’’ published by the National Institutes of Health. The graft was removed by ligation of native femoral artery directly adjacent to the suture locations.

16. Histological and immunohistochemical examination

We took 3 sites sample from each implanted grafts for further analysis, the distal part, proximal part and the middle part. The distal and proximal part included the interface between the engineered tissue and native tissue. Segments of the blood vessels harvested 4 weeks after implantation were fixed in 10% buffered formaldehyde solution, dehydrated with a graded ethanol series, and embedded in paraffin. The specimens were cut into 4 mm-thick sections and stained with hematoxylin and eosin (H&E). Immunohistochemical staining was used to analyze the sections with the following primary antibodies: CD31, and CD34 along with FITC-IgG secondary antibody and double confirmed following staining with 3, 3'-Diaminobenzidine (DAB). Native femoral artery from rabbits served as positive controls for all stains.

Immunohistochemistry images were captured with a fluorescence microscope.

Results

1. Preparation and surface characterization of PU and the PU-Au nanocomposites films

The preparation of PU-Au nanocomposites (PU-Au) was represented in Fig 1 A. The AFM surface topography and phase diagrams of PU and PU-Au 43.5 ppm was shown in Fig 1B. Comparing topography and phase diagrams, the darker area in topography corresponded to the brighter area in phase, i.e. the hard domains appeared to descend slightly. The presence of Au at concentration of 43.5 ppm induced a significant change in surface morphology from hard-segment lamellae of soft micells was caused by the different state of phase separation on the material surface [60].

2. Characterization of Wharton's jelly stem cells (WJCs)

The predominant morphology of WJCs used in this study was similar fibroblast-like in shape (Fig 2A). WJCs could be culture for over 20 passages, without spontaneous differentiation. As shows a representative WJCs preparation with uniform positive expression of CD29 (88.2 %), CD44 (94.34 %), CD73 (94.41 %), CD90 (96.64 %) and CD105 (95.59 %) and negative expression of CD14 (20.98 %), CD34 (0.01 %) and CD45 (0.02 %) by using flow cytometery analysis as shown in Fig 2B. Similar results were obtained in all other experiments [40].

3. PU-Au enhanced the migration ability of WJCs

The migration ability of stem cells plays a critical role in vascular regeneration [24]. Stem cells migration requires the cross-talk between molecular signaling cascades, which has been shown to be mainly the vascular endothelial growth factor (VEGF) [48] and stromal-derived factor-1 (SDF-1) [50] signal pathway. As FAK phosphorylation is involved in cell focal adhesion and migration through integrin activation [57]. Based on these reports, we further explore whether PU-Au could induced integrin/FAK activation was modulated by VEGF or SDF-1 during the migration event. Additionally, both VEGF and SDF-1 can significantly promote the p-FAK protein expression level (Fig 3). Beside, the induction of p-FAK expression level after treatment with VEGF was more significantly enhancement than that after SDF-1 treatment. As FAK phosphorylation is involved in cell adhesion and migration through integrin, we also observed whether PU-Au could promote FAK activation during WJCs migration. FAK can modulate cell migration through the Rho GTPases, and leading to direction cell movement [57]. As shown in Fig 4, WJCs expressed p-RhoA and p-Rac/Cdc42 proteins on PU-Au was more prominently than on PU. These suggested that the FAK/RhoA/Rac/Cdc42 signaling pathway may be involved cell migration of WJCs on PU-Au. The possible role of PI3K/Akt activation in the eNOS protein expression induced by PU-Au was observed in our previous study [59]. After cultured WJCs on PU-Au, the expression of both p-Akt and p-eNOS by PU-Au were significantly reduced (Fig 4). This result was not consistent to our previous on ECs, it was indicate that the PI3K/Akt/eNOS pathway may not be involved by PU-Au in WJCs. Based on these finding, it was suggested that PU-Au may be induced a more prominent migration event via the NO-independent pathway in WJCs. The extracellular matrix (ECM) facilitate cell to migration were matrix metalloproteinase (MMPs) and play a major role in angiogenesis

or chemotaxis [58]. The adhered WJCs expressed readily detectable MMP-2 and MMP-9 protein expression on PU-Au, but this observation was not as evident for PU control group (Fig 5).

4. CXCR4 and α5β3 are activated by angiogenic factors on PU-Au.

Integrin were critical for cell adhesion and angiogenesis between cells and extracellular matrix [50]. The effect of PU-Au of α5β3 and CXCR4 in WJCs was further investigated by flow cytometry assay and immunofluorescence. The α5β3 and CXCR4 integrins activation for WJCs was highest on PU-Au, followed on PU, and lowest on TCPS after 48 hr incubation as depicted in Fig 6. Meanwhile, after treatment with VEGF or SDF-1, the inductions of both α5β3 and CXCR4 integrins by PU-Au were markedly enhanced. As evident from Fig 7 (at 8 hrs and 48 hrs), PU-Au was promoted the more homogenous co-localization of α5β3 (red color) and CXCR4 (green color) integrins expression in the cytoplasma, followed by PU and TCPS. The α5β3/CXCR4 integrins expression was possibility correlated with the FAK signaling in WJCs. The expression of CXCR4 and α5β3 integrins was significantly enhanced by VEGF of WJCs after 8 hrs treatment (Fig 7). Interestingly on PU-Au, the expressed of CXCR4 and α5β3 integrins were more prominently after SDF-1 treatment than with VEGF treatment for 48 hrs. Together these finding, we found that VEGF to be as a critical upstream molecular in the regulation of WJCs migration function after cultured on PU-Au nanocomposites.

5. Number of $CD34^+$ cells in the peripheral blood mononuclear cells.

PBMNCs were obtained from young healthy adults and the percentage of $CD34^+$ cells in the PBMNCs were determined by flow cytometry after MultiSort separation procedure. The flow cytometry showed about 1.09% of PBMNCs expressed $CD34^+$ and G-mean fluorescence intensity of $CD34^+$ was 367.29 whereas the PBMNCs was 56.10 (Fig 8).

6. Characterization of $CD34^+$ endothelial progenitor cells.

At 1, 7, and 14 days of incubation, the morphology of EPCs was visualized by microscopy. The defined cells morphology exhibited as a central core of round cells in day1 and exhibited with elongated cells at the periphery was shown from the day 7 to day 14 (Fig 9A). Indeed, cells were also identified by staining for endothelial lineage markers as shown in Fig 9B. The endothelial cells phenotype was characterized by immunostaining with antibodies specific for endothelial markers (vWF and eNOS) at day 21.

7. Maturation of EPCs by SDF-1 stimulated on PU-Au

The CD31, VEGF-R2, and CD34 are all known to crucial important role in angiogenesis [18]. Thus, we investigated whether the effect of PU-Au on these surface markers of EPCs is mediated via the chemoattract effect of SDF-1. The CD31 and VEGF-R2 surface markers

expression level of EPCs significantly enhanced by PU-Au. Indeed, a slightly activation of CD34 expression also has been observed (Fig 10A). Furthermore, we pretreated cells with CXCR4 neutralizing antibody and AMD3100 (10 nM) (an inhibitor of CXCR4) 1 hr before PU-Au treatment. It was found that CD34 expression level was abolished by these inhibitor treatments after the cells cultured on PU-Au (Fig 10B).

8. PU-Au nanocomposites promote vascularization in damage vessel tissue.

The EPCs-seeded materials of rabbit femoral artery divided in 3 groups (catheter treated, PU-Au with catheter, PU-Au plus EPCs with catheter). To clarify the repairing capacity of long-term biomimetic remodeling of cellular vascular grafts coated with EPCs on PU-Au nanocomosites, we furthermore performed long-term experiments to examine the vascular lumen of cellular grafts. Because thrombosis is the major high risk factor of vascular grafts, especially for small diameter of vascular, we carried out more detailed analysis on platelet adhesion and thromous formation. HE staining assay revealed that a cellular graft (with control group) had significant amounts of platelet aggregation after 28 day implantation (Fig 11). However, the EPCs grafts exhibited very little platelet aggregation on the lumen surface, which coated with the PU-Au nanocomposites, followed by PU-Au (without implantation of EPCs) treatment group. Cross-section staining showed thrombus formation on the luminal surface of a cellular grafts (with treatment) but not of EPC-implantated grafts. Platelet aggregation and thrombus are an index of host response to foreign-body biomaterials; our results demonstrated that when seeded EPCs with PU-Au nanocomposites could have better

antithrombogenic capacity. Consistently, the results at 1 month significant intimal thickening in acellular grafts but not in EPCs-seeded grafts (Fig. 11). It is conceivable that the long-term patency of EPCs-seeded vascular grafts (coated with PU-Au nanocomposites) was mainly because of the antithrombogenic property of EPCs in the early phase.

Immunohistochemical examination of vascular graft coated with PU-Au nancomposites after1 month post-implantation of EPCs showed regeneration of vascular tissues of the artery on endothelial layer. Immunohistochemical analysis showed that cells on the luminal sides (endothelial layer) of the vascular grafts stained significantly stained positively expression for CD31 and CD34, further indicating the endothelium regeneration (Figs 12A and 12B).

Discussion

Cardiovascular tissue engineering introduced the prospect of a completely biological, living, and autologous blood vessel produced in vitro to fill the critical need for functional small diameter vascular grafts [7]. It was observed in our previous report that the surface morphology of the HDI-based PU was significantly modified by the existence of a small amount of gold nanoparticles [45]. The surface morphology of the PU and PU-Au nanocomposites showed dominantly hard segment micelles embedded in a soft-segment-rich matrix. The change in the diameter (from 93 to 22 nm) of the hard segment micelles upon addition of the gold nanoparticles actually played an important role in the cellular response to these nanocomposites. Therefore, we believed the increased cell migration was not a result of the quantity of gold but the quality of gold that can modify the two-phase morphology. It has been reported that in ECs, PI3K/Akt and FAK signaling could be activated by material nanotopography [59]. These molecular signaling between cells and nanomaterials can cause actin fibers and lamellopidia formation, leading to cell motibility. However, the effect of nanocomposites on the behavior of stem cells has less studied.

MSCs have been reported to play an important role in vascularization and angiogenesis [33], and also have been used in the construction of tissue-engineered blood vessels [64]. The functions of MSCs are not only due to its potential to differentiate into endothelial cells, but also depend on the paracrine effects, including enhanced survival of implanted MSCs, mobilization and migration of stem cells, which contribute to the repair of vascular. MSCs secreted numerous cytokines including VEGF, SDF-1, bFGF, IGF-1 and HGF [27]. These paracrine factors, especially VEGF and SDF-1, are important maintaining or improving vascular tissue

repairing.

Previous studies demonstrate that overexpression of SDF-1 in the vascular provides a cue for stem cells to mobilize and home into the damaged vascular tissue [50]. Consequently, interactions between SDF-1 and CXCR4 contribute to ischemic tissue repair [51]. Mobilization from the bone marrow can increase the local number of MSCs, VEGF or SDF-1 can mobilize MSCs to promote the formation of new blood vessels [52]. We found that PU-Au induced MSC co-stimulation with growth factors, i.e. VEGF and SDF-1 and expressed its surface receptors, i.e. CXCR4 and $\alpha 5\beta 3$ on PU-Au represent an important mechanism directing MSC-mediated repair of vascular tissue (Fig 7). Our results showed that PU-Au can improve the adhesion effectively of WJCs (Fig 6). In particular, it can significantly enhance the mobilization function of VEGF and SDF-1, indicating that PU-Au can promote WJCs proliferation alone and in synergy with VEGF or SDF-1. As a result, the specific mechanisms of cross-talk between the vascular tissue in WJCs mobilization deserve further study.

Cell attachment is the single most important factor during cell–implant interactions [23], and is critical in determining the initial success of a bioengineered implant. The biological activity of the immobilized VEGF plays a dominant role during neovascularization of an implant in vivo and endothelial cells will come into direct contact with the implant surface [27]. Our previously report indicated that PI3K/Akt and FAK has a marked effect on the ability of endothelial cells to involve migration event [59]. In particular, endothelial cell chemotaxis is linked to the production of proteolytic enzymes (i.e., metalloproteinases) and phosphorylation of fast signaling as FAK [65]. At the same time, endothelial cell survival, adhesion and migration correlate with proper expression and organization of the adhesion on biomaterials. We next

explored on evaluating the effects and bioactivity of the VEGF and SDF-1 immobilized on the PU-Au coated substrate. In this study, we also intend explore this more detail and further identify in the signaling pathway by which PU-Au cause adhesion and migration during the cardiovascular regeneration process in the presence of Au nanoparticle of WJCs. As shown in this work, PU-Au induced greater FAK expression intensity after 48 hrs of incubation (Fig 3). It is suppose that the levels of p-FAK may be more relevant to functions such as regulation of gene expression and cell migration effect. To explore the molecular mechanism by which MMP proteins activity was induced for WJCs on PU-Au, the expression of MMP-2 and MMP-9 was also induced after a co-treatment of PU-Au with VEGF or SDF-1, respectively in Fig 5. Thus, additional protein components of cell-cell interaction may be affected by signals triggered by FAK.

eNOS plays an essential role in endothelial cell proliferation and is a central mediator of several endothelium growth stimulators, such as VEGF [19]. Recent studies have been shown that paracrine release of SDF-1 by Akt in MSCs promotes vascular repair [51]. VEGF has been reported to stimulate PI3K/Akt expression in endothelial cells [52]. This strategy might become a novel chemokine therapy for next generation therapeutic neovascularization [47-48]. Migration of EPCs was mediated by SDF-1/CXCR4 via PI3K/Akt/eNOS signal transduction pathway [52]. Nevertheless, these data suggest that the increased expression and function of VEGF with subsequent activation of Akt and eNOS were involved, at least in part, in the mechanisms by which SDF-1α enhanced ischemia-induced neovascularization. Akt signaling appears to be critical for VEGF-induced postnatal angiogenesis [52]. Interesting, we found that PU-Au attenuated Akt/eNOS phosphorylation in WJCs after containment treated with SDF-1 or VEGF (Fig 4). It was suggested that PI3K/Akt

signaling may not play as a crucial role as PI3K/Akt signaling in promoting WJCs migration on PU-Au.

Tissue engineered vascular conduits need to have the mechanical and biological properties of arteries in order to have superior patency rates. The conduits need to be non-thrombogenic and need to simulate arteries. The capacity of PBMNCs derived EPCs has important implications in the repair of vascular tissue. Reports also suggested that EPCs are derived from PBMNCs and that accumulate at sites of angiogenesis [62]. These studies support the notion that EPCs could be a cell source for ECs and would be an ideal cell source for tissue engineering of autologous vascular grafts [16]. An ideal strategy is to prepare a material which is inherently nonthrombogenic, compliant and has the ability to promote endothelialization from EPCs directly from the blood [16]. So far, anti-thrombotic modifications of the intima of vascular grafts can inhibit thrombosis, but these anticoagulant effects are temporary, and vascular grafts are meant to last for the life of the patient [11]. Since EPCs play important roles in thrombosis, endothelialization of the vascular graft is the most effective way to deal with thrombosis and intima hyperplasia [13]. Based on our current research, we took peripheral mononuclear cells and isolated the EPCs from the monocytes by changing the culture medium after the first day. Using a combination of surface marker discrimination and adhesion-based EPCs isolation, we developed a new PU-Au nanocompsites to explore the vascular tissue research.

During the implantation of vascular stents, percutaneous transluminal coronary angioplasty (PTCA) tends to damage the vascular endothelium [8]. If EPCs can be mobilized from bone marrow to peripheral blood, homing to the damages site will repair the injured blood vessel [13]. Based on these finding, it was suggested that PU-Au can promote EPCs

mobilization and homing to promote endothelium of vascular graft. To test this concept, we prepared a “commercial catheter”, coated PU-Au nanocomposites on the surface and seed EPCs on the “vascular graft”, and then transplanted the vascular graft in the rabbit femoral artery model (Fig 11).

The present results showed that the degree of endothelialization in PU-Au seeded with EPCs was significantly higher than the control vascular graft, consistent with the conclusion that PU-Au promotes CD34 and CD31 expression level of EPCs *in vivo* (Fig 12). Our results demonstrate that PU-Au nanocomposites allow the remodeling of vascular tissue in EPCs, similar to that the native vascular tissue. The effect of the antithrombogenic property of EPCs has also observed in this study (Fig 11). In this study we showed that the PU-Au nanocomoposites coated with the catheter allowed efficient promote endothelialization and that EPCs remodeling into lumen in the vascular wall, as in the native wall (Fig 11). The combination of antithrombic and implantation EPCs into PU-Au nanocomposites is a promising approach to fabricate ideal vascular grafts (allogenetic or autologus) that may be offer a new way for applied clinical setting. Although PU-Au had significantly induced of CD34 surface markers expression has been found in this study (Fig 12B), however, it is still not obvious how much EPCs to the cell recruitment process from the host tissue. One important observation is the CD34 surface markers of vascular graft was continuous present in the vascular wall after 1 month implantation with PU-Au nanocomopsites. The relative contribution to endothelialization by the surrounding vascular and the circulating EPCs needs further investigation.

Given the EPCs from the vascular niche for endothelial cell differentiation and that vascular grafts are compatible with host vascular tissue in circulation. It was suggested that PU-Au nanocomposites can be

a good model system for implantation of EPCs and to promote the endothelialization capacity after vascular graft implantation. Besides, our data also demonstrate that the antithrombosis property of EPCs depends on PU-Au nanocomposites, which provides a novel strategy for the approach of modifying vascular graft with anti-platelet adhesion/aggregation effects. The use of EPCs which was isolation from PBMNCs to construct vascular graft by PU-Au nanocomposites could be a new insight for vascular tissue engineering. However, besides having an antithrombogenic effect on EPCs on PU-Au nanocomposites, EPCs could participate in other vascular repairing processes at the postimplantation, such as paracrine signaling (ex: SDF-1α/CXCR4) or ECM remodeling, which also warrants further studies.

Noteworthy, administration of EPCs into subjects with vascular disease has had lower proliferative efficacy with regard new vessel formation, which limited their clinical application. To solve this problem, how to seek for other sources of hemoatopoietic stem cells for the better proliferative property will be worth exploration in the further. This is also supported by the significantly up-regulated expression of CD34 surface marker by PU-Au nanocomposites both in vitro (Fig 10) and in vivo (Fig 12). Therefore, implantation of EPCs with PU-Au nanocomposites was shown to enhance in vivo endothelialization and the subsequent expression the CD34 marker in vascular damaged model. We further show that the CD34 surface marker of EPCs from PBMNCs can efficiency significantly induced by PU-Au nanocomposites under in vivo condition. The potential of CD34 surface marker to access recruit circulation EPCs from the host tissue and to differentiate into endothelial cells could be greatly beneficial for vascular tissue engineering application.

In this study, we propose to elucidate the specific angiogenic

processes downstream of VEGF/SDF-1 receptor activated by PU-Au in the WJCs, and further to explore how critical role played by angiogenesis in the whole process. We believe our findings will provide new insights into the development of more effective cell therapy strategies directed at angiogenic processes for restoring vascular function. Therefore, strategies aimed to apply PU-Au to amplify VEGF/SDF-1 signaling could significantly promote angiogenic cell mobilization and vascularization in stem cell-based therapies. The molecular mechanism behind the enhanced endothelialization by such combination requires further exploration.

The use of more abundant PBMNCs (ex: $CD14^+$ cells), could may offer other way to overcome limitation in cell number of EPCs. Because EPCs express functional SDF-1α/CXCR4 and interaction between eNOS and VEGF signaling pathway, it may form a positive-feedback loop to further enhance therapeutic neovascularization in vivo. The present study might have significant clinical implications in that induced CD34 surface markers by PU-Au nanocomposites has therapeutic potential for enhancing ischemia-induced neovascualrization.

References

1. Moreno PR, Purushothaman KR, Zias E, Sanz J, Fuster V. Neovascularization in human atherosclerosis. Curr Mol Med 2006; 6: 457-77.
2. Malle E, Waeg G, Schreiber R, Gröne EF, Sattler W, Gröne HJ. Immunohistochemical evidence for the myeloperoxidase/H_2O_2/halide system in human atherosclerotic lesions: colocalization of myeloperoxidase and hypochlorite-modified proteins. Eur J Biochem 2000; 267: 4495-503.
3. Fuster V, Badimon JJ, Badimon L. Clinical-pathological correlations of coronary disease progression and regression. Circulation 1992; 86: 1-11.
4. Meltem Avci-Adali, Gerhard Ziemer, Hans P. Wendel. Induction of EPC homing on biofunctionalized vascular grafts for rapid in vivo self-endothelialization: A review of current strategies. Biotechnology Advances 2010; 28:119-129.
5. Enterline DS, Kapoor G. A practical approach to CT angiography of the neck and brain. Tech Vasc Interv Radiol 2006; 9: 192-204.
6. Giacconi R, Caruso C, Lio D, Muti E, Cipriano C, Saba V, Boccoli G, Gasparini N, Malavolta M, Mocchegiani E. HSP70-2 polymorphism as a risk factor for carotid plaque rupture and cerebral ischaemia in old type 2 diabetes-atherosclerotic patients. Mech Ageing Dev 2005; 126: 866-73.
7. Nissen SE. Atherosclerosis in 2010: new therapeutic insights. Nat Rev Cardiol 2011; 8: 70-2.

8. Kulik A, Ruel M. Statins and coronary artery bypass graft surgery: preoperative and postoperative efficacy and safety. Expert Opin Drug Saf 2009; 8: 559-71.
9. Du X, Soon JL. Mild to moderate aortic stenosis and coronary bypass surgery. J Cardiol 2011; 57: 31-5.
10. Molisse T, Tunick PA, Kronzon I. Role of echocardiography in aortic atherosclerotic disease and stroke. Minerva Cardioangiol 2007; 55: 267-74.
11. Chen MC, Chang Y, Liu CT, Lai WY, Peng SF, Hung YW, Tsai HW, Sung HW. The characteristics and in vivo suppression of neointimal formation with sirolimus-eluting polymeric stents. Biomaterials 2009; 30: 79-88.
12. De Scheerder IK, Wilczek KL, Verbeken EV, Vandorpe J, Lan PN, Schacht E, De Geest H, Piessens J. Biocompatibility of polymer-coated oversized metallic stents implanted in normal porcine coronary arteries. Atherosclerosis 1995; 114: 105-14.
13. de Mel A, Bolvin C, Edirisinghe M, Hamilton G, Seifalian AM. Development of cardiovascular bypass grafts: endothelialization and applications of nanotechnology. Expert Rev Cardiovasc Ther 2008; 6: 1259-77.
14. Jackson KA, Majka SM, Wang H, Pocius J, Hartley CJ, Majesky MW, Entman ML, Michael LH, Hirschi KK, Goodell MA. Regeneration of ischemic cardiac muscle and vascular endothelium by adult stem cells. J Clin Invest 2001; 107: 1395-402.
15. Kocher AA, Schuster MD, Szabolcs MJ, Takuma S, Burkhoff D, Wang J, Homma S, Edwards NM, Itescu S. Neovascularization of

ischemic myocardium by human bone-marrow-derived angioblasts prevents cardiomyocyte apoptosis, reduces remodeling and improves cardiac function. Nat Med 2001; 7: 412-3.

16. Strauer BE, Brehm M, Zeus T, Köstering M, Hernandez A, Sorg RV, Kögler G, Wernet P. Repair of infarcted myocardium by autologous intracoronary mononuclear bone marrow cell transplantation in humans. Circulation 2002; 106: 1913-8.
17. Silva EA, Kim ES, Kong HJ, Mooney DJ. Material-based deployment enhances efficacy of endothelial progenitor cells. Proc Natl Acad Sci U S A 2008; 105: 14347-52.
18. Asahara T, Murohara T, Sullivan A, Silver M, van der Zee R, Li T, Witzenbichler B, Schatteman G, Isner JM. Isolation of putative progenitor endothelial cells for angiogenesis. Science 1997; 275: 964-967.
19. Yu J, deMuinck ED, Zhuang Z, Drinane M, Kauser K, Rubanyi GM, Qian HS, Murata T, Escalante B, Sessa WC. Endothelial nitric oxide synthase is critical for ischemic remodeling, mural cell recruitment, and blood flow reserve. Proc Natl Acad Sci U S A 2005; 102: 10999-11004.
20. Kwon SM, Suzuki T, Kawamoto A, Ii M, Eguchi M, Akimaru H, Wada M, Matsumoto T, Masuda H, Nakagawa Y, Nishimura H, Kawai K, Takaki S, Asahara T. Pivotal role of lnk adaptor protein in endothelial progenitor cell biology for vascular regeneration. Circ Res 2009; 104: 969-977.
21. Massa M, Campanelli R, Bonetti E, Ferrario M, Marinoni B, Rosti V. Rapid and large increase of the frequency of circulating endothelial colony-forming cells (ECFCs) generating late outgrowth endothelial cells in patients with acute myocardial infarction. Exp Hematol 2009;

37: 8-9.

22. Kim DI, Kim MJ, Joh JH, Shin SW, Do YS, Moon JY, Kim NR, Lim JE, Kim AK, Eo HS, Kim BS, Cho SW, Yang SH, Park CJ, Shim JS. Angiogenesis facilitated by autologous whole bone marrow stem cell transplantation for Buerger's disease. Stem Cells 2006; 24: 1194-1200.
23. Leone AM, Rutella S, Giannico MB, Perfetti M, Zaccone V, Brugaletta S, Garramone B, Niccoli G, Porto I, Liuzzo G, Biasucci LM, Bellesi S, Galiuto L, Leone G, Rebuzzi AG, Crea F. Effect of intensive vs standard statin therapy on endothelial progenitor cells and left ventricular function in patients with acute myocardial infarction: Statins for regeneration after acute myocardial infarction and PCI (STRAP) trial. Int J Cardiol 2008; 130: 457-462.
24. Jackson KA, Majka SM, Wang H, Pocius J, Hartley CJ, Majesky MW, Entman ML, Michael LH, Hirschi KK, Goodell MA. Regeneration of ischemic cardiac muscle and vascular endothelium by adult stem cells. J Clin Invest 2001. 107; 11: 1395-402.
25. Kocher AA, Schuster MD, Szabolcs MJ, Takuma S, Burkhoff D, Wang J, Homma S, Edwards NM, Itescu S. Neovascularization of ischemic myocardium by human bone-marrow-derived angioblasts prevents cardiomyocyte apoptosis, reduces remodeling and improves cardiac function. Nat Med 2001. 7; 4: 412-3.
26. Strauer BE, Brehm M, Zeus T, Köstering M, Hernandez A, Sorg RV, Kögler G, Wernet P. Repair of infarcted myocardium by autologous intracoronary mononuclear bone marrow cell transplantation in humans. Circulation 2002. 106; 15: 1913-8.
27. Bruder SP, Jaiswal N, Haynesworth SE. Growth kinetics,

self-renewal, and the osteogenic potential of purified human mesenchymal stem cells during extensive subcultivation and following cryopreservation. J Cell Biochem 1997; 4: 278-294.

28. Jaiswal N, Haynesworth SE, Caplan AI, Bruder SP. Osteogenic differentiation of purified, culture-expanded human mesenchymal stem cells in vitro. J Cell Biochem 1997; 64: 295-312.
29. Kadiyala S, Young RG, Thiede MA, Bruder SP. Culture expanded canine mesenchymal stem cells possess osteochondrogenic potential in vivo and in vitro. Cell Transplant 1997; 6: 125-134.
30. Ferrari G, Cusella-De Angelis G, Coletta M, Paolucci E, Stornaiuolo A, Cossu G, Mavilio F. Muscle regeneration by bone marrow-derived myogenic progenitors. Science 1998; 279: 1528-1530.
31. Dennis JE, Merriam A, Awadallah A, Yoo JU, Johnstone B, Caplan AI. A quadripotential mesenchymal progenitor cell isolated from the marrow of an adult mouse. J Bone Miner Res 1999; 14: 700-709.
32. Young RG, Butler DL, Weber W, Caplan AI, Gordon SL, Fink DJ. Use of mesenchymal stem cells in a collagen matrix for Achilles tendon repair. J Orthop Res 1998; 16: 406-413.
33. Dominici M, Le Blanc K, Mueller I, Slaper-Cortenbach I, Marini F, Krause D, Deans R, Keating A, Prockop Dj, Horwitz E. Minimal criteria for defining multipotent mesenchymal stromal cells. The International Society for Cellular: Therapy position statement. Cytotherapy 2006; 8: 315-317.
34. Oswald J, Boxberger S, Jørgensen B, Feldmann S, Ehninger G, Bornhäuser M, Werner C. Mesenchymal stem cells can be differentiated into endothelial cells in vitro. Stem Cells 2004; 22:

377-384.

35. Stenderup K, Justesen J, Clausen C, Kassem M. Aging is associated with decreased maximal life span and accelerated senescence of bone marrow stromal cells. Bone 2003; 33: 919-926.
36. Nishida S, Endo N, Yamagiwa H, Tanizawa T, Takahashi HE. Number of osteoprogenitor cells in human bone marrow markedly decreases after skeletal maturation. J Bone Miner Metab 1999; 17: 171-177.
37. Mueller SM, Glowacki J. Age-related decline in the osteogenic potential of human bone marrow cells cultured in three-dimensional collagen sponges. J Cell Biochem 2001; 82: 583-590.
38. Zhang H, Fazel S, Tian H, Mickle DA, Weisel RD, Fujii T, Li RK. Increasing donor age adversely impacts beneficial effects of bone marrow but not smooth muscle myocardial cell therapy. Am J Physiol Heart Circ Physiol 2005; 289: H2089-H2096.
39. Mitchell KE, Weiss ML, Mitchell BM, Martin P, Davis D, Morales L, Helwig B, Beerenstrauch M, Abou-Easa K, Hildreth T, Troyer D, Medicetty S. Matrix cells from Wharton's jelly form neurons and glia. Stem Cells 2003; 21: 50-60.
40. Ming-Yan Chena, Pu-Chang Liea, Zhi-Ling Lib, and Xing Weia. Endothelial differentiation of Wharton's jelly–derived mesenchymal stem cells in comparison with bone marrow–derived mesenchymal stem cells. Experimental Hematology 2009; 37: 629-640.
41. De Mel A, Bolvin C, Edirisinghe M, Hamilton G, Seifalian AM. Development of cardiovascular bypass grafts: endothelialization and applications of nanotechnology. Expert Rev Cardiovasc Ther 2008; 6:

1259-77.

42. Gilmore JL, Yi X, Quan L, Kabanov AV. Novel nanomaterials for clinical neuroscience. J Neuroimmune Pharmacol 2008; 3: 83-94.
43. Hsu S, Tseng H, Wu M. Comparative in vitro evaluation of two different preparations of small diameter polyurethane vascular grafts. Artif Organs 2000; 24: 119-128.
44. Gu H, Chen Z, Sa R, Yuan S, Chen H, Ding Y, Yu A. The immobilization of hepatocytes on 24 nm sized gold colloid for enhanced hepatocytes proliferation. Biomaterials 2004; 25: 3445-3451.
45. Hsu SH, Tang CM, Tseng HJ. Biocompatibility of poly(ether)urethane-gold nanocomposites. J Biomed Mater Res A 2006; 79: 759-70.
46. Dotsenko O, Xiao Q, Xu Q, Jahangiri M. Bone marrow resident and circulating progenitor cells in patients undergoing cardiac surgery. Ann Thorac Surg 2010; 90: 1944-51.
47. Sata M. Molecular strategies to treat vascular diseases: circulating vascular progenitor cell as a potential target for prophylactic treatment of atherosclerosis. Circ J 2003; 67: 983-91.
48. Norment AM, Bevan MJ. Role of chemokines in thymocyte development. Semin Immunol 2000; 12: 445-55.
49. Aicher A, Zeiher AM, Dimmeler S. Mobilizing endothelial progenitor cells. Hypertension 2005; 45: 321-5.
50. Moll NM, Ransohoff RM. CXCL12 and CXCR4 in bone marrow physiology. Expert Rev Hematol 2010; 3: 315-22.
51. Zaruba MM, Franz WM. Role of the SDF-1-CXCR4 axis in stem

cell-based therapies for ischemic cardiomyopathy. Expert Opin Biol Ther 2010; 10: 321-35.

52. Aiuti A, Webb IJ, Bleul C, Springer T, Gutierrez-Ramos JC. The chemokine SDF-1 is a chemoattractant for human $CD34^+$ hematopoietic progenitor cells and provides a new mechanism to explain the mobilization of $CD34^+$ progenitors to peripheral blood. J Exp Med 1997; 185: 111-20.
53. Müller A, Homey B, Soto H, Ge N, Catron D, Buchanan ME, McClanahan T, Murphy E, Yuan W, Wagner SN, Barrera JL, Mohar A, Verástegui E, Zlotnik A. Involvement of chemokine receptors in breast cancer metastasis. Nature 2001; 410: 50-6.
54. Sun YX, Wang J, Shelburne CE, Lopatin DE, Chinnaiyan AM, Rubin MA, Pienta KJ, Taichman RS. Expression of CXCR4 and CXCL12 (SDF-1) in human prostate cancers (PCa) in vivo. J Cell Biochem 2003; 89: 462-73.
55. Vaday GG, Hua SB, Peehl DM, Pauling MH, Lin YH, Zhu L, Lawrence DM, Foda HD, Zucker S. CXCR4 and CXCL12 (SDF-1) in Prostate Cancer: Inhibitory Effects of Human Single Chain Fv Antibodies. Clin Cancer Res 2004; 10: 5630-9.
56. Lapidot T, Dar A, Kollet O. How do stem cells find their way home? Blood 2005; 106: 1901-10.
57. Rebecca A Moyer, Michael K Wendt, Priscilla A Johanesen, Jerrold R Turner, and Michael B Dwinell. Rho activation regulates CXCL12 chemokine stimulated actin rearrangement and restitution in model intestinal epithelia. Laboratory Investigation 2007; 87: 807-817.
58. Ramesh K. Ganju, Stephanie A. Brubaker, Joshua Meyer, Parmesh

Dutt, Yangming Yang, Shixin Qin, Walter Newman, and Jerome E. Groopman. The a-Chemokine, Stromal Cell-derived Factor-1, Binds to the Transmembrane G-protein-coupled CXCR-4 Receptor and Activates Multiple Signal Transduction Pathways. J Biol Chem 1998; 27: 23169-75

59. Hung HS, Wu CC, Chien S, Hsu SH. The behavior of endothelial cells on polyurethane nanocomposites and the associated signaling pathways. Biomaterials 2009; 30: 1502-11.
60. Hsu SH, Tang CM, Tseng HJ. Gold nanoparticles induce surface morphological transformation in polyurethane and affect the cellular response. Biomacromolecules 2008; 9: 241-8.
61. Wang HS, Hung SC, Peng ST, Huang CC, Wei HM, Guo YJ, Fu YS, Lai MC, Chen CC. Mesenchymal stem cells in Wharton jelly of the human umbilical cord. Stem Cells 2004; 22: 1330-1337.
62. Wu H, Riha GM, Yang H, Li M, Yao Q, Chen C. Differentiation and proliferation of endothelial progenitor cells from canine peripheral blood mononuclear cells. J Surg Res 2005; 126: 193-8.
63. Kumar AH, Caplice NM. Clinical potential of adult vascular progenitor cells. Arterioscler Thromb Vasc Biol 2010; 30: 1080-7.
64. Cho SW, Lim SH, Kim IK, Hong YS, Kim SS, Yoo KJ, Park HY, Jang Y, Chang BC, Choi CY, Hwang KC, Kim BS. Small-diameter blood vessels engineered with bone marrow-derived cells. Ann Surg 2005; 241: 506-15.
65. Pezzatini S, Morbidelli L, Solito R, Paccagnini E, Boanini E, Bigi A, Ziche M. Nanostructured HA crystals up-regulate FGF-2 expression and activity in microvascular endothelium promoting angiogenesis.

Bone 2007; 41: 523-34.

66. Hung HS, Hsu SH. The response of endothelial cells to polymer surface composed of nanometric micelles. N Biotechnol 2009; 25: 235-43.

Figure 1

(A)

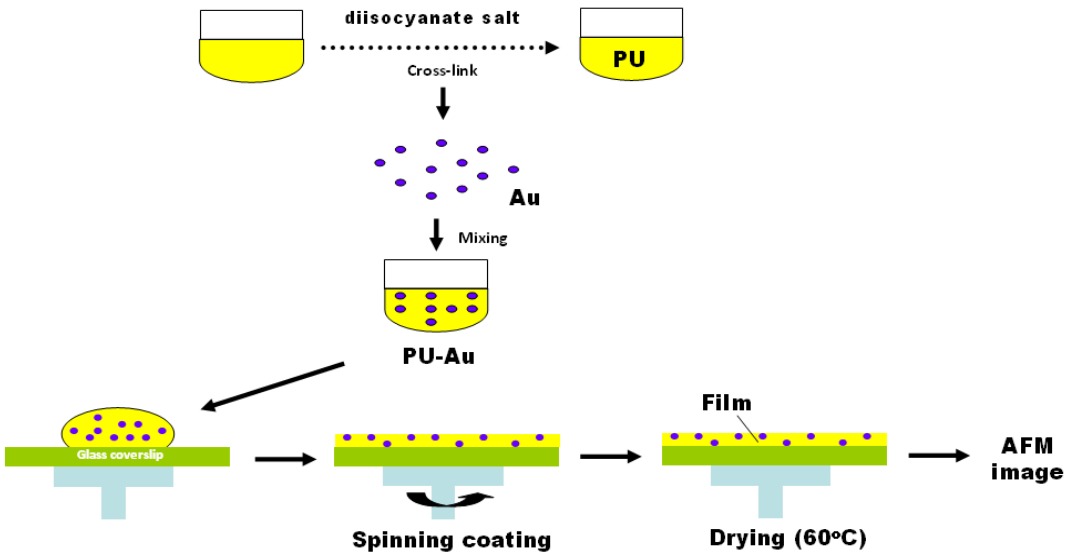

(B)

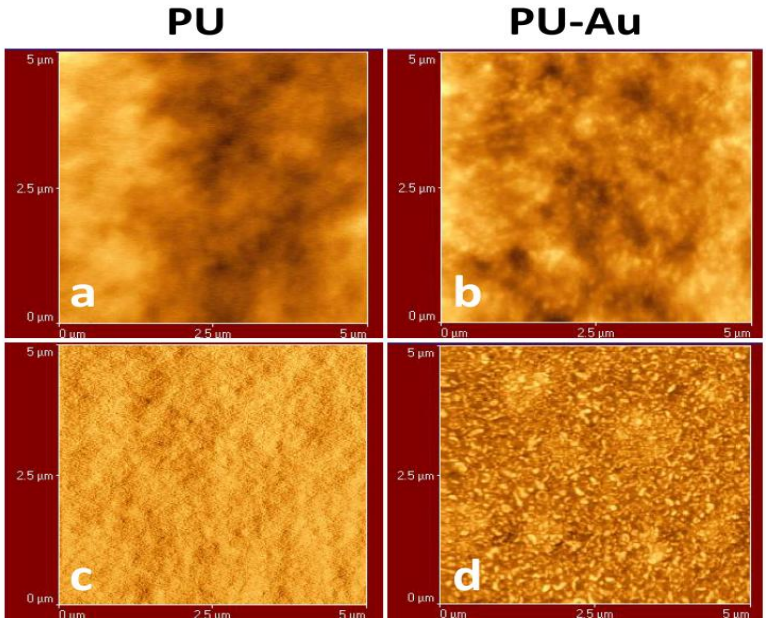

Figure 1: (A) Preparation of polyurethane (PU) and PU nanocomposites containing 43.5 ppm of gold nanoparticles (PU-Au) films. (B) The AFM images of topography (upper) and phase (below) for pure PU (a) (c); and PU-Au nanocomposites (b) (d).

Figure 2

(A)

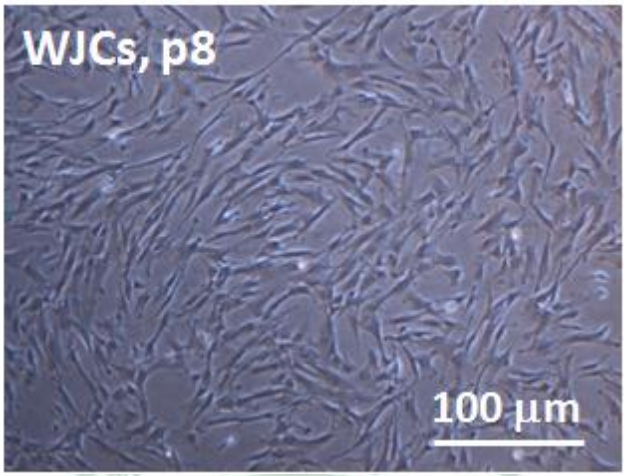

(B)

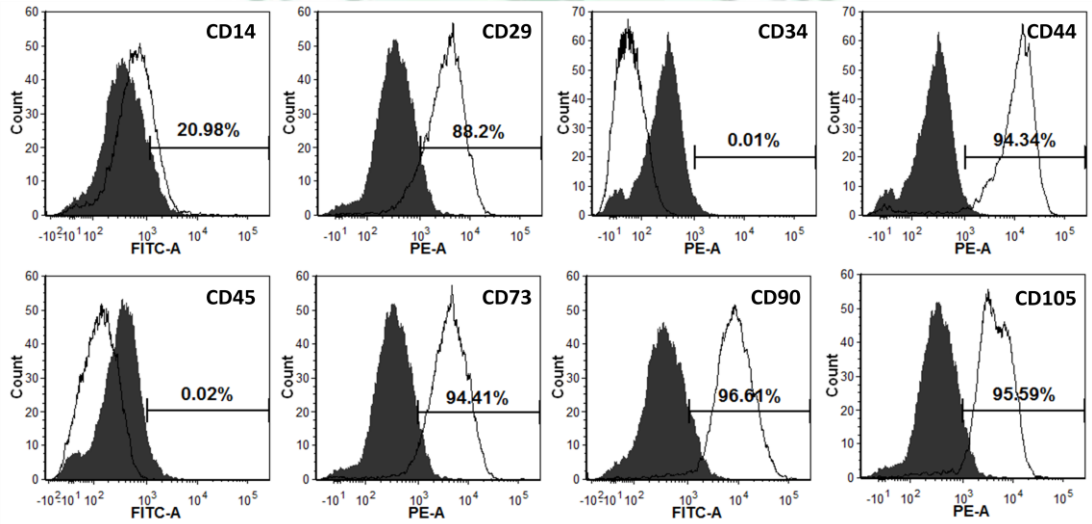

Figure 2: Characterization of WJCs. (A) Cell morphology of WJCs by optical microscope**.** (B) Detection of WJCs specific markers expression by flow cytometry analysis. An open area represents an antibody isotype control for background fluorescence and a shaded area shows signal from WJCs surface marker. WJCs were stained with PE or FITC-conjugated antibodies against the indicated markers: CD14-FITC, CD29-PE, CD34-FITC, CD44-FITC, CD45-PE, CD73-PE, CD90-FITC and CD105-PE.

Figure 3

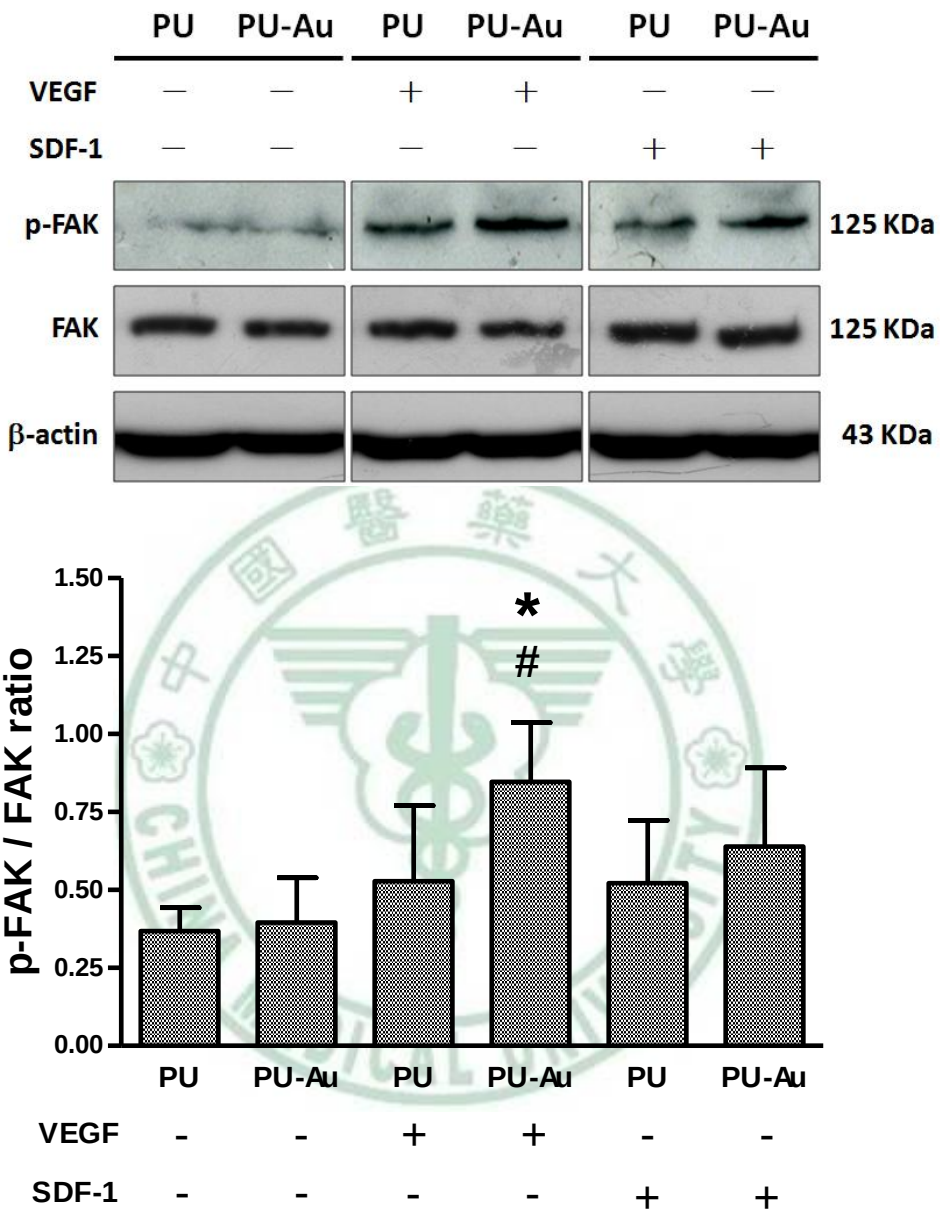

Figure 3: FAK phosphorylation of WJCs on nanocomposites was activated by angiogenic factor. WJCs were cultured on PU or PU-Au, and stimulated with VEGF and SDF-1 for 48 hrs. Cell lysates were collected and analyzed by Western Blot. Data are mean ± SD. *: greater than PU (without treated); #: greater than PU-Au (without treated).

Figure 4

(A)

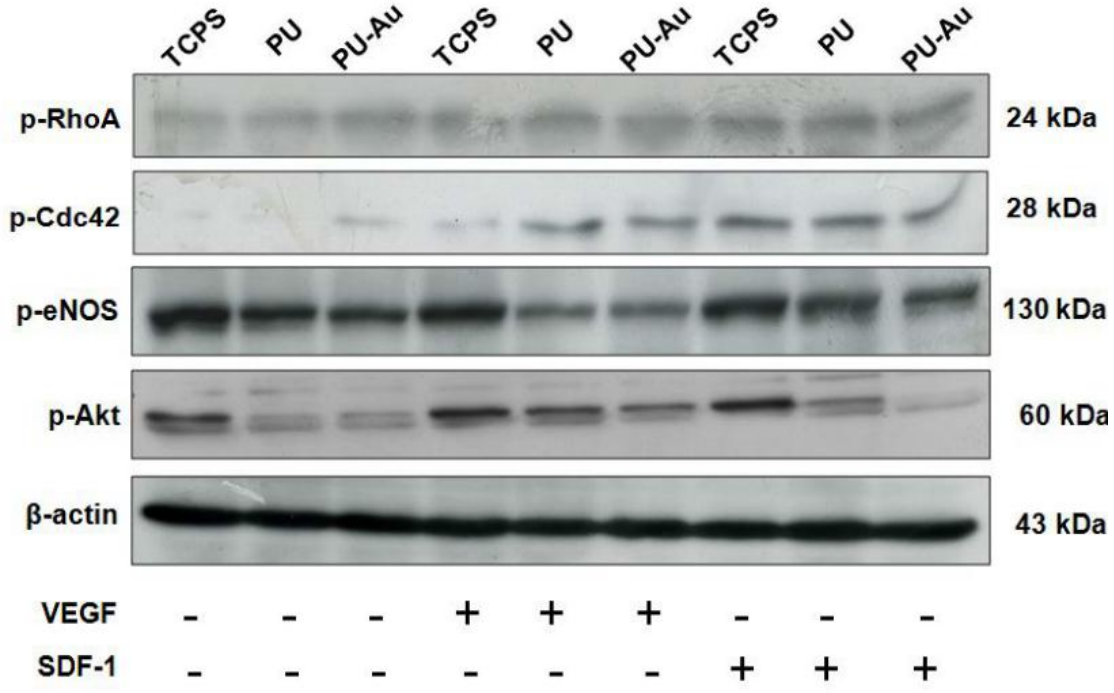
TCPS
PU
PU-Au
p-RhoA
24 kDa
p-Cdc42
28 kDa
p-eNOS
130 kDa
p-Akt
60 kDa
β-actin
43 kDa
VEGF
SDF-1

(B)

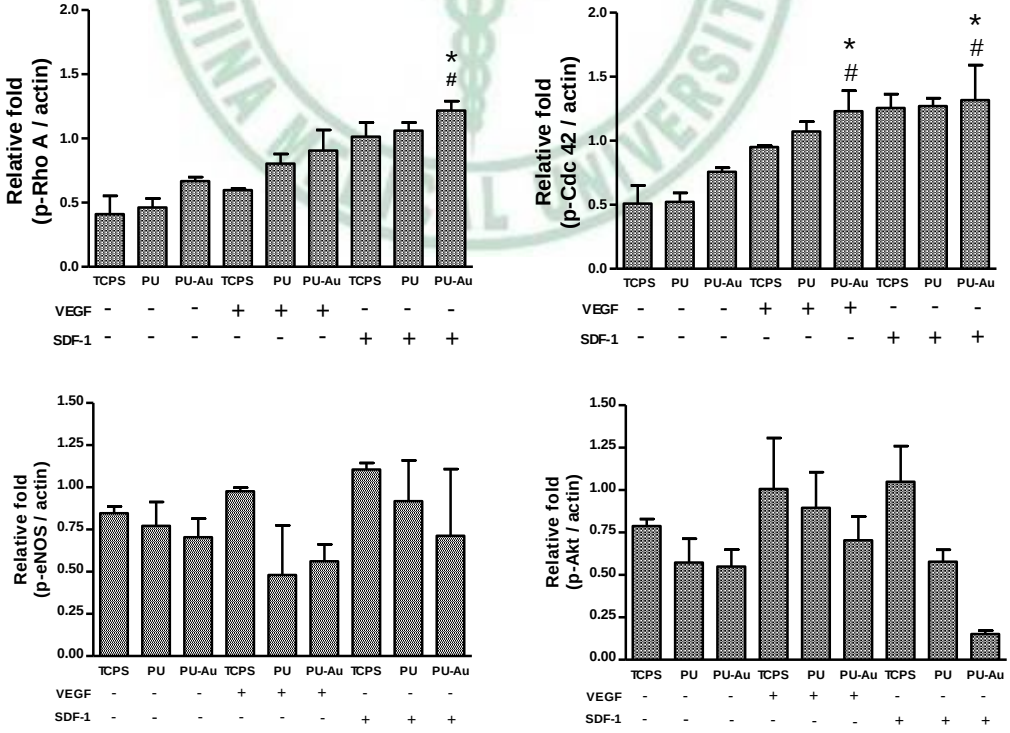
Relative fold (p-Rho A / actin)
Relative fold (p-Cdc 42 / actin)
Relative fold (p-eNOS / actin)
Relative fold (p-Akt / actin)
TCPS
PU
PU-Au
VEGF
SDF-1

Figure 4: The expressions of (A) Rho A, Cdc42, Akt, eNOS protein of WJCs cultured for 48 hrs by VEGF or SDF-1 stimulated on nanocomposites. WJCs were cultured on TCPS, PU and PU-Au, and stimulated with VEGF and SDF-1 for 48 hrs. Cell lysates were collected and analyzed by Western blot. (B) Columns, mean of three separate experiments. Data are mean ± SD. * $p < 0.05$: greater than TCPS (without treated), # $p < 0.05$: greater than PU (without treated).

Figure 5

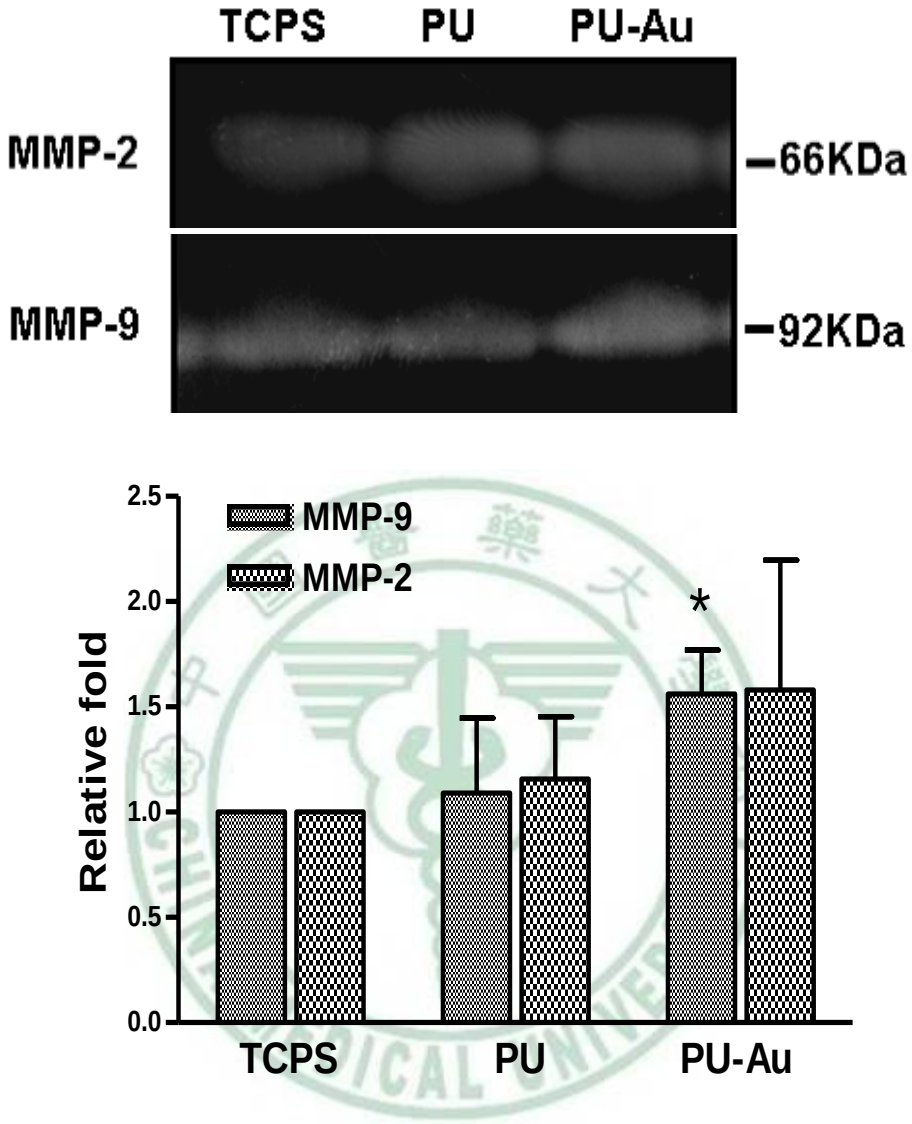

Figure 5: The MMP enzymatic activity in WJCs cultured on nanocomposites for 48 hrs. Cell lysates were collected and analyzed by MMP Gelatin Zymography. Data are mean ± SD. * $p < 0.05$: greater than TCPS.

Figure 6

(A)

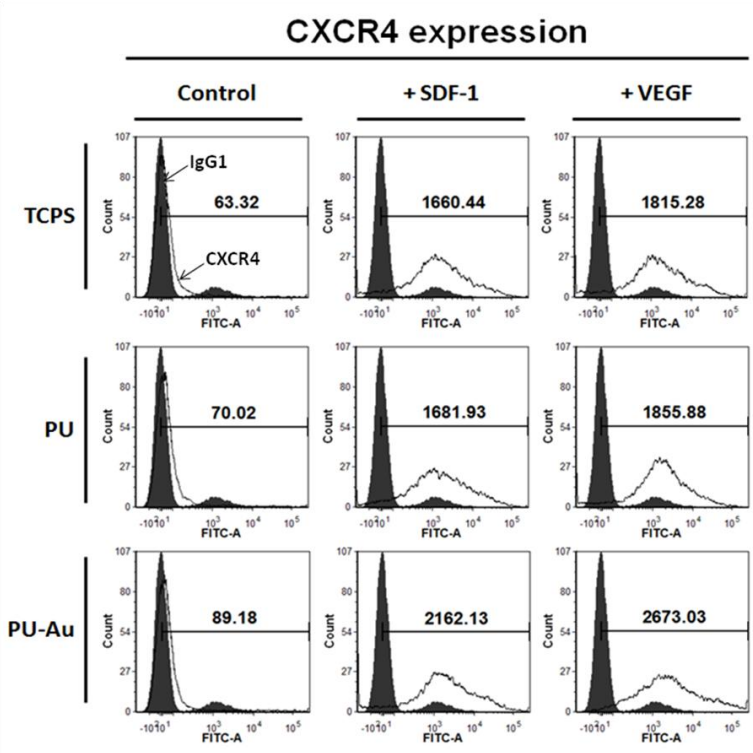
CXCR4 expression
Control
+ SDF-1
+ VEGF
TCPS
PU
PU-Au
IgG1
CXCR4
63.32
1660.44
1815.28
70.02
1681.93
1855.88
89.18
2162.13
2673.03
Count
FITC-A

(B)

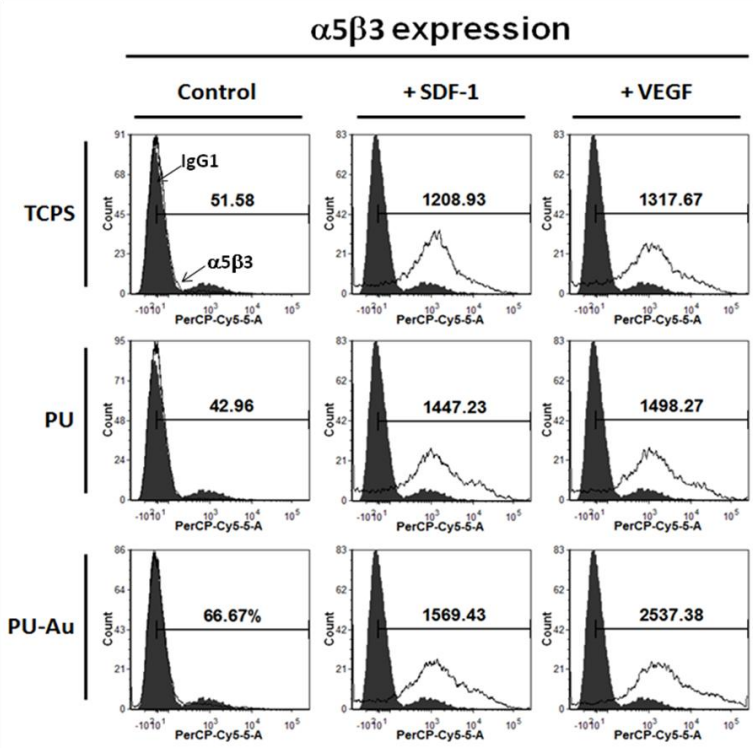
α5β3 expression
Control
+ SDF-1
+ VEGF
TCPS
PU
PU-Au
IgG1
α5β3
51.58
1208.93
1317.67
42.96
1447.23
1498.27
66.67%
1569.43
2537.38
Count
PerCP-Cy5-5-A

Figure 6: FACS analysis of CXCR4 and α5β3 integrin of WJCs with or without VEGF and SDF-1 treatment. WJCs were seeded on PU or PU-Au, and cultured with VEGF and SDF-1 for 48 hrs. CXCR4 or α5β3 integrin were induction on PU-Au after VEGF and SDF-1 treatment compared to PU. A shaded area represents an antibody isotype control for background fluorescence and an open area shows CXCR4 and α5β3 integrin expression.

Figure 7

(A)

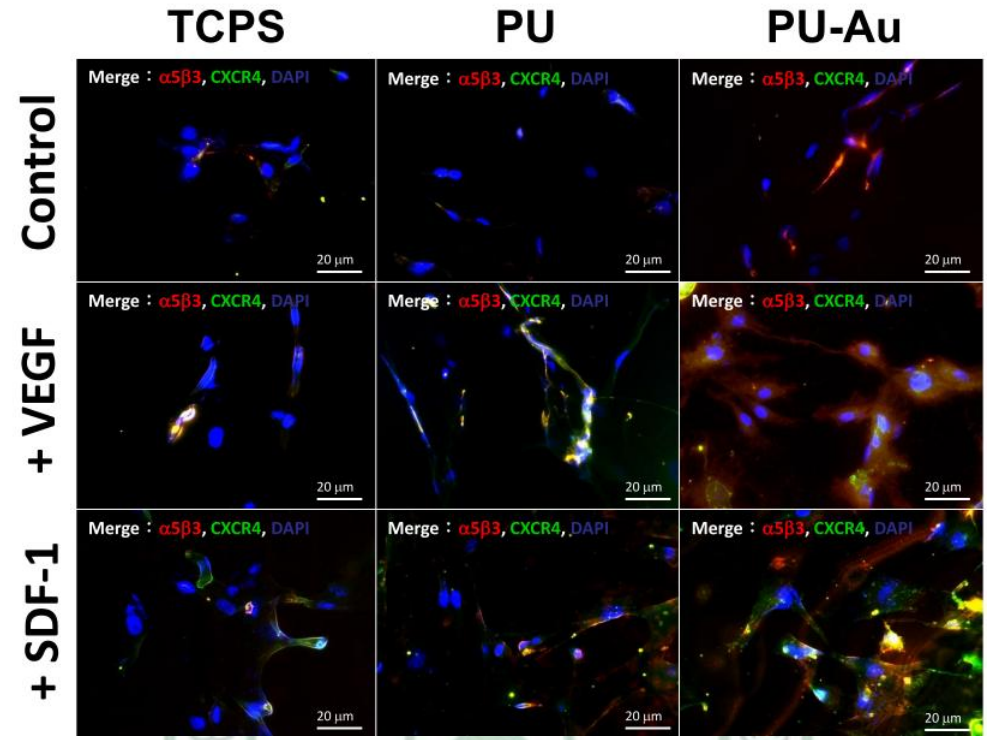
TCPS
PU
PU-Au
Control
+ VEGF
+ SDF-1
Merge : α5β3, CXCR4, DAPI
20 μm

(B)

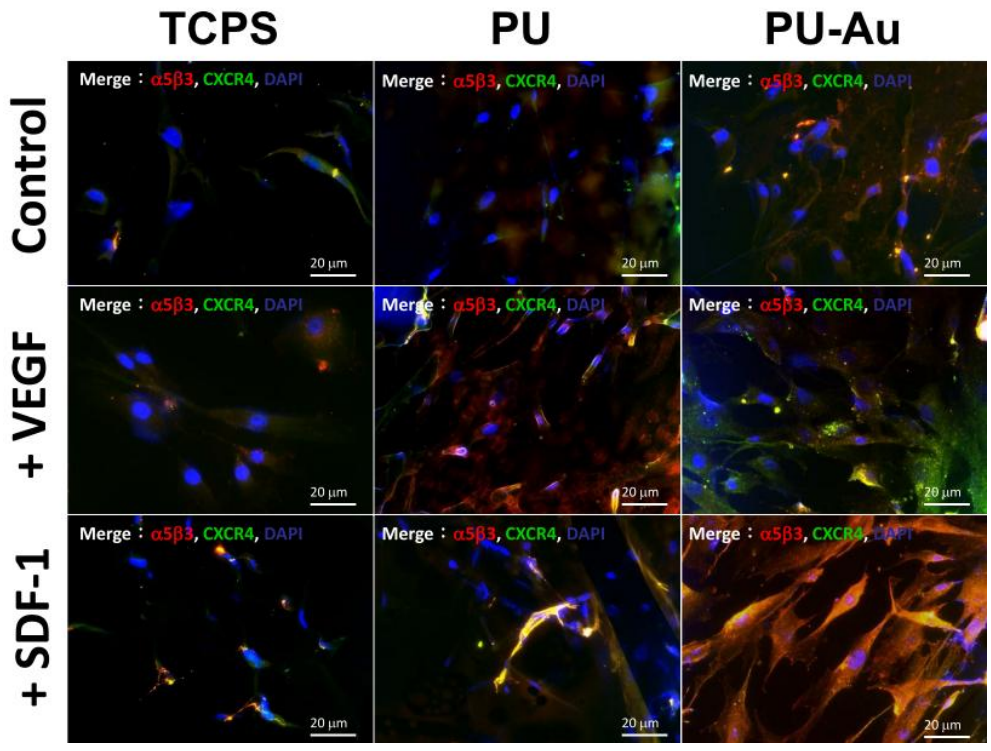
TCPS
PU
PU-Au
Control
+ VEGF
+ SDF-1
Merge : α5β3, CXCR4, DAPI
20 μm

Figure 7: Immunofluorescence staining of CXCR4 and α5β3 integrin of WJCs with or without VEGF and SDF-1 treatment. WJCs were seeded on PU or PU-Au, and stimulated with VEGF or SDF-1 for 8 (A) or 48 (B) hrs. Cells were incubated with primary anti-CXCR4 and anti-α5β3 antibodies followed by stained with FITC-conjugated immunoglobulin (green color fluorescence) or Cyc 5.5–conjugated immunoglobulin (red color fluorescence), cell nuclear staining was performed by 4', 6'-diamidino-2-phenylindole (DAPI) (blue color staining) (indicated by thin arrows). The merge of CXCR4, α5β3 and nuclei were shown. Bar=20 μm.

Figure 8

(A)

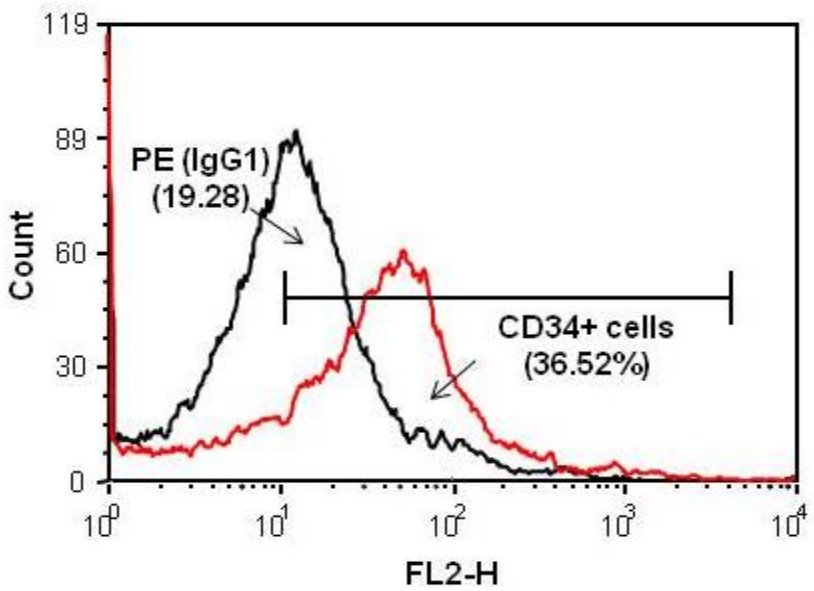

(B)

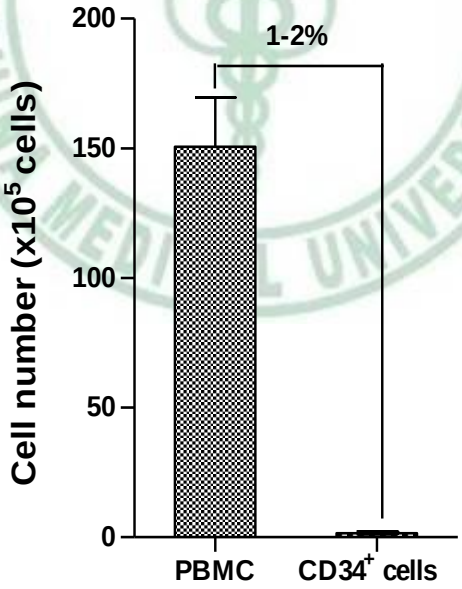

Figure 8: (A) Number of $CD34^+$ cells and (B) FACS analysis of CD34 after MultiSort separation procedure. A small proportion (1-2%) of PBMNC expressed CD34 determined by fluorescence-activated cell sorter (FACS) analysis.

Figure 9

(A)

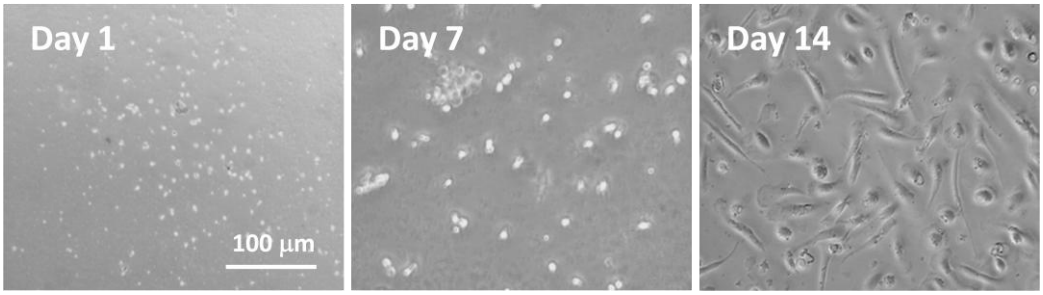

(B)

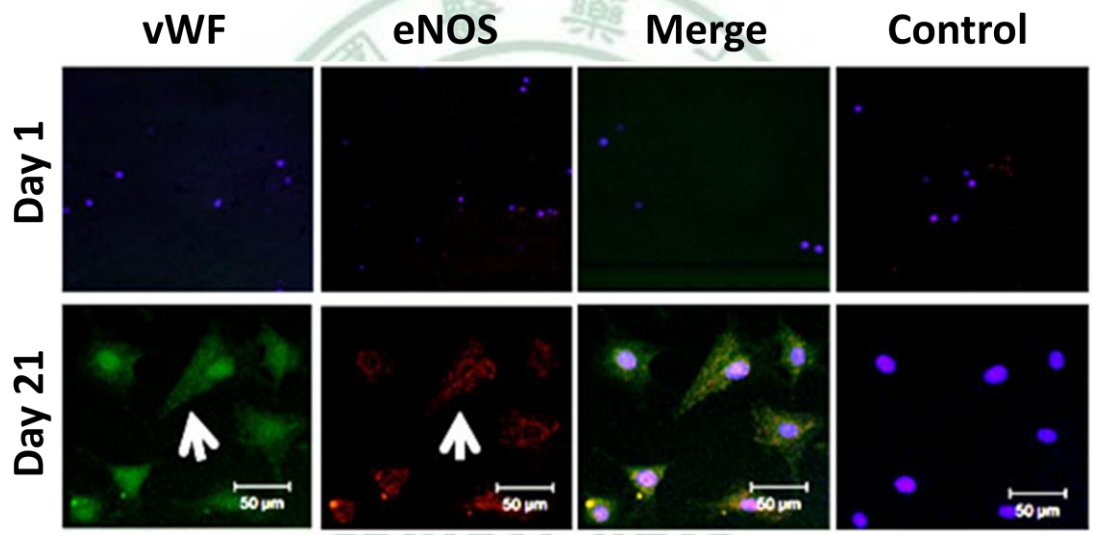

Figure 9: (A) Phase-contrast micrograph of endothelial progenitor cells (EPCs) morphology after cultured with fibronectin. (B) The endothelial phenotype was confirmed by immunostaining with antibodies specific for endothelial markers, eNOS; cell membrane and on cells border to border (arrow); vWF contained within cytoplasmic granule (arrow); representative control sections where nuclear staining alone is visible. All cells were counterstained with DAPI showing the nucleus as blue. (FITC: green color; cyc5.5: red color; DAPI: blue color) (day 1 and day 21). Bar=50 μm.

Figure 10

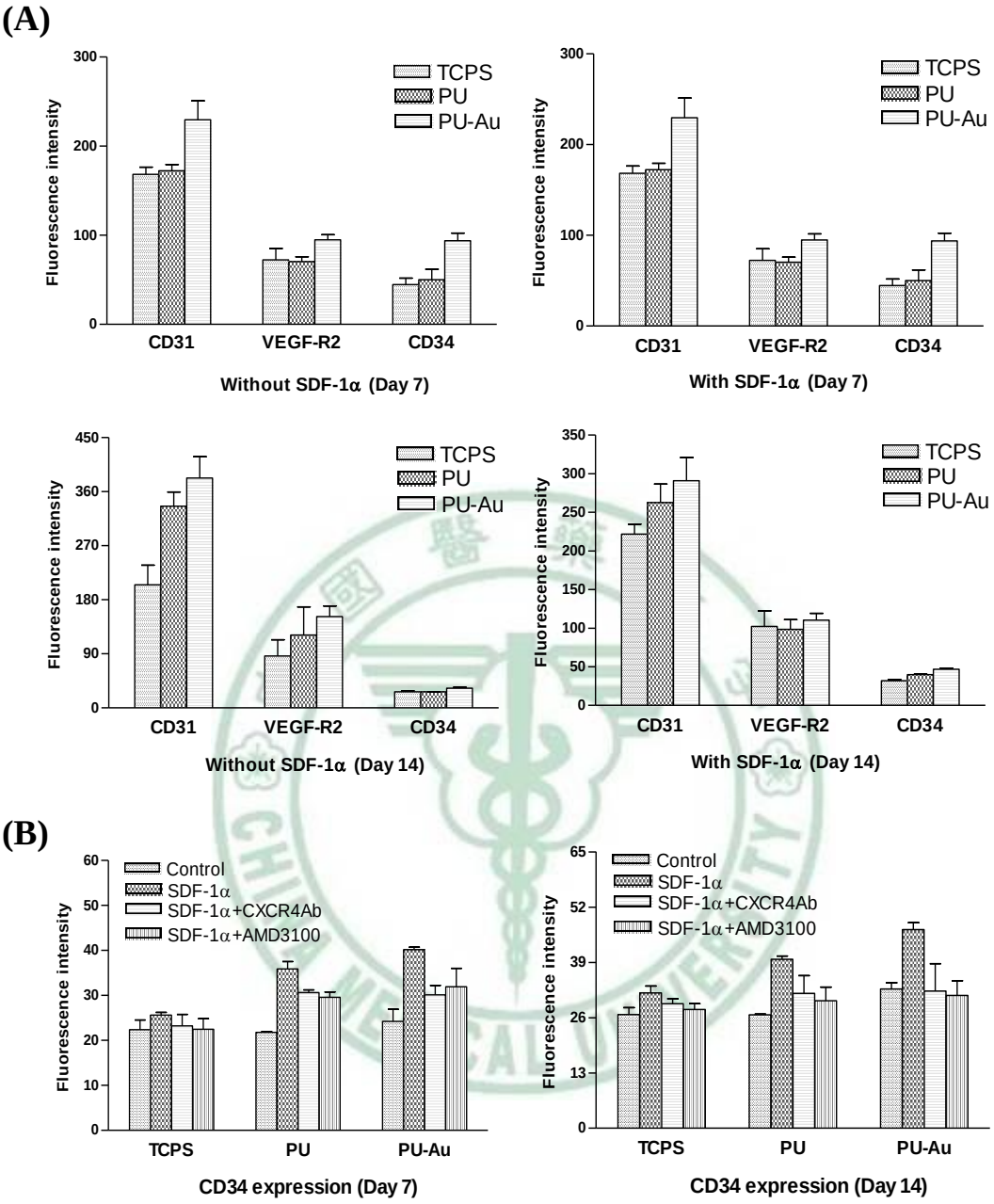

Figure 10: (A) Induction of CD31, VEGF-R2 and CD31 expression of EPCs with or without SDF-1 (100 ng/ml) treatment on TCPS, PU and PU-Au. (B) Flow cytometry analysis showed that CD34 surface marker expression increased in PU-Au for day 7 and day 14, whereas pretreatment with AMD3100 (10 nM) (an inhibitor of CXCR4) and CXCR4 neutralizating antibody with among the positively stained surface markers of the clusters. Data are mean ± SD.

Figure 11

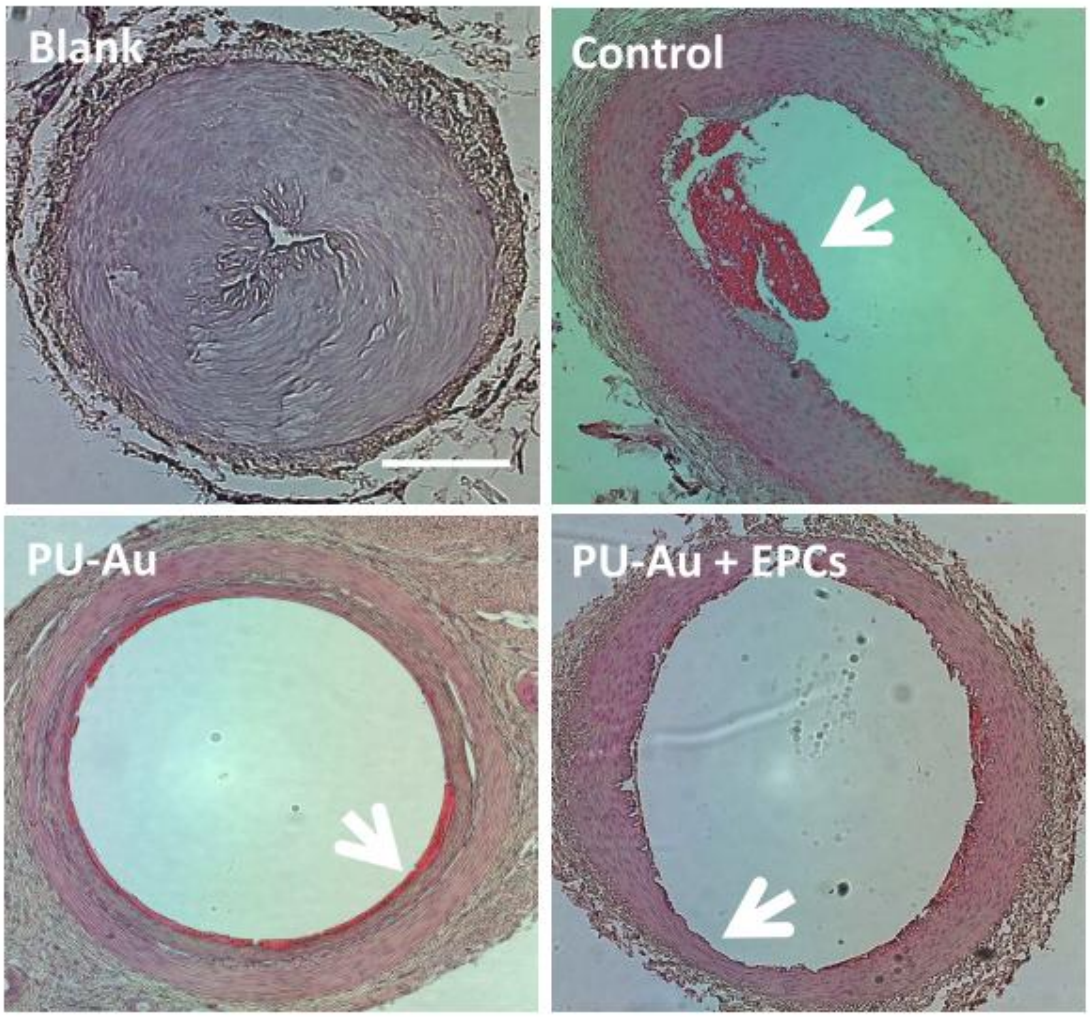

Figure 11: Anti-thrombogenic property after 28 days for EPCs implantation on PU-Au nanocomposites vascular graft in vivo. The samples were stained with Hematoxylin/eosin (H&E). Images are representative from at least four independent groups (indicated by thin arrows). Bar=100 μm.

Figure 12

(A)

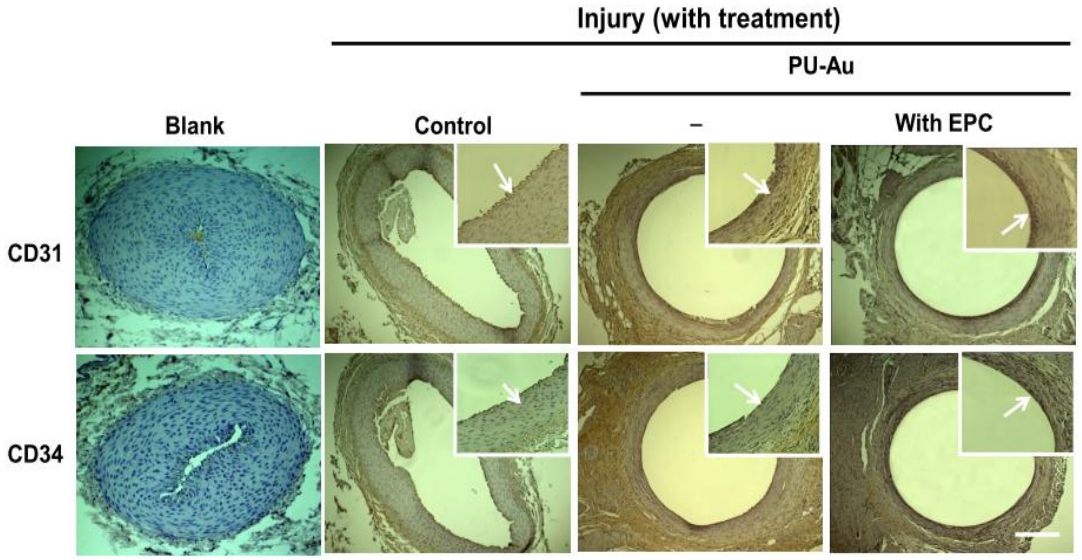

(B)

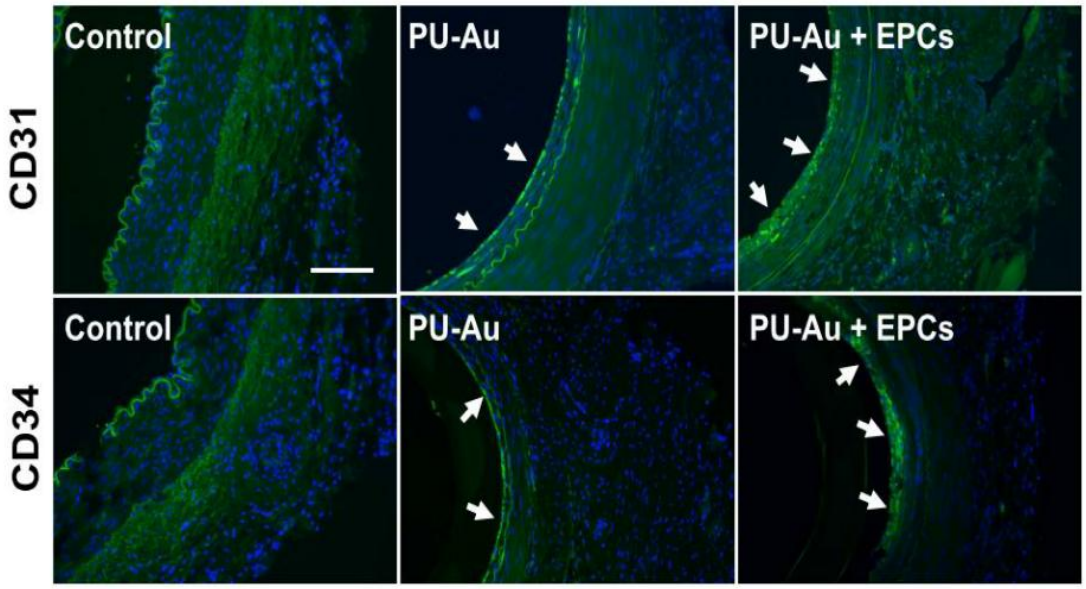

Figure 12: PU-Au nanocomposites promoted ECPs to differentiate into ECs after repairing rabbit femoral artery injured by wire. EPCs were incubated with PU-Au or not for 48 hrs and implantation into injured

artery. The injured artery were separated from rabbit and immunostainined with anti-CD31 antibody and CD34 antibody, cells followed by stained with (A) 3,3-Diaminobenzidine (DAB) and stained with (B) FITC-conjugated immunoglobulin (green color fluorescence), cell nuclear staining was performed by 4', 6'-diamidino-2-phenylindole (DAPI) (blue color staining) (indicated by thin arrows). (A) Bar=100 μm. (B) Bar=25 μm.

第二部分

探討 Wharton's jelly stem cells 在纖維連接蛋白-奈米金之複合基材上 VEGF/CXCR4 之分子機制

Part II

The molecular mechanism of Wharton's jelly stem cells on fibronectin-gold nanocomposites associated with VEGF/CXCR4 pathway

中文摘要

最近我們發展出一系列的纖維連接蛋白奈米金複合基材 (fibronectin-gold nanocomposites, FN-Au) 作為一模式系統，探討 Wharton's jelly stem cells (WJCs) 在 FN-Au 上之移動 (migration) 能力。我們利用 AFM 以及 FTIR 來分析 FN-Au 之結構，並且以 WJCs、單核球細胞以及血小板在 FN-Au 上之生物相容性測試。研究顯示， FN-Au 43.5 ppm 或是與單獨 FN、FN-Au 17.4 ppm 或 FN-Au 174 ppm 比較之下， FN-Au 43.5 ppm 可以增加生物的相容性 (例如:細胞增生、減少單核球細胞活化、血小板活化與氧化壓力)。此外，當給予 50 ng/ml 血管內皮生長因子 (vascular endothelial growth factor, VEGF) 以及 50 ng/ml 基質衍生因子 (stromal cell derived factor-1α, SDF-1) 的刺激，並培養在 FN-Au 43.5 ppm 之環境條件下可以增強細胞的增生與移動能力。此外，將 CXCR4 siRNA 轉染至 WJCs 中更降低了細胞的移動能力。研究顯示，FN-Au 可能誘導 VEGF/CXCR4 路徑同時活化 PI3K/Akt/eNOS 以及 MMP-9 之訊息途徑來增加 WJCs 的增生與移動能力。

Abstract

Recently we have developed a series of fibronectin-gold nanocomposites (FN-Au) as a model system to study the behavior of Wharton's jelly stem cells (WJCs) on biomaterials with nanophase separation. The structure and biology function of the FN-Au were characterized by AFM, ATR-IR analysis biocompatibility assay. FN-Au nanocomposites had a different surface morphology from FN, especially of FN-Au 43.5 ppm. The FN-Au 43.5 ppm showed promoted biocompatibility (i.e. cell proliferation) and reduced monocyte activation, platelet activation and oxidative stress, compared with the original FN or other FN-Au nanocomposites. Two different growth factors, i.e. vascular endothelial growth factor (VEGF) and stromal-derived factor-1 (SDF-1) were used to elucidate the respective contribution. The better cell proliferation and migration effect on the more phase-separated FN-Au 43.5 ppm than on the less phase-separated control (FN, FN-Au 17.4 and FN-Au 174 ppm) after cells were concomitantly treated with VEGF (50 ng/ml) or SDF-1 (50 ng/ml) was observed. Indeed, the enhancement in the migration event for WJCs transfected with CXCR4 siRNA was more prominent reduced for cells on FN-Au 43.5 ppm. Our findings suggested that the VEGF/CXCR4 pathway may be induced by nanophase-separated FN-Au nanocomposites in WJCs and promote their proliferation/migration effect, and that the crosstalk between PI3K/Akt/eNOS signaling pathway and MMP-9 activation may have caused a greater effect in WJCs.

Content

Introduction

1. Fibronectin

Fibronectin (FN) is a well studied glycoprotein of the extracellular matrix (ECM), and it is found in connective tissue throughout the body in humans and in blood plasma [1]. FN is also expressed as a membrane glycoprotein in some cells, and FN-like domains are found in large glycoprotein complexes in the ECM, such as tenascin. FN can be found in monomeric and dimeric forms ranging in size from 146,000 to 450,000 Da [2]. Being a major extracellular connective tissue component, fibronectin is distributed extensively on basement membranes [3]. FN exists in two main forms: 1) as an insoluble glycoprotein dimer that serves as a linker in the ECM, and; 2) as a soluble disulphide linked dimer found in the plasma [4]. The plasma form is synthesized by hepatocytes, and the ECM form is made by fibroblasts, chondrocytes, endothelial cells, macrophages, as well as certain epithelial cells [5]. FN sometimes serves as a general cell adhesion molecule by anchoring cells to collagen or proteoglycan substrates. It also can serve to organize cellular interaction with the ECM by binding to different components of the extracellular matrix and to membrane-bound FN receptors on cell surfaces [6]. The importance of FN in cell migration events during embryogenesis has been documented in several contexts, e.g.: 1) mesodermal cell migration during gastrulation can be blocked by injection of Arg-Gly-Asp (RGD) tripeptides that block cellular FN receptors (integrins) [7]; 2) injection of anti-FN antibodies into chick

embryos blocks migration of precardiac cells to the embryonic midline [8], and; 3) the patterns of FN deposition in developing vertebrate limbs determines the patterns of precartilage cell adhesion to the ECM, thereby specifying limb-specific patterns of chondrogenesis [9].

2. Nanotopographical Cues

The ECM presents an abundance of macromolecules with feature sizes at the nanometer scale. For example, fibronectin, the most abundant ECM macromolecule, exhibit dimensions among the nanoscale regime, with single fibronectin monomers approximately 25 nm in width and 5 nm in diameter [10] and self-assembled fibrillar structures extending several micrometers in length and hundreds of nanometers in diameter [11]. Cells interact with these nanometer-sized molecular structures [12-13] via contact guidance, the widely known principle that cellular behavior and function is influenced by physical topography [14]. This is thought to occur through the reorganization of membrane-bound integrins, initiating the alteration of the cytoskeleton and modulating the formation of associated focal adhesion proteins that ultimately activate specific signaling cascades, thereby inducing such cellular events as adhesion, proliferation, migration, and differentiation [15-17]. It is well known that cells receive instructive cues from their topographical environment [18]; with the progress of micro- and nanotechnology, many studies have investigated specific cellular behavior in response to engineered micro- and nanoscale substrates [19-20] and have demonstrated that topographical geometry and dimension clearly

correlate with cellular response [21]. 2D patterned cues have been fabricated in the nanoscale regime, and have demonstrated a profound effect on cellular response, including adhesion [22-23], motility [24], and stem cell function [25]. Although there have been recent advances in nanopatterning techniques and complexities, these designs have yet to be utilized to study stem cell differentiation [26]. One important factor to consider is that tissue development occurs in a transient environment with bidirectional signaling between cells and their ECM [27]. However, many of the scaffolds developed so far may not be conducive to incorporating this dynamic behavior to truly mimic the extracellular environment [28]. Cell behavior is constantly governed by instructive biochemical and biophysical cues from the ECM; likewise, cells are continuously remodeling the ECM. Furthermore, the ECM is variable across different cell types [29], and synthetic environments should be individually constructed with distinct cell lineages in mind.

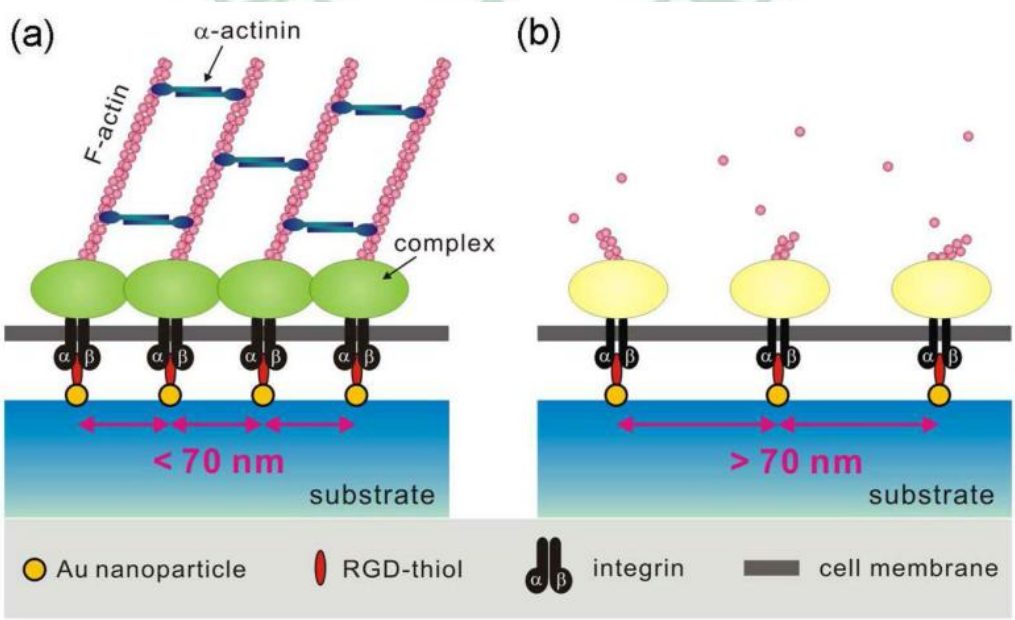

Nano Lett 2009; 9: 1111-6.

3. Roles of FN in diseases

Vascular remodeling due to hemodynamic changes or vessel injury causes changes in the architecture of blood vessels and is associated with coronary artery disease and atherosclerosis. Repair of injured cardiac tissue after a myocardial infarct is a regulated process in which plasma FN and fibrinogen play an important role in establishing the provisional matrix after the inflammatory phase [30]. In humans, administration of a naturally occurring peptide that blocks fibrin's interaction with vascular endothelial cadherin did not affect infarct size, but reduced area of necrosis as described in ref [30]. Vascular remodeling causes changes in the media/lumen ratio of vessels as well as alterations in matrix synthesis, cell proliferation, and apoptosis [31]. Periadventitial administration of functional upstream domain to mice after partial ligation of the left internal and external carotid arteries resulted in decreased measures of post-stenotic vascular remodeling including intima-media thickness and FN and collagen deposition [32]. This implicates FN in the extracellular matrix as a key pathologic process in vascular pathophysiology.

4. Cell migration

Cell migration is an extensively studied process that depends on several dynamic actin assemblies. The protrusive structures at the leading edge of a motile cell are called lamellipodia and filopodia [33]. A lamellipodium is a thin (0.1~0.2 μm) sheet-like protrusion that is filled with a branched network of actin. By contrast, filopodia are thin (0.1~0.3

μm), finger-like structures that are filled with tight parallel bundles of filamentous (F)-actin. In both cases, the fast-growing barbed ends of actin filaments are orientated towards the plasma membrane. The elongation of these filaments pushes the leading edge forward, and thus promotes cell migration or extension [34].

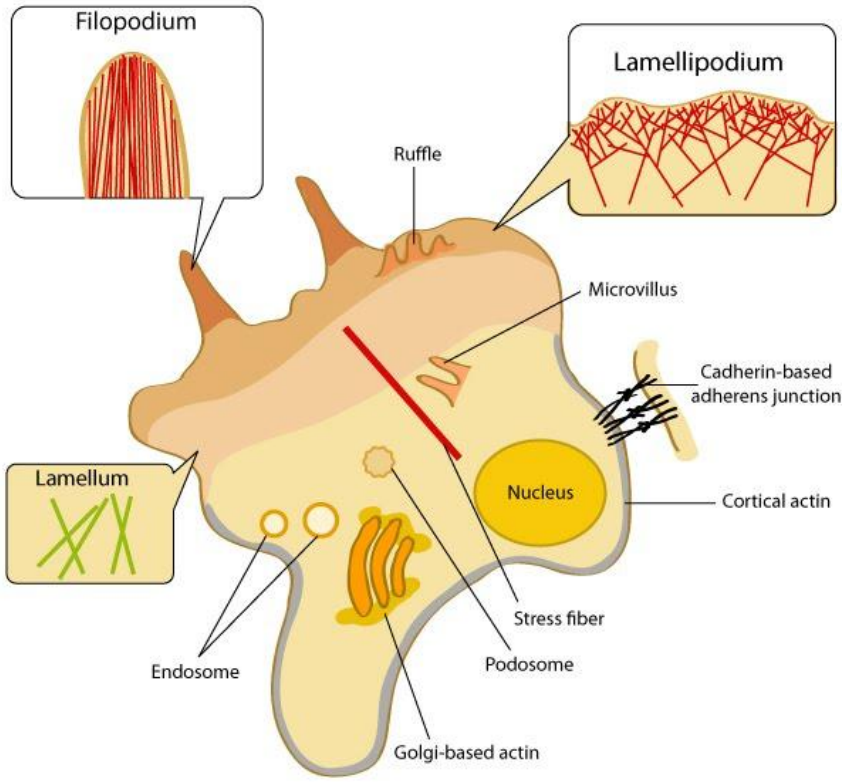

MSCs mobilization from bone marrow enables migration to peripheral blood and homing to peripheral tissues. This process is tightly controlled by specialized signals [35]. Chemoattractant cytokines, growth factors, and hormones are modulators that control the egress of HSPCs from BM [36]. Particularly, the SDF-1 (CXCL-12)/CXCR4 axis plays a pivotal role for MSCs positioning in the BM compartment [37]. Abrogation of SDF-1/CXCR4 mediated cell signaling results in rapid mobilization of MSCs from BM niches [38]. SDF-1 also mediates a variety of other cellular functions such as engraftment in peripheral

tissues.

5. Angiogenesis

Angiogenesis is a complex multi-step process that follows a characteristic sequence of events mediated and controlled by growth factors, cellular receptors and adhesion molecules [39-40]. In this process, five phases can be distinguished: (1) endothelial cell activation, (2) basement membrane degradation, (3) endothelial cell migration, (4) vessel formation, and (5) angiogenic remodeling [41]. The activation of pre-existing quiescent vessels can be triggered by hypoxia. Hypoxia induces the expression of hypoxia inducible factor (HIF), which binds to the hypoxic response element. As a result, the expression of hypoxia inducible genes, such as vascular endothelial growth factor (VEGF), platelet derived growth factor (PDGF), transforming growth factor (TGF) is induced [41]. Activated endothelial cells express the dimeric transmembrane integrin $\alpha 5\beta 3$, which interacts with extracellular matrix proteins (vitronectin, tenascin, fibronectin) and regulates migration of the endothelial cell through the extracellular matrix during vessel formation [42-43]. The activated endothelial cells synthesize proteolytic enzymes, such as matrix metalloproteinases (MMPs), used to degrade the basement membrane and the extracellular matrix [44]. Initially, endothelial cells assemble as solid cords. Subsequently, the inner layer of endothelial cells undergoes apoptosis leading to the formation of the vessel lumen. Finally this primary, immature vasculature undergoes extensive remodeling during which the vessels are stabilized by pericytes and smooth muscle

cells [44].

6. Chemokines

Chemokines are small (8-10 kDa) proteins able to chemically attract lymphocytes, neutrophils and other immune cell types to the sites of inflammation. Several families of chemokines and their receptors exist, each with different characteristics and abilities. Activation by chemokines is an important step during recruitment of a reasonable number of stem cells or progenitor cells to the ischemic tissue. The chemokine SDF-1 is expressed on osteoblasts and endothelial cells and the interaction with CXCR4 is thought to regulate trafficking of hematopoietic stem cell (HSCs) in the bone marrow [45]. In the perivascular niche, sinusoidal reticular cells express high levels of SDF-1 and were found to be in close contact with HSCs [46]. Interestingly, these SDF-1 expressing reticular cells were also located at the endosteal niche. The fact that HSCs express the receptor CXCR4 [47] suggests that the SDF-1/CXCR4 system would be crucial for the modulation of activation or quiescence of the HSC niche in bone marrow. Furthermore, ischemia-induced VEGF acts as a chemoattractant to endothelial progenitor cells (EPCs) [48]. Interestingly, VEGF is sufficient to induce the organ recruitment of bone marrow derived circulating myeloid cells and their perivascular localization via induction of SDF-1 expression by perivascular myofibroblasts, suggesting that different cytokines may cooperate during homing of bone marrow cells [49]. Proteases are well established to be involved in angiogenesis, in particular in migration of endothelial cells. Meanwhile

growing evidence suggests that pericellular proteases play also an important role in vasculogenesis. Extracellular proteases, such as MMPs may affect neovascularization by degradation of the extracellular matrix and cell surface receptors and activation, liberation and modification of angiogenic growth factors [50]. Thus, the mobilization, recruitment and invasion of stem and progenitor cells during vasculogenesis involve proteolytic activity [51]. On the other hand, nitric oxide (NO) plays a crucial role in progenitor cell function and the expression of endothelial nitric oxide synthase (eNOS) is required for bone marrow-derived mobilization of EPCs and $eNOS^{-/-}$ progenitor cells showed a reduced homing capacity in ischemia models [51]. Thus, MMP and eNOS are required for the basal, VEGF, and SDF-1 induced migration of EPCs or bone marrow-derived progenitor cells in vitro and in vivo.

Materials and Methods

1. Preparation of fibronectin-gold (FN-Au) nanocomposite films

FN-Au solutions were prepared by mixing fibronectin solution (1 mg/ml) with a certain amount of Au nanoparticles (containing 17.4 to 174 ppm of Au in the final weight). The mixture was stirred and covered on the culture dish or 15 mm round glass coverslips to obtain the films of fibronectin (denoted "FN") or fibronectin-gold (denoted "FN-Au") nanocomposites. The thicker films surface morphology and microphase separation were confirmed by atomic force microscopy and used in the monocyte activation, oxidative stress, cell proliferation and cell morphological experiments by biocompatibility test [52].

2. Surface characterization of FN and the FN-Au nanocomposites

The surface morphology was examined by the atomic force microscope (AFM) equipped with a 100-mm piezoelectric scanner. The images were obtained in the tapping mode in air with a triangular cantilever (force constant of 21–78 N/m) supporting anintegrated pyramidal tip of Si_3N_4. Topography and phase images were recorded simultaneously. Phase images provide a sharp contrast of fine structural features and emphasize differences in mechanical properties of different sample components. Tapping mode AFM generates phase images with dark features corresponding to regions of lower modulus (soft domains) and bright features corresponding to regions of high modulus (hard

domains). The size (average diameter) of hard domains from phase images was obtained by image analysis using Image Pro Plus 4.5 software. The average diameter was calculated based on the average length of diameters passing through the centroid of each hard domain. The desorbed wavelength of FN and FN-Au solutions were measured by a UV/IVS spectrophotometer. FN and FN-Au nanocomposites were also chemically analyzed using a FTIR (fourier transform infrared spectrometer). Each sample was scanned eight times in the spectral region of 400–4000 cm^{-1} with a resolution setting of 2 cm^{-1} and averaged to produce each spectrum. [54]

3. Monocyte activation test

Human blood monocytes were isolated from the venous blood of unmediated donors. Monocytes were isolated by density gradient centrifugation using Percoll. Cell viability was determined by trypan blue staining. Monocytes were suspended in a medium of DMEM containing 10% FBS and 1% (v/v) antibiotic (10,000 U/ml penicillin G and 10 mg/ml streptomycin) and the cell concentration was adjusted to 1×10^5 cells/ml. The samples were sterilized by 70% ethanol for 30 min and placed into the bottom of 24-well tissue culture plates. One milliliter of the cell suspension was added to each well and allowed to adhere for 96 hrs at 37℃ in 5% CO_2. After incubation, the adherent cells were trypsinized, centrifuged, and resuspended for cell counting by using a hemocytometer combined with the inverted phase contrast microscope.

The number of monocytes and macrophages were determined respectively by their morphology. The percent conversion of monocytes was defined by dividing the number of adherent macrophages by the sum of attached monocytes and macrophages.

4. Cell proliferation test

Human Wharton's jelly stem cells (WJCs) were cultured in high-glucose Dulbecco's modified Eagle's medium (DMEM) supplemented with 10% FBS, 2 mM glutamine and 1% (v/v) antibiotics (10,000 U/ml penicillin G, 10 mg/ml streptomycin, and 0.025 mg/ml amphotericin B). Cells of passages 8~20 were used. The FN and FN-Au were coated into the bottom of 96-well tissue culture plates. Two hundred μl of cell suspension with a density of 6×10^3 cells/mL was injected into each well of the culture plates. After 24, 48 and 72 hrs of incubation, add 500 μl of MTT [3-(4, 5-cimethylthiazol-2-yl)-2, 5-diphenyl tetrazolium bromide] solution from step one to each well containing cells. Incubate the plate in a CO_2 incubator at 37 ℃ for 3 hrs. Remove media with pipette and add 500 μl DMSO to each well and pipette up and down to dissolve crystals. Transfer to plate reader and measure absorbance at 570 nm.

5. Platelet activation test

For platelet adhesion and activation, substrates were placed in a

24-well culture plate, and 0.5 ml of platelet-rich plasma (～2×10^6 platelets/ml, obtained from the Chinese Blood Foundation, Taiwan) was added to each well. After incubation for 1 hr, samples were taken out and gently rinsed with the buffered saline. In one duplicate, the adherent platelets were detached by trypsin, and counted by cell counter. In another duplicate, samples were fixed by HEPES-buffered glutaraldehyde, dehydrated in increasing ethanol solutions, critical point-dried, sputter-coated with gold, and examined by SEM [51]. The common morphological change (including five stages) during platelet activation was used as a tool routinely [65] to define the degree of activation of a platelet quantitatively in this study: 0 = round (unactivated), 1/4 = dendritic (pseudopodial but no flattening), 1/2 = spread-dendritic (flattened pseudopodia), 3/4 = spreading (late pseudopodial with hyaloplasm spreading), and 1 = fully spread (totally activated). The average degree of platelet activation (0.0-1.0) was calculated based on～50 adherent platelets observed under SEM.

6. Cell morphology

The FN and FN-Au were coated into the bottom of 24-well tissue culture plates. WJCs were seeded in 24-well plates with coverslips at a density of 0.5×10^4 cells per well and incubated under standard conditions for 8 hrs and 48 hrs. After incubation, samples were taken out and gently rinsed with the buffered saline. In one duplicate, samples were fixed by HEPES-buffered glutaraldehyde, dehydrated in increasing ethanol

solutions, critical point-dried, sputter-coated with gold, and examined by SEM. In another duplicate, the cells were washed with PBS buffer, fixed with 4% paraformaldehyde for 15 min, and permeabilized with 0.5% (v/v) Triton X-100 in PBS for 10 min prior to staining. Following fixation and permeabilization, non-specific binding was blocked by adding 5% (w/v) FBS for 30 min at room temperature. Following further extensive washing, the cells were stained with rhodamine phalloidin (1:1000) for 30 min. After three additional washes, the coverslips were mounted on microscope slides and sealed with a synthetic mount. Images were collected on the fluorescence microscope.

7. Western blotting

WJCs (2×10^5 cells) were seeded into each well of a 6-well tissue culture plate containing 32-mm material-coated coverslips cultured with 50 ng/ml VEGF and 50 ng/ml SDF-1 treatment. After 48 hrs of incubation, cells were washed three times with the ice-cold PBS, lysed in the RIPA lysis buffer [50 mM Tris, pH 7.4, 1 mM EDTA, 1 mM phenylmethyl sulfonyl fluoride (PMSF), 25 mg/ml leupeptin, 0.1 mg/ml aprotinin, 1 mM dithiothreitol, 1 mM NaF, and 1% NP-40]; scraped from the dish, rotated for 1 hr at 4 ^{o}C, and centrifuged for 15 min at 14,000×g. The protein concentration in the supernatant was quantified by using a protein assay kit, and 30 μg proteins of each sample were subjected to SDS-PAGE. For immunoblotting, separated proteins were transferred onto a nitrocellulose membrane by a semi-dry blotting technique. The membrane was blocked with 5% non-fat dry milk in PBS for 1 hr at room temperature before overnight incubation at 4℃ with the primary

antibodies [anti-phospho-eNOS antibody (1:500 dilution), anti-phospho-Akt antibody (1:500 dilution), anti-phospho-ERK antibody (1:500 dilution), anti-phospho-p38 MAPK antibody (1:500 dilution), anti-phospho-STAT-3 antibody (1:500 dilution), anti-Bax antibody (1:500 dilution), anti-caspase-3 antibody (1:500 dilution), anti-Bcl-2 antibody (1:500 dilution), anti-CXCR4 antibody (1:500 dilution)] and controls [anti-actin antibody (1:5000 dilution)] to ensure uniformity of loading. After incubation with the primary antibodies, the membrane was washed, incubated for 1 hr with peroxidase-conjugated secondary antibodies, and then treated with the ECL Western blotting detection system, according to the manufacturer's instructions. Quantification was performed by densitiometric analysis with the LabWork Image Acquisition and Analysis software. The tests were performed three times and the representative data are shown.

8. CXCR4 transient transfection

For transient expression experiments of CXCR4 in WJCs, 50–70% confluent cells were transfected for 12~16 hrs with 2 μl of CXCR4 siRNA by using 3 μl of Lipofectamine and 1 ml of medium without serum. One day later, The transfection of siRNA into WJCs were harvested in lysis buffer and analyzed by Western Blotting.

9. Migration assay

WJCs were seeded onto each well of an Oris$^{(TM)}$ Cell Migration Assay Tri-Coated plate with a Cell Seeding Stopper at 8000 cells/well

containing materials-coated. The plate was then incubated overnight at 37 ℃, and transfected with CXCR4 siRNA in WJCs. The following day the Cell Seeding Stoppers were removed from the plate. Subsequently, 200 µl Calcein AM-free medium was added to each wells and treated with VEGF (50 ng/ml) at 12, 24, 36 and 48 hrs. Images were collected on the fluorescence microscope.

10. Gelatin zymography

WJCs (5×10^5 cells) were seeded in 10 cm culture dish with material-coated and transfected CXCR4 siRNA into cells overnight. Subsequently, added VEGF (50 ng/ml) for 48 hrs. After 48 hrs the conditioned medium was collected, centrifuged and assayed for gelatin zymography as previously described. The gels were stained with 0.5% Coomassie brilliant blue R-250 in 10% acetic acid and 45% methanol and destained with 10% acetic acid and 45% methanol. Bands of gelatinase activity appeared as transparent areas against a blue background. MMP-2 and MMP-9 gelatinase activity was then evaluated by quantitative densitometry. Data were normalized on the protein amount measured in cell supernatant.

11. Immunofluorescence analysis of eNOS expression

WJCs (2×10^4 cells on each 15-mm material-coated coverslips placed in the 24-well plate) were incubated in the complete medium. After transfected CXCR4 siRNA into cells overnight and subsequently added

VEGF (50 ng/ml) for 48 hrs, they were fixed with 4% paraformaldehyde and permeabilized with 0.5% (v/v) Triton X-100 in phosphate buffered saline (PBS) for 10 min prior to staining. Following fixation and permeabilization, non-specific binding was blocked by adding 5% (w/v) FBS for 30 min at room temperature. Cells were incubated in the primary anti-eNOS antibody solution for 60 min, washed extensively and then incubated with the appropriate secondary FITC-conjugated immunoglobulin (green color fluorescence) (1:150 dilution) for 60 min. Following further extensive washing, the nuclei were stained with DAPI (1:500 dilution) for 20 min. After two further washes, coverslips were mounted on microscope slides with the storage solution (glycerol/PBS) and sealed with a synthetic mount. In each case a primary antibody free control was produced. Images were collected on a fluorescence microscope.

Results

1. Characterization of FN and FN-Au nanocomposites

The surface morphology of FN and FN-Au nanocomposites are shown in Figure 1. The rms roughness of FN and FN-Au obtained from the AFM topography was in a narrow range of 1.95–3.12 nm, indicating that the surface was similarly flat for all nanocomposites. The topography diagrams indicated about the surface morphology of materials, while the phase diagrams revealed more details information. By comparing the topography with phase diagrams, the darker area in topography corresponded to the brighter area in phase. The size domain of the original FN surface was dominated by hard segment lamellae (26.31 nm). FN-Au 17.4 ppm demonstrated fewer hard segment lamellae (32.447 nm). On the surface of FN-Au 43.5 ppm, the lamellae were completely absent and replaced with plenty of soft segment micelles (20.04 nm). When Au concentration was further increased (as in FN-Au 174 ppm), hard domains expanded in size with areas of aggregation and the size domain of the lamellae became thicker (43.0 nm). The changes of nanometric surface morphology in FN upon addition of Au nanoparticle are depicted in Fig 1. Fig 2 showed that the FN (at 290 nm) intermediate with pure Au nanoparticle (at 525 nm) by UV/VIS spectrophotometer analysis. Interestingly, the peak (525 nm) was more obvious when added different concentrations of Au nanoparticle. Indeed, the conformation of FN and FN-Au nanocomposites by FTIR were examined in Fig 3. It was showed that the addition of Au with different concentration did not cause a remarkable change in FN. Furthermore, a high resolution scan of the Amide I and Amide II (C-N) region revealed that there also did not

significantly change [55]. These results indicated that the physical property of FN was changed by Au nanoparticles rather than in chemical property.

2. Monocyte activation test

As in the normal progression of adherent monocytes, the cell morphology progressed from the expected round monocyte morphology into the spread cytoplasm morphology of macrophages. The chances for human monocytes to become the activated macrophages on the materials after 96 hrs culture are shown in Fig 4. FN-Au 43.5 ppm had the lowest percent conversion, indicating the least monocyte activation. FN-Au 17.4 ppm and FN-Au 174 ppm were comparable in provoking the activation of monocytes. FN-Au 174 ppm had the most monocyte activation among all nanocomposites. Nevertheless, on all FN-Au nanocomposites, the chances for monocytes to become activated macrophages were still lower than that on the original TCPS.

3. Cell proliferation test

The numbers of cells that attached and proliferated on the TCPS, FN and FN-Au nanocomposite were showed in Fig 5. The proliferation and adhesion ability of WJCs on all nanocomposites were greater than on TCPS at 24, 48 and 72 hrs. FN-Au 43.5 ppm was promoted highest proliferation ability compared to FN-Au 17.4 ppm and FN-Au 174 ppm.

4. Cellular oxidative stress

The oxidative stress of WJCs on the nanocomposites were used DCF-DA to measure intracellular reactive oxygen species (ROS) by flow cytometry. DCF-DA has been used as a detector of ROS for a number of years in many applications such as fluorescence microscopy and flow cytometry [56]. The Fig 6 showed that the presence of Au nanoparticles at all contents (17.4~174 ppm) in FN-Au nanocomposites suppressed the oxidative stress of WJCs compared to original FN. Especially, the oxidative stress of WJCs on FN-Au 43.5 ppm was the lowest among all nanocomposites.

5. Platelet activation test

In the platelet activation test, however, platelets were less activated on all FN-Au nanocomposites, as shown by the scanning electron microscopy (SEM) of platelets in Fig 7. Some of the platelets on the original FN were already spread. In contrast, most platelets on FN-Au 17.4 ppm and FN-Au 43.5 ppm were either round or pseudopodial but not flattened.

6. The morphology of wharton's jelly stem cells on nanocomposites

The morphology of Wharton's jelly stem cells on nanocomposites were determined by SEM. When cell adhesion or migration, they were initiated by the protrusion of lamellipodia and filopodia, leading to direct

cell movement [33]. In the Fig 8 showed that WJCs were not protrusion formation on TCPS. However, cells were more protrusion formation, like lamellipodia or filopodia on the FN-Au (43.5 ppm) at 48 hrs compared with other groups. Taken together, FN-Au 43.5 ppm exhibited better biocompatibility compared than other groups. Next, FN-Au 43.5 ppm (denote the FN-Au) was used in this study.

7. VEGF and SDF-1 enhanced the survival capability of WJCs on FN-Au

VEGF and SDF-1 have been identified as a key component in the development and maturation of blood vessels [35, 37]. The molecular between VEGF and SDF-1 enhanced the WJCs survival capability on FN-Au nanocomposites have less studied. In the Fig 9 showed that the caspase-3 and Bax protein expression level of WJCs were significantly decreased on FN-Au when treated with VEGF (50 ng/ml) or SDF-1 (50 ng/ml). Indeed, Bcl-2 protein level was significantly enhanced on FN-Au when treated with VEGF or SDF-1, respectively (Fig 9). Taken together, VEGF or SDF-1 were enhanced the WJCs survival capability and suppressed apoptosis on FN-Au.

8. VEGF stimulated migration of WJCs on FN-Au through CXCR4

The involvement of CXCR4 in VEGF induced WJCs migration was confirmed by CXCR4 siRNA treatment. Fig 10A showed that CXCR4 expression level was significantly suppressed by CXCR4 siRNA

treatment. As show in Fig 10B, transfected with CXCR4 siRNA into the WJCs were labeled Calcein-AM (green) after treated with VEGF (50 ng/ml) for 0, 12, 24, 36 and 48hrs. This result showed that VEGF enhanced WJCs migration were significant in a time dependent manner on FN-Au compared to TCPS or FN groups. The migration of WJCs was most significantly reduced after the treatment of CXCR4 siRNA, but was slightly promoted after co-treatment with VEGF. Meanwhile, the migration ability of WJCs on FN or FN-Au quantified as the fluorescence intensity by labeled with Calcein-AM staining.

9. VEGF activated MMP-9 activity of WJCs on FN-Au through CXCR4

To explore the mechanisms by which MMP protein activity was induced for WJCs on FN-Au, the expression of MMP-2 and MMP-9 were evaluated after co-treatment of VEGF with CXCR4 siRNA, respectively. Fig 11 shows a representative MMPs expression of WJCs upon transfection with CXCR4 siRNA by using Gelatin zymography. The adhered WJCs expressed more readily detectable MMP-9 after VEGF stimulation than other control groups on FN-Au. Besides, MMP-9 expression level at 48 hrs was significantly reduced in WJCs transfected with CXCR4 siRNA, especially for those on FN-Au.

10. VEGF promoted eNOS expression of WJCs on FN-Au through CXCR4

The expression and cellular localization of eNOS at 48 hrs observed by the immunofluorescence image analysis shown in Fig 12. A higher fluorescence intensity in the cytoplasm distribution of eNOS protein labeling was found on FN-Au compared to TCPS and FN groups (Fig 12). Indeed, the eNOS induction by FN-Au on WJCs was obvious reduced by the addition of CXCR4 siRNA. This result indicated VEGF/CXCR4 signaling was involved in eNOS induction on FN-Au (Fig 12). It was also confirmed by Western Blot (Fig 13).

11. VEGF modulated CXCR4 downstream signaling pathway on FN-Au

Previous reports indicated that cell migration ability was promoted by the CXCR4 signaling and via the downstream protein such as PI3K-Akt-eNOS, MAPK family and JAk2/STAT3 [41-42]. So far, the investigated the roles of angiogenic factor in WJCs on FN-Au has less studied. Next, we further explored the molecular mechanism of WJCs on FN-Au. When cultured WJCs on materials after VEGF stimulation, the increased in p-Akt/eNOS protein on FN-Au was significantly higher than on TCPS or FN (Fig 13). The mechanism on p38 MAPK, ERK and STAT-3, however, was not remarkable (Fig 13). Besides, it was further noticed that the p-Akt/eNOS expression level was blocked by CXCR4 siRNA. Together these results in Fig 13, it was suggested that CXCR4 may play as a upstream crucial role as in roles p-Akt/eNOS signaling in promoting WJCs migration on FN-Au.

Discussion

In this current study, all the FN nanocomposites at 17.4-174 ppm of Au nanoparticle showed increased cell proliferation, reduced monocyte activation, and greater free radical scavenging ability, than the original FN. FN-Au 43.5 ppm had the best performance among the nanocomposites, followed by FN-Au 17.4 ppm. Previously it has been demonstrated that the presence of Au nanoparticles at 43.5 ppm significantly improved the thermal and mechanical properties, as well as the biostability of other PU model system [51]. These effects were similar to those in the presence of an appropriate amount (43.5 ppm) of Au nanoparticles.

The surface morphology of the FN was significantly modified by the existence of a small amount of gold nanoparticles has been observed in this study. The change in nanometric surface morphology was reported in our published work, where the hard segment micelles changed their size upon addition of Au nanoparticles [53]. In this model system, the surface of the original FN showed hard segment lamellae (≈26.31 nm), which was the common surface morphology of FN when the hard segment content was relatively higher (≈3.123 nm). Also, it seemed that the added of Au nanoparticles on the surface processed micelle formation and interfered with the ability of the hard segments to form lamellae of PU-Au 17.4 ppm. The soft segments formed isolated micelles, and the extent of phase separation was greatest was occurred on PU-Au 43.4 ppm. It was agreed and compared to our previously report that phase separation was probably stabilized by hydrogen bonds brought about by the Au nanoparticles [51]. The above observations demonstrated that nanoparticles had the ability to induce significant morphological transformation in FN-Au nanocomposites. From the present report and

the previous other PU system, Au nanoparticles with a size of 5 nm with hard segment, it seemed could participate in the phase separation process of FN, leading to nanometric surface morphological changes. It is thus readily to fabricate the material properties of original FN material surface by applying small amount of Au nanoparticle of the optimal size domain and concentrations. So far, many literatures have reported the influence of the height of nanometric features on the cellular response could change the cellular behavior. For example, surface nanoislands (13-27 nm) were indicated to promote the response of fibroblasts [54]. Also, the other model system of poly(ε-caprolactone)/poly(ethylene glycol) diblock copolymer with 27 nm high islands obtained by phase separation was shown to have better biocompatibility [45]. Compared to our previous work with PU-Au nanocomposites, the characteristic size in the lateral dimension had a similar tendency of change as in the present study, and FN-Au 43.5 ppm with the smallest hard domain size (≈20.04 nm) exhibited the best cell biocompatibility effect.

It is worth to notice the effect regarding how the appearance of thing of FN-Au nanocomposites was related to the biological response. Monocyte-derived macrophages are key regulators of the host response to biomaterial implants [51]. In the current report, the monocyte activation was attenuated by FN-Au nanocomposites (Fig 4). We suggested that macrophages, by morality of their ability to adhere and spread on FN surfaces, may be associated with the in vivo biostability capacity. Au nanoparticles in FN were found to reduce the adherence of monocytes as well, especially at 43.5 ppm of FN-Au. Therefore, Au nanoparticles appeared to provide a reasonable means to attenuate the inflammatory response to biomaterials.

The scavenging ability of ROS appeared to exert a crucial effect on the implantation of biomaterials into in host body. Previously, we have

showed that free radicals may be derived from the surface of Au nanoparticles and may be responsible for the against ROS generation activity of the Au nanoparticles [51]. In the current study, Au nanoparticles at 43.5 ppm in water exhibited some free radical scavenging ability (Fig 6). Therefore, the previous hypothesis regarding the mechanism of the inhibitory effects of Au nanoparticles on ROS scavenging appeared undiscovered. Interestingly, the pure Au nanoparticles (50 ppm in solution) exhibited excellent free radical scavenging ability has also been found in our recently published work [54]. It was possible that the Au could function to modulate the cellular response, especially the biocompatibility of the other PU-Au system. Antioxidation was associated with reduced host inflammation after implantation of biomaterials [57]. A report indicated that after the implantation of superoxide dismutase-modified PU into rats, PMN-rich acute inflammatory infiltrates were reduced [58]. Thus, it is possible that FN containing Au could reduce the amount of free radicals and the inflammatory response as well. However, the elimination of free radicals generation effect by Au nanoparticles on FN could not be completely ruled out in the current work and required further exploration.

It is logical to suppose two molecular mechanisms related to enhanced ECs migration, that is, the NO-dependent (such as PI3K/Akt pathway) and NO independent (such as the mentioned Rho GTPase pathways) [52]. eNOS is known to be activated by ECs migration effect [50]. The greater migration rate of ECs on the other model system PU-Au was association with the PI3K/Akt signaling to eNOS molecular mechanism on PU-Au has been well studied in our previous work [52]. It was found that ECs tended to elongate and form lamellipodia on PU-Au. Lamellipodia formation may be a result of activation of small Rho GTPase (ex: Rac) and induced edge ruffling and stress fiber formation in

cultured ECs, it can induce cell motility. Indeed, when signaling was abolished by Y-27632 (specific inhibitor of Rho-GTPase), actin fiber extension was significantly reduced. Many recent reports have mentioned the Rho family of small GTPases as the key regulator of the cytoskeletal reorganization [59]. In spite of the association with PI3K/Akt signaling pathway, FN-Au 43.5ppm, which exerted a stronger Akt/eNOS activation effect than other materials (Fig 13). The present study also has shown that the migration of WJCs on FN-Au was significantly enhanced over the original FN (Fig 10). Based on this finding, it was to say that upregulation of eNOS and p-Akt proteins, which was simultaneously associated NO-independent pathway (FAK/Rho-GTPase/MMP-9) signaling pathway to promote cell migration by FN-Au.

Abundant evidence suggests that EPCs contribute to vascular repair, remodeling, and lesion formation under physiological and pathological conditions. Systemic administration of EPCs also improves functions of ischemic tissues after stroke [39] or myocardial infarction [19]. However, administration of for EPCs or bone marrow-derived cell populations enriched for EPCs into subjects with cardiovascular disease has had limited lower proliferative efficacy, with regard to new vessel formation. Although less studied, we have aimed to as WJCs [24], from human umbilical cord in order to seek for other substitution source of vascular stem cells. MSCs secrete numerous cytokines including VEGF, SDF-1, bFGF, IGF-1, and HGF [23]. These paracrine factors, especially VEGF, are important for maintaining or improving vascular function in MSCs-mediated vascular repair [37]. The functions of MSCs are not only due to its potential to differentiate into endothelial cells [36], but also depend on the paracrine effects, including enhanced repairing capacity of implanted MSCs mobilization and migration [35]. Previous studies indicated that overexpression of SDF-1 provides a cue for stem cells to

mobilize and home into the damaged vascular sites [32]. Consequently, interactions between SDF-1 and CXCR4 contribute to tissue repair [33]. Because vascular damage appears to be an important signaling cue in the migratory responses of MSCs, we next investigated in MSCs the expression of CXCR4, which are the receptors for SDF-1 and VEGF. The VEGF siRNA significantly inhibited migration capacity of MSCs toward SDF-1 stimulation (Appexdix 1), further confirming that the SDF-1/CXCR4 mechanism regulates the migratory responses of MSCs on FN-Au. The present studies provide a further support for the paracrine function of MSCs in response to FN-Au nanometric surface.

Although BM has been the main source of MSCs for both experimental and clinical studies, recent work has shown that MSCs could also be isolated from umbilical cord vein [23] and cord blood [60]. In our studies, we were able to establish MSCs cultures from Wharton jelly in human umbilical cord *(*WJCs*)*-derived stem cells which survived past the 20th passage. One difference between BM- and CB-derived MSCs that we observed was expression of VEGFR-2, which we found in MSCs from CB but not from BM [60]. Recently, MSCs derived from umbilical cord vein were shown to express endothelial markers [24]. VEGF overexpressed from MSCs first activates SDF-1α/CXCR4 pathway. Activated SDF-1 then induces mobilization and migration of MSCs into damaged areas [32]. Accordingly, we observed that MSCs from WJCs proliferated better than on FN-Au, and our results also are consistent with the notion that confluences MSCs results in the induced of VEGF expression level (Appexdix 1). VEGF siRNA reduces SDF-1 promoted CXCR4 expression level on FN-Au (Appexdix 1) has been found. By the stimulation of VEGF and SDF-1, MSCs became more readily differentiates to endothelial-like cells, leading to the enhanced eNOS protein (Fig 12). Meanwhile, the eNOS protein expression level

was more completely abolished after CXCR4 siRNA treatment (Fig 12). Based on this finding, it was suggested that VEGF may has as a upstream regulator of SDF-1/CXCR4/eNOS by FN-Au induction.

The expression of MMPs by MSCs is important, as it has recently been shown to be upregulated under hypoxic conditions and to promote the migration and capillary-tube formation by MSCs [41]. This is suppose that secreted proteinases such as MMP-2 and MMP-9 are contributing to promote cell migration also through its ability to process and activate cell surface molecules such as integrin α5β3 [61]. In our study, migration ability by FN-Au on MSCs toward VEGF/SDF-1 cross interaction (Fig 10) and was significantly reduced by CXCR4 siRNA treatment (Fig 10), further underlining the role of MMP in MSCs migration via the involvement of MMPs on FN-Au, especially MMP-9. SDF-1 stimulation also promoted the expression of cell surface marker (ex: α5β3 integrin) involved in stem cells homing to the damaged vascular site and the secretion of MMPs, which are involved in enhancing cell migration and vascular remodeling [49]. Our data are in agreement with the role of SDF-1 in the regulation of MMP-9 expression level (Fig. 11) with respectively MMP-9 involved in stem cells adhesion on FN-Au nanometric surface. Also, activation of integrin CXCR4 or α5β3 integrin are thus crucial for regulating of VEGF-stimulated MSCs to FN-Au, which has a positive effect on these events in response to nanometric surface.

The binding of SDF-1 to CXCR4 was reported to cause activation of multiple signal transduction pathways, including PI3K, MAP kinases and ERK signaling pathway [41-42]. Both PI3K/Akt and MAPK/ERK signal transduction pathways have been shown to mediate the cell migration induced by chemokines or cytokines in different cell types [41]. Akt signaling appears to be critical for VEGF-induced angiogenesis [62].

Recently, studies in MSCs have demonstrated that VEGF could improve migration, proliferation, in which the activation of the PI3K/Akt signal transduction pathway may play an important role [41]. Wang *et al.* have reported that PI3K/Akt, but not MAPK/ERK, is required for SDF-1–mediated migration of hematopoietic progenitor cells [63]. Moreover, some studies have showed that both PI3K/Akt and MAPK/ERK signal transduction pathways are involved in the regulation of SDF-1α–mediated migration [64]. To investigate the functional roles of PI3K/Akt and MAPK/ERK signaling cascades in VEGF/SDF-1–induced cell migration of MSCs by FN-Au, CXCR4 siRNA nearly totally blocked VEGF induced Akt protein expression on WJCs with FN-Au (Fig 13). In contrast, had no significant effect on VEGF-induced p38MAPK, ERK and STAT-3 signaling activation (Fig 13). Thus, it may suggest that PI3K/Akt activation is required for VEGF/SDF-1-induced WJCs migration on MSCs with FN-Au.

VEGF and SDF-1 have been shown to regulate cell proliferation, migration, and angiogenesis, including the activation of eNOS activity, via the PI3K/Akt signaling pathway [62]. Activation of Akt has been shown to stimulate phosphorylation of eNOS and then increases endothelial NO production, which leads to subsequent cells growth and migration [50]. Our data also demonstrated that eNOS activation was required for VEGF mediated MSCs migration on Fn-Au (Fig 13), the induction of eNOS by FN-Au was significantly reduced by a co-treatment with CXCR4 siRNA and VEGF on MSCs (Fig 13). These finding suggested that VEGF may act as upstream regulator leading to PI3K/Akt/eNOS expression in response to FN-Au nanometric surface.

Conclusion

It is necessary to be able to offer the endothelial cell proliferation, migration and function of ECs for successful implantation of biomaterials into cardiovascular. This study suggested that WJCs could react to nanometric surface in a FN by changing morphology, relating to NO-dependent and NO-dependent pathway and increasing motility event. Cytoskeletal reorganization and VEGF/SDF-1 regulation played key roles in this process. Our data are the first to report a molecular mechanism of WJCs in response to surfaces featured with nanometric domains. Practically, such defining clearly could help to fabricate the more effective biomaterials for vascular tissue engineering application.

References

1. Ross R. Atherosclerosis — an inflammatory disease. N Engl J Med 1999; 340: 115-26.
2. Libby P. Inflammation in atherosclerosis. Nature 2002; 420:868-74.
3. Hansson GK. Inflammation, atherosclerosis, and coronary artery disease. N Engl J Med 2005; 352: 1685-95.
4. Levi M, Ten Cate H. Disseminated intravascular coagulation. N Engl J Med1999; 341: 586-92.
5. Levi M, van der Poll T, Buller HR. Bidirectional relation between inflammation and coagulation. Circulation 2004; 109: 2698-704.
6. Esmon CT. The interactions between inflammation and coagulation. Br J Haematol 2005; 131: 417-30.
7. Klassman L. Therapeutic hypothermia in acute stroke. J Neurosci Nurs. 2011; 43: 94-103.
8. He, W.; Yong, T.; Teo, W. E.; Ma, Z.; Ramakrishna, S. Fabrication and endothelialization of collagen-blended biodegradable polymer nanofibers: potential vascular graft for blood vessel tissue engineering. Tissue Eng 2005; 11: 1574-1588.
9. Nair, L. S.; Bhattacharyya, S.; Bender, J. D.; Greish, Y. E.; Brown, P. W.; Allcock, H. R.; Laurencin, C. T. Fabrication and optimization of methylphenoxy substituted polyphosphazene nanofibers for biomedical applications. Biomacromolecules 2004; 5: 2212-2220.
10. Tsuda, Y.; Shimizu, T.; Yamato, M.; Kikuchi, A.; Sasagawa, T.; Sekiya, S.; Kobayashi, J.; Chen, G.; Okano, T. Cellular control of tissue architectures using a three-dimensional tissue fabrication

technique. Biomaterials 2007; 28: 4939-4946.

11. Alobaid, N.; Salacinski, H. J.; Sales, K. M.; Ramesh, B.; Kannan, R. Y.; Hamilton, G.; Seifalian, A. M. Nanocomposite containing bioactive peptides promote endothelialisation by circulating progenitor cells: an in vitro evaluation. Eur. J. Vasc. Endovasc. Surg 2006; 32: 76-83.
12. Kofidis, T.; Muller-Stahl, K.; Haverich, A. Myocardial restoration and tissue engineering of heart structures. Methods Mol. Med 2007; 140: 273-290.
13. Chai, C.; Leong, K. W. Biomaterials approach to expand and direct differentiation of stem cells. Mol. Ther 2007; 15: 467-480.
14. Nair, L. S.; Bhattacharyya, S.; Bender, J. D.; Greish, Y. E.; Brown, P. W.; Allcock, H. R.; Laurencin, C. T. Fabrication and optimization of methylphenoxy substituted polyphosphazene nanofibers for biomedical applications. Biomacromolecules 2004; 5: 2212-2220.
15. Gafni, Y.; Zilberman, Y.; Ophir, Z.; Abramovitch, R.; Jaffe, M.; Gazit, Z.; Domb, A.; Gazit, D. Design of a filamentous polymeric scaffold for in vivo guided angiogenesis. Tissue Eng 2006; 12: 3021-3034.
16. Li, J.; Ding, M.; Fu, Q.; Tan, H.; Xie, X.; Zhong, Y. A novel strategy to graft RGD peptide on biomaterials surfaces for endothelization of small-diamater vascular grafts and tissue engineering blood vessel. J. Mater. Sci. Mater. Med 2008; 19: 2595-2603.
17. Yim, E. K.; Reano, R. M.; Pang, S. W.; Yee, A. F.; Chen, C. S.; Leong, K. W. Nanopattern-induced changes in morphology and motility of smooth muscle cells. Biomaterials 2005; 26: 5405-5413.
18. Franz WM, Zaruba M, Theiss H, David R. Stem-cell homing and

tissue regeneration in ischaemic cardiomyopathy. Lancet 2003; 362: 675-676.

19. Kocher AA, Schuster MD, Szabolcs MJ, Takuma S, Burkhoff D, Wang J, Homma S, Edwards NM, Itescu S. Neovascularization of ischemic myocardium by human bone marrow-derived angioblasts prevents cardiomyocyte apoptosis, reduces remodeling and improves cardiac function. Nat Med 2001; 7: 430-436.

20. Cho SW, Moon SH, Lee SH, Kang SW, Kim J, Lim JM, Kim HS, Kim BS, Chung HM. Improvement of postnatal neovascularization by human embryonic stem cell derived endothelial-like cell transplantation in a mouse model of hindlimb ischemia. Circulation 2007; 116: 2409-2419.

21. Gambini E, Pompilio G, Biondi A, Alamanni F, Capogrossi MC, Agrifoglio M, Pesce M. C-kit^{+} cardiac progenitors exhibit mesenchymal markers and preferential cardiovascular commitment. Cardiovasc Res 2011; 89: 362-73.

22. Fu YS, Cheng YC, Lin MY, Cheng H, Chu PM, Chou SC, Shih YH, Ko MH, Sung MS. Conversion of human umbilical cord mesenchymal stem cells in Wharton's jelly to dopaminergic neurons in vitro: potential therapeutic application for Parkinsonism. Stem Cells 2006; 24: 115-24.

23. Troyer DL, Weiss ML. Wharton's jelly-derived cells are a primitive stromal cell population. Stem Cells 2008; 26: 591-599.

24. Chen MY, Lie PC, Li ZL, Wei X. Endothelial differentiation of Wharton's jelly-derived mesenchymal stem cells in comparison with bone marrow-derived mesenchymal stem cells. Exp Hematol 2009; 37:

629-40.

25. Louis F. Reichardt and Kevin J. Tomaselli. Extracellular matrix molecules and their receptors: functions in neural development. Annu Rev Neurosci 1991; 14: 531-570.
26. Anthony D Metcalfe and Mark W.J Ferguson. Tissue engineering of replacement skin: the crossroads of biomaterials, wound healing, embryonic development, stem cells and regeneration. J R Soc Interface 2007; 4: 413-437.
27. Martin Handfield, Henry V. Baker, and Richard J. Lamont. Beyond Good and Evil in the Oral Cavity: Insights into Host-Microbe Relationships Derived from Transcriptional Profiling of Gingival Cells. J Dent Res 2008; 87: 203-223.
28. Pollard TD, Borisy GG. Cellular motility driven by assembly and disassembly of actin filaments. Cell 2003; 112: 453-65.
29. Chhabra ES, Higgs HN. The many faces of actin: matching assembly factors with cellular structures. Nat Cell Biol 2007; 9: 1110-21.
30. Welner RS, Kincade PW. Stem cells on patrol. Cell 2007; 131:842–4.
31. Pitchford SC, Furze RC, Jones CP, Wengner AM, Rankin SM. Differential mobilization of subsets of progenitor cells from the bone marrow. Cell Stem Cell 2009; 4: 62-72.
32. Lapidot T, Kollet O. The essential roles of the chemokine SDF-1 and its receptor CXCR4 in human stem cell homing and repopulation of transplanted immune-deficient NOD/SCID and NOD/SCID/B2m(null) mice. Leukemia 2002; 16: 1992-2003.
33. Broxmeyer HE, Orschell CM, Clapp DW, Hangoc G, Cooper S, Plett PA, et al. Rapid mobilization of murine and human hematopoietic

stem and progenitor cells with AMD3100, a CXCR4 antagonist. J Exp Med 2005; 201: 1307-18.

34. Semerad CL, Christopher MJ, Liu F, Short B, Simmons PJ, Winkler I, Levesque JP, Chappel J, Ross FP, Link DC. G-CSF potently inhibits osteoblast activity and CXCL12 mRNA expression in the bone marrow. Blood 2005; 106: 3020-3027.

35. Sugiyama T, Kohara H, Noda M, Nagasawa T. Maintenance of the hematopoietic stem cell pool by CXCL12-CXCR4 chemokine signaling in bone marrow stromal cell niches. Immunity 2006; 25: 977-988.

36. Peled A, Petit I, Kollet O, Magid M, Ponomaryov T, Byk T, Nagler A, Ben-Hur H, Many A, Shultz L, Lider O, Alon R, Zipori D, Lapidot T. Dependence of human stem cell engraftment and repopulation of NOD/SCID mice on CXCR4. Science 1999; 283: 845-848.

37. Kalka C, Masuda H, Takahashi T, Gordon R, Tepper O, Gravereaux E, Pieczek A, Iwaguro H, Hayashi SI, Isner JM, Asahara T. Vascular endothelial growth factor (165) gene transfer augments circulating endothelial progenitor cells in human subjects. Circ Res 2000; 86: 1198-202.

38. Grunewald M, Avraham I, Dor Y, Bachar-Lustig E, Itin A, Jung S, Chimenti S, Landsman L, Abramovitch R, Keshet E. VEGF-induced adult neovascularization: recruitment, retention, and role of accessory cells. Cell 2006; 124: 175-89.

39. Chavakis E, Urbich C, Dimmeler S. Homing and engraftment of progenitor cells: a prerequisite for cell therapy. J Mol Cell Cardiol 2008; 45: 514-22.

40. Aicher A, Heeschen C, Mildner-Rihm C, Urbich C, Ihling C, Technau-Ihling K, Zeiher AM, Dimmeler S. Essential role of endothelial nitric oxide synthase for mobilization of stem and progenitor cells. Nat Med 2003; 9: 1370-6.
41. Lee SH, Lee YJ, Song CH, Ahn YK, Han HJ. Role of FAK phosphorylation in hypoxia-induced hMSCS migration: involvement of VEGF as well as MAPKS and eNOS pathways. Am J Physiol Cell Physiol 2010; 298: 847-56.
42. Gao H, Priebe W, Glod J, Banerjee D. Activation of STAT3 and FAK by SDF-1 is required for migration of human mesenchymal stem cells in response to tumor cell-conditioned medium. Stem Cells 2009; 27: 857-65.
43. Ma PX, Schloo B, Mooney D, Langer R. Development of biomechanical properties and morphogenesis of in vitro tissue engineered cartilage. J Biomed Mater Res 1995; 29: 1587-95.
44. Siao-Wei Yeh, Kung-Hwa Wei. CdS nanoparticles induce a morphological transformation of poly(styrene-b-4-vinylpyridine) from hexagonally packed cylinders to a lamellar structure. Macromolecules 2005; 38: 6559-6565.
45. Dalby MJ, Giannaras D, Riehle MO, Gadegaard N, Affrossman S, Curtis AS. Rapid fibroblast adhesion to 27nm high polymer demixed nano-topography. Biomaterials 2004; 25: 77-83.
46. Dalby M, Yarwood S, Riehle M, Johnstone H,Affrossman S, Curtis A. Increasing fibroblast response to materials using nanotopography: Morphological and genetic measurements of cell response to 13-nm-high polymer demixed islands. Exp Cell Res 2002; 276: 1-9.

47. Aicher A, Zeiher AM, Dimmeler S. Mobilizing endothelial progenitor cells. Hypertension 2005; 45: 321-5.
48. Tang JM, Wang JN, Zhang L, Zheng F, Yang JY, Kong X, Guo LY, Chen L, Huang YZ, Wan Y, Chen SY. VEGF/SDF-1 promotes cardiac stem cell mobilization and myocardial repair in the infarcted heart. Cardiovasc Res 2011.
49. Heissig B, Hattori K, Dias S, Friedrich M, Ferris B, Hackett NR, Crystal RG, Besmer P, Lyden D, Moore MA, Werb Z, Rafii S. Recruitment of stem and progenitor cells from the bone marrow niche requires MMP-9 mediated release of kit-ligand. Cell 2002; 109: 625-37.
50. Aicher A, Heeschen C, Mildner-Rihm C, Urbich C, Ihling C, Technau-Ihling K, Zeiher AM, Dimmeler S. Essential role of endothelial nitric oxide synthase for mobilization of stem and progenitor cells. Nat Med 2003; 9: 1370-6.
51. Hsu SH, Tang CM, Tseng HJ. Biocompatibility of poly(ether)urethane-gold nanocomposites. J Biomed Mater Res A 2006; 79: 759-70.
52. Hung HS, Wu CC, Chien S, Hsu SH. The behavior of endothelial cells on polyurethane nanocomposites and the associated signaling pathways. Biomaterials 2009; 30: 1502-11.
53. Hsu SH, Tang CM, Tseng HJ. Gold nanoparticles induce surface morphological transformation in polyurethane and affect the cellular response. Biomacromolecules 2008; 9: 241-8.
54. Hung HS, Hsu SH. The response of endothelial cells to polymer surface composed of nanometric micelles. N Biotechnol 2009; 25:

235-43.

55. L. Baujard-Lamotte, S. Noinville, F. Goubard, P. Marque, E. Pauthe. Kinetics of conformational changes of fibronectin adsorbed onto model surfaces. Colloids and Surfaces B: Biointerfaces 2008; 63: 129-137.

56. Kuznetsov AV, Kehrer I, Kozlov AV, Haller M, Redl H, Hermann M, Grimm M, Troppmair J. Mitochondrial ROS production under cellular stress: comparison of different detection methods. Anal Bioanal Chem 2011; 400: 2383-90.

57. Chou CW, Hsu SH, Wang PH. Biostability and biocompatibility of poly(ether)urethane containing gold or silver nanoparticles in a porcine model. J Biomed Mater Res A 2008; 84: 785-94.

58. Horie M, Nishio K, Fujita K, Kato H, Endoh S, Suzuki M, Nakamura A, Miyauchi A, Kinugasa S, Yamamoto K, Iwahashi H, Murayama H, Niki E, Yoshida Y. Cellular responses by stable and uniform ultrafine titanium dioxide particles in culture-medium dispersions when secondary particle size was 100 nm or less. Toxicol In Vitro 2010; 24: 1629-38.

59. Wang Z, Thurmond DC. Mechanisms of biphasic insulin-granule exocytosis - roles of the cytoskeleton, small GTPases and SNARE proteins. J Cell Sci 2009; 122: 893-903.

60. Ishige I, Nagamura-Inoue T, Honda MJ, Harnprasopwat R, Kido M, Sugimoto M, Nakauchi H, Tojo A. Comparison of mesenchymal stem cells derived from arterial, venous, and Wharton's jelly explants of human umbilical cord. Int J Hematol 2009; 90: 261-9.

61. van Hinsbergh VW, Engelse MA, Quax PH. Pericellular proteases in

angiogenesis and vasculogenesis. Arterioscler Thromb Vasc Biol 2006; 26: 716-28.

62. Lu L, Payvandi F, Wu L, Zhang LH, Hariri RJ, Man HW, Chen RS, Muller GW, Hughes CC, Stirling DI, Schafer PH, Bartlett JB. The anti-cancer drug lenalidomide inhibits angiogenesis and metastasis via multiple inhibitory effects on endothelial cell function in normoxic and hypoxic conditions. Microvasc Res 2009; 77: 78-86.
63. Qiu FY, Song XX, Zheng H, Zhao YB, Fu GS. Thymosin beta4 induces endothelial progenitor cell migration via PI3K/Akt/eNOS signal transduction pathway. J Cardiovasc Pharmacol 2009; 53: 209-14.
64. Liao CH, Sang S, Ho CT, Lin JK. Garcinol modulates tyrosine phosphorylation of FAK and subsequently induces apoptosis through down-regulation of Src, ERK, and Akt survival signaling in human colon cancer cells. J Cell Biochem 2005; 96: 155-69.
65. Hsu Sh, Tseng H, Wu M. Comparative In vitro evaluation of two different preparations of small diameter polyurethane vascular grafts. Artif Organs 2000; 24: 119-28.

Figure 1

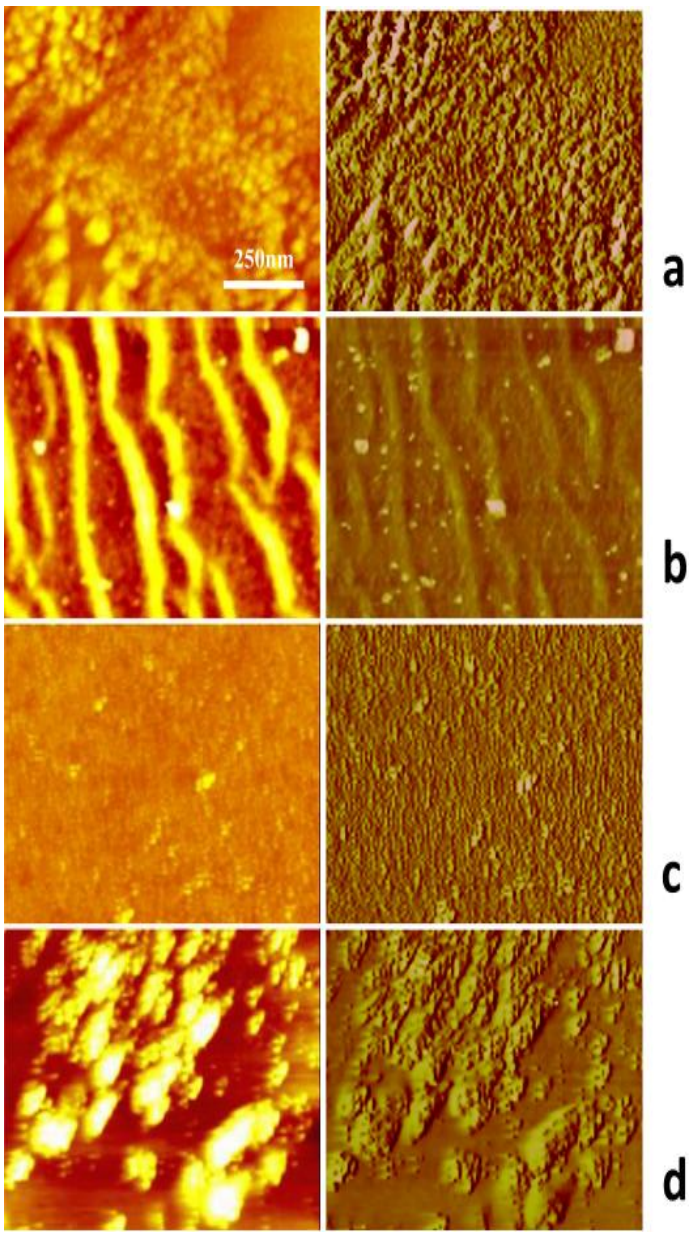

Materials	rms roughness (nm)	main surface morphology (nm)
FN	3.123 ± 0.03	26.312 ± 3.21
FN-Au (17.4 ppm)	2.685 ± 0.11	32.447 ± 4.39
FN-Au (43.5 ppm)	0.95 ± 0.012	20.042 ± 2.24
FN-Au (174 ppm)	1.951 ± 0.06	43.005 ± 4.98

Figure 1: The AFM images of topography (left) and phase (right) for (a) pure FN, and FN-Au nanocomposites containing (b) 17.4 ppm, (c) 43.5 ppm, and (d) 174 ppm of Au nanoparticles. Data are mean ± SD.

Figure 2

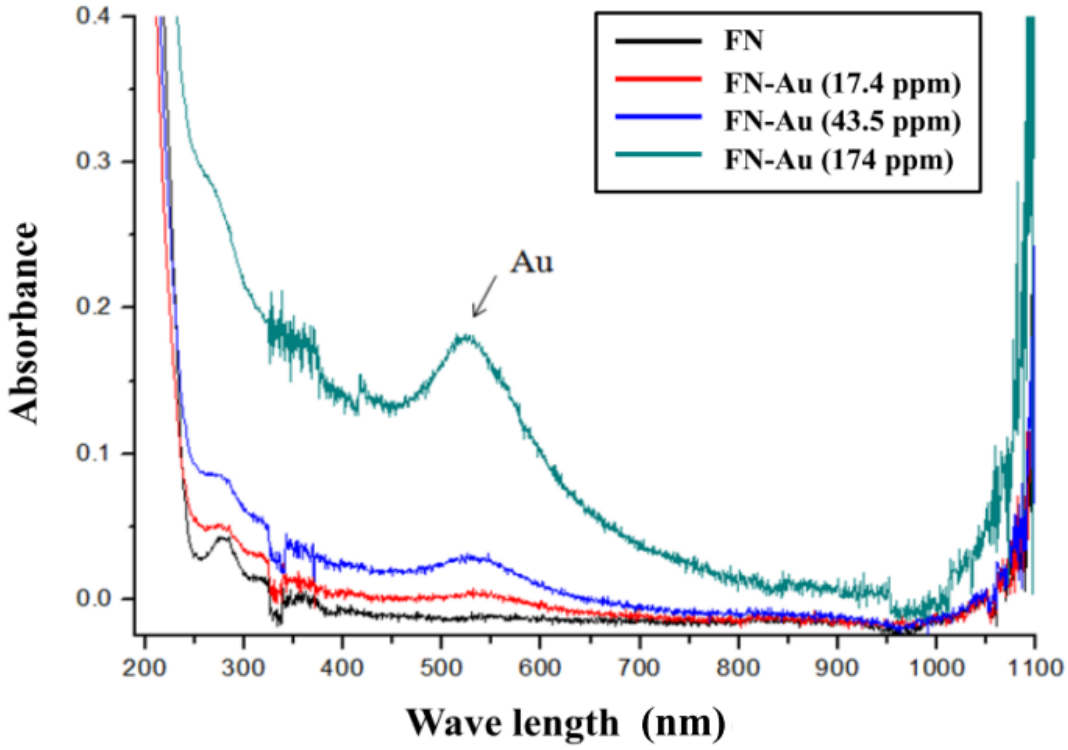

Figure 2: Characterization of the nanocomposites by UV/VIS Spectrophotometer. The pure FN, and FN-Au nanocomposites containing 17.4 ppm, 43.5 ppm, and 174 ppm of Au nanoparticles were analyzed the absorbance wavelength by UV/VIS Spectrophotometer.

Figure 3

(A)

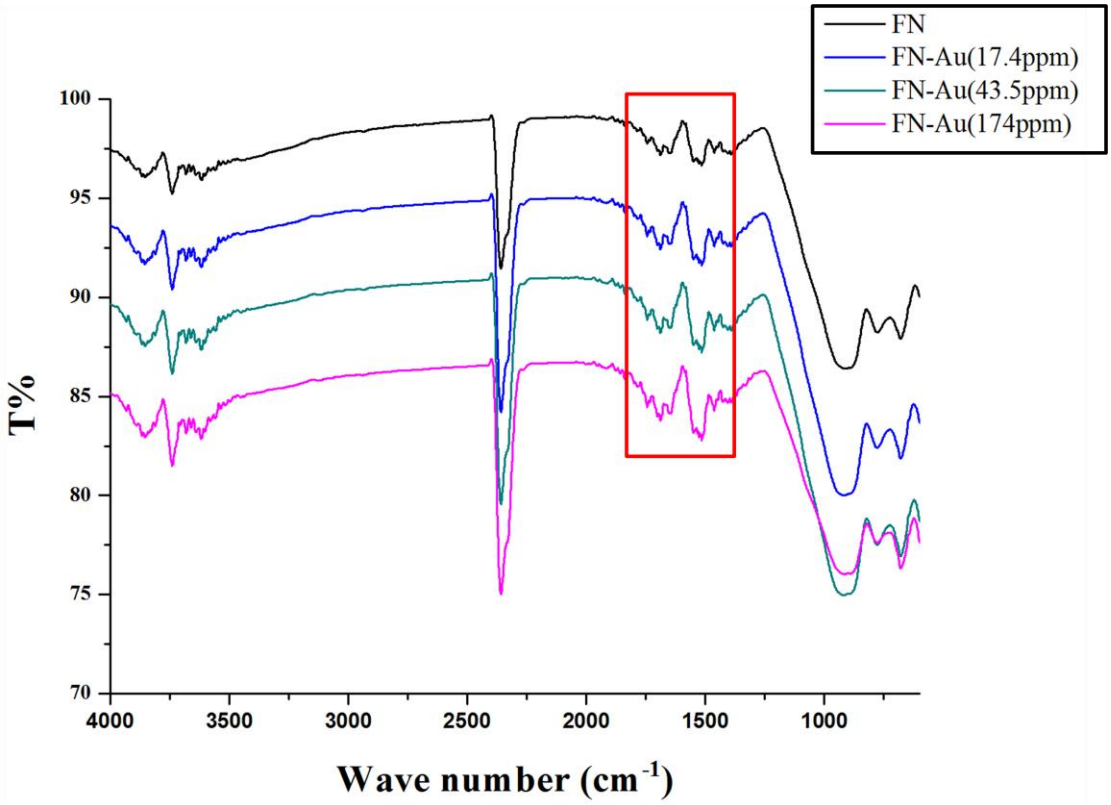
FN
FN-Au(17.4ppm)
FN-Au(43.5ppm)
FN-Au(174ppm)
T%
100
95
90
85
80
75
70
4000
3500
3000
2500
2000
1500
1000
Wave number (cm-1)

(B)

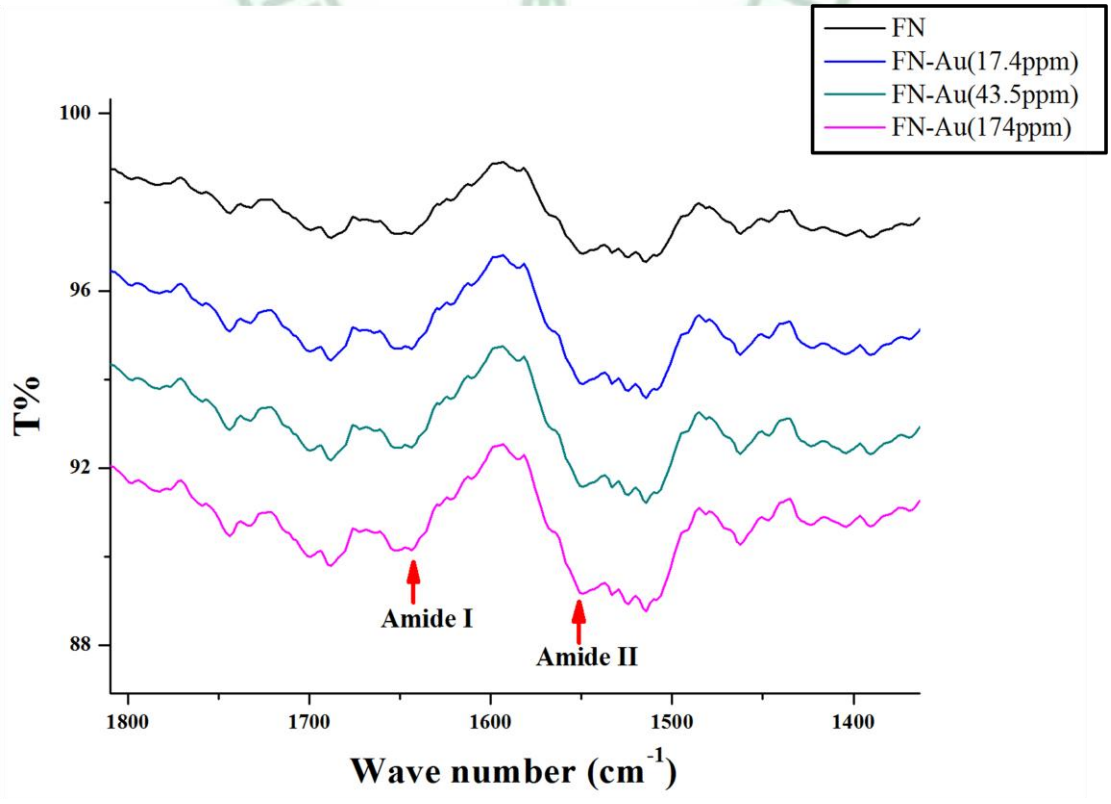
FN
FN-Au(17.4ppm)
FN-Au(43.5ppm)
FN-Au(174ppm)
T%
100
96
92
88
Amide I
Amide II
1800
1700
1600
1500
1400
Wave number (cm-1)

Figure 3: Characterization of the nanocomposites by FTIR. (A) FTIR spectra of pure FN, and FN-Au nanocomposites containing 17.4 ppm, 43.5 ppm, and 174 ppm of Au nanoparticles in the total absorbance wavenumber region (700 cm^{-1} to 4000 cm^{-1}) or (B) in the Amide I (1640 cm^{-1}) and Amide II (1550 cm^{-1}) (C-N) region.

Figure 4

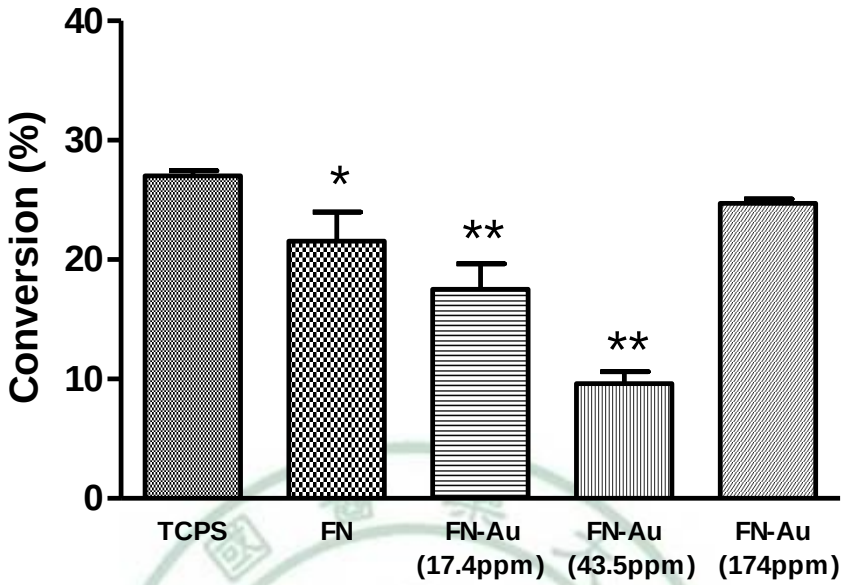

Materials	The neuber of monocyte ($\times 10^3$)	The neuber of macrophage ($\times 10^3$)	Conversion yield (%)
TCPS	8.463 ± 2.12	2.958 ± 0.52	27.008 ± 5.11
FN	8.618 ± 2.37	2.275 ± 0.81	21.565 ± 5.41 *
FN-Au (17.4 ppm)	9.091 ± 1.79	1.186 ± 0.33	17.501 ± 3.76 **
FN-Au (43.5 ppm)	9.322 ± 1.28	0.825 ± 0.11	9.622 ± 2.11 **
FN-Au (174 ppm)	8.525 ± 1.69	2.683 ± 0.81	24.704 ± 3.92

Figure 4: Human monocyte activation on the surface of pure FN, and FN containing 17.4 ppm, 43.5 ppm, and 174 ppm of Au nanoparticles. Data are mean ± SD. * $p < 0.05$, ** $p < 0.01$: greater than TCPS.

Figure 5

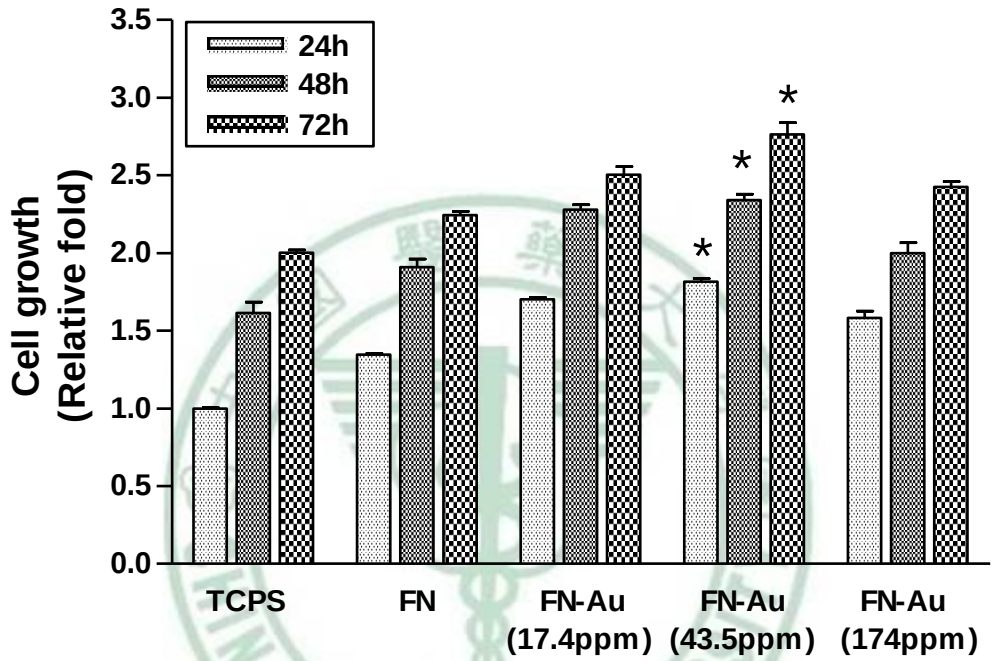

Figure 5: WJCs attachment and proliferation on the surface of pure FN, and FN containing 17.4 ppm, 43.5 ppm, and 174 ppm of Au nanoparticles. Data are mean ± SD. * $p < 0.05$: greater than FN.

Figure 6.

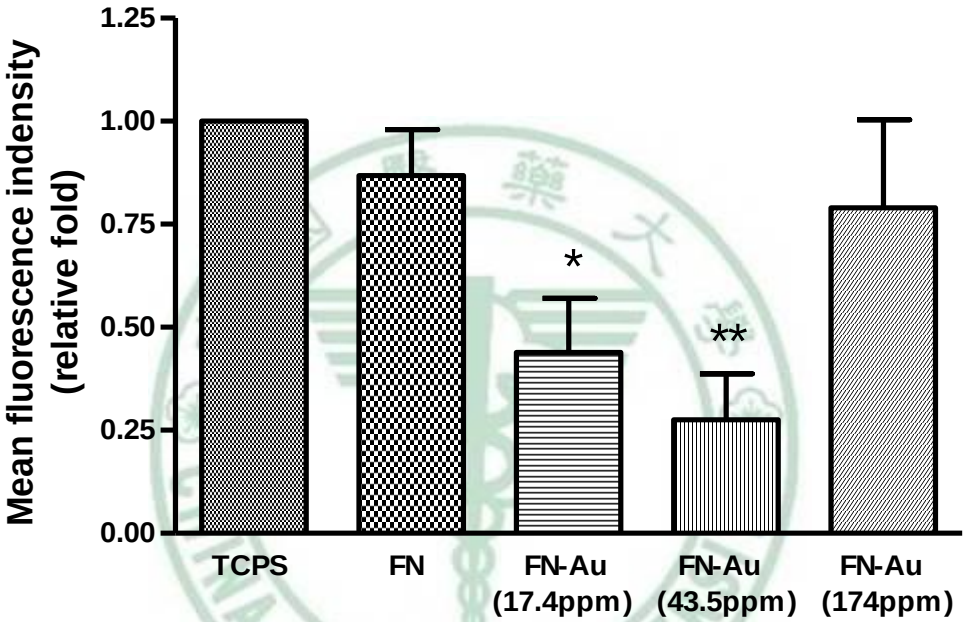

Figure 6: Oxidative stress of WJCS on the surface of pure FN, and FN containing 17.4 ppm, 43.5 ppm, and 174 ppm of Au nanoparticles. Data are mean ± SD. * $p < 0.05$, ** $p < 0.01$: greater than FN.

Figure 7

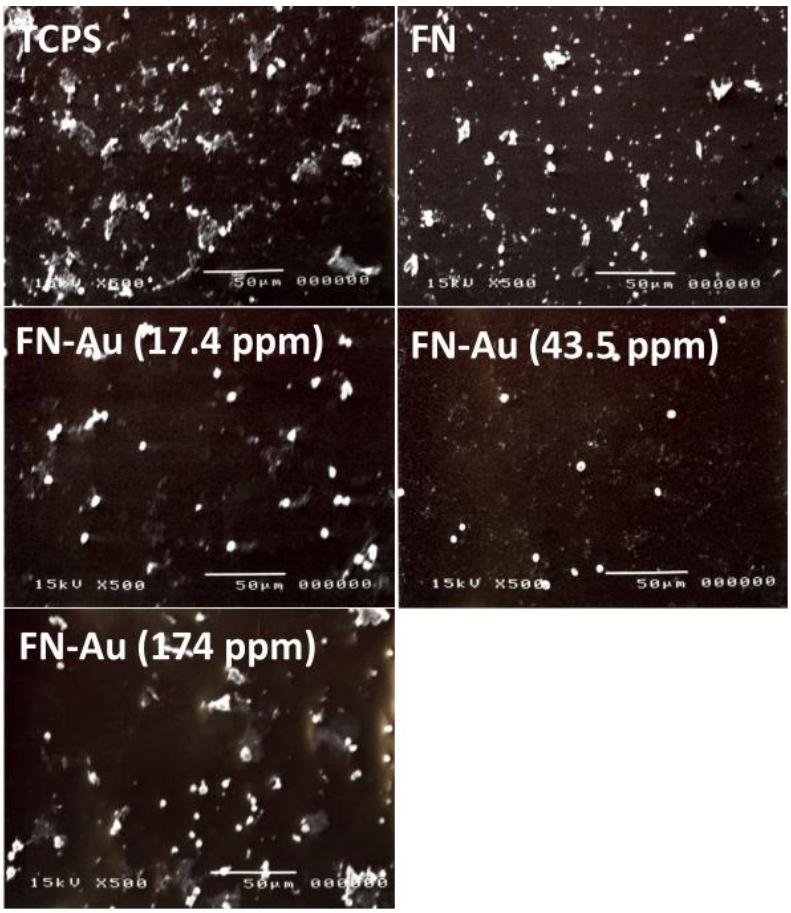

Materials	Number of Adhered Platelets ($\times 10^3$)	Average Degree of Activation (0.0-1.0)
TCPS	3.72 ± 0.14	0.788 ± 0.23
FN	2.41 ± 0.21	0.706 ± 0.31
FN-Au (17.4 ppm)	0.42 ± 0.03 *	0.311 ± 0.09 *
FN-Au (43.5 ppm)	0.07 ± 0.01 **	0.071 ± 0.02 **
FN-Au (174 ppm)	2.95 ± 0.41	0.747 ± 0.35

Figure 7: Scanning electron microscopy analysis of platelets adhered and activated on the TCPS, pure FN and FN-Au nanocomposites containing 17.4 ppm, 43.5 ppm, and 174 ppm of Au nanoparticles . Data are mean ± SD. * $p < 0.05$, ** $p < 0.01$: greater than TCPS. Bar=50 μm.

Figure 8

(A)

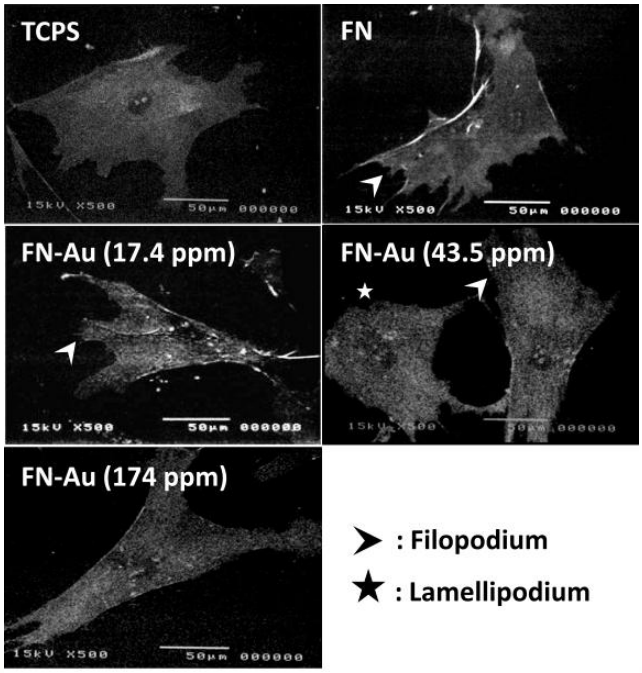
TCPS
FN
FN-Au (17.4 ppm)
FN-Au (43.5 ppm)
FN-Au (174 ppm)
: Filopodium
: Lamellipodium

(B)

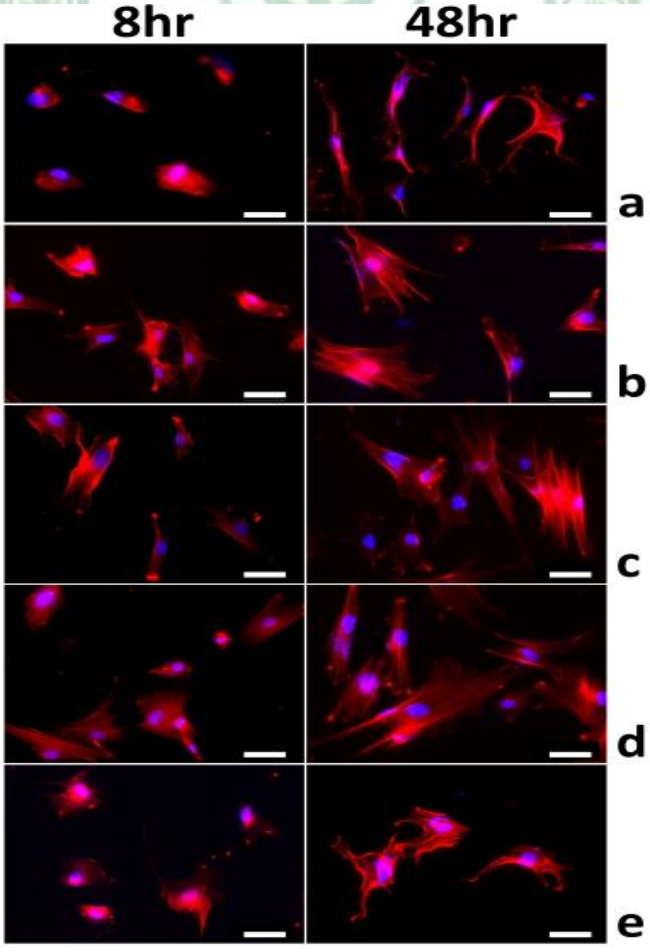
8hr
48hr
a
b
c
d
e

Figure 8: The morphology of WJCs on nanocomposites. (A) WJCs morphological on the surface of pure FN, and FN containing 17.4 ppm, 43.5 ppm, and 174 ppm of Au nanoparticles were observed by scanning electron microscopy analysis. Arrow means filopodium; Star means lamellipodium. Bar=50 μm. (B) Actin staining of WJCs on the TCPS (a), FN (b) and FN containing 17.4 ppm (c), 43.5 ppm (d), and 174 ppm (e) of Au nanoparticles at 8 and 48 hrs were observed by fluorescence microscopy. Additionally, experiments were obtained the same result. Bar=100 μm.

Figure 9

(A)

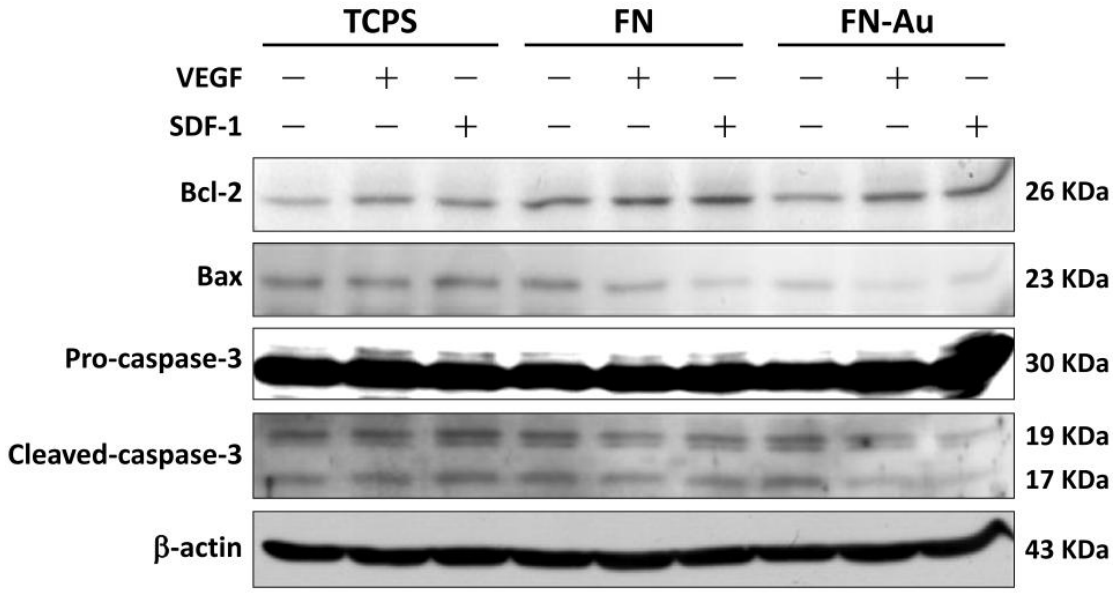
TCPS
FN
FN-Au
VEGF
SDF-1
Bcl-2
26 KDa
Bax
23 KDa
Pro-caspase-3
30 KDa
Cleaved-caspase-3
19 KDa
17 KDa
β-actin
43 KDa

(B)

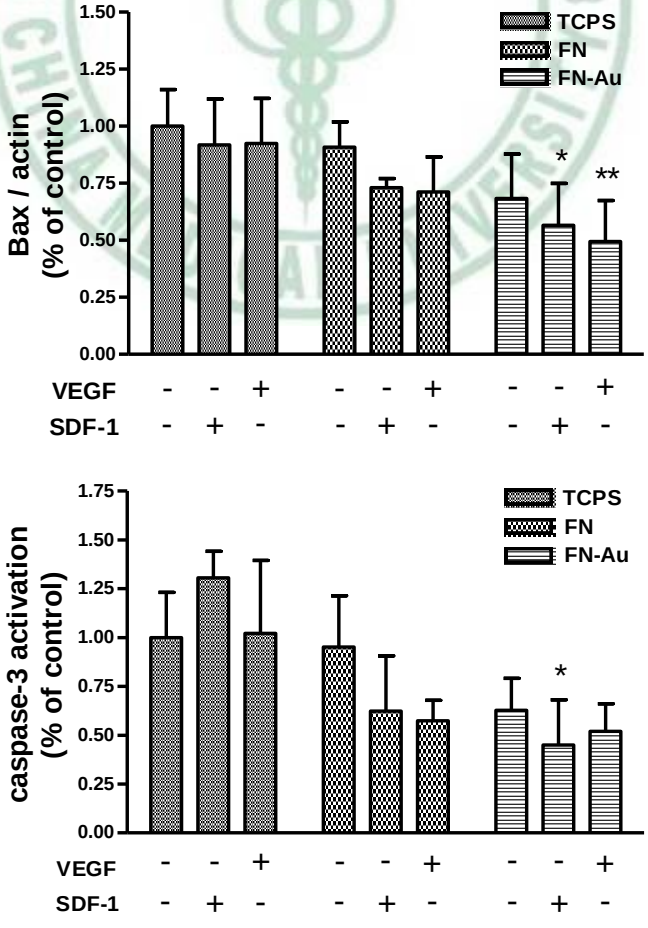
Bax / actin
(% of control)
1.50
1.25
1.00
0.75
0.50
0.25
0.00
TCPS
FN
FN-Au
*
**
VEGF - - + - - + - - +
SDF-1 - + - - + - - + -
caspase-3 activation
(% of control)
1.75
1.50
1.25
1.00
0.75
0.50
0.25
0.00
TCPS
FN
FN-Au
*
VEGF - - + - - + - - +
SDF-1 - + - - + - - + -

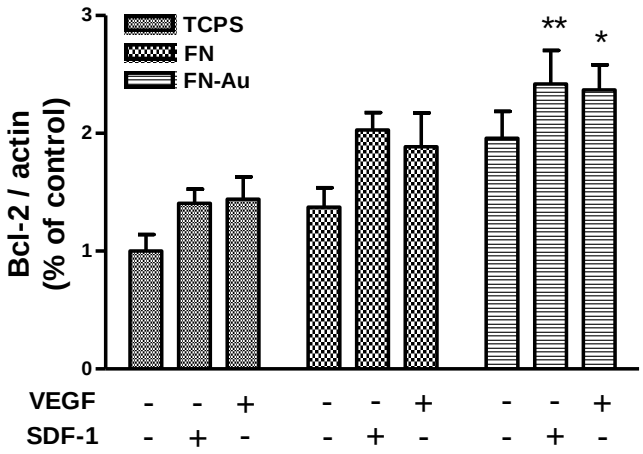

Figure 9: The survival capability of WJCs on FN-Au after VEGF or SDF-1 stimulation for 48 hrs. (A) The Bax, caspase 3 and Bcl-2 proetin expression level were analyzed by Western Blot analysis after treatment with VEGF (50 ng/ml) or SDF-1 (50 ng/ml) for 48 hrs. β-actin was used as a loading control. (B) Columns, mean of three separate experiments. Data are mean ± SD. * $p < 0.05$, * * $p < 0.01$: greater than TCPS (without treated).

Figure 10

(A)

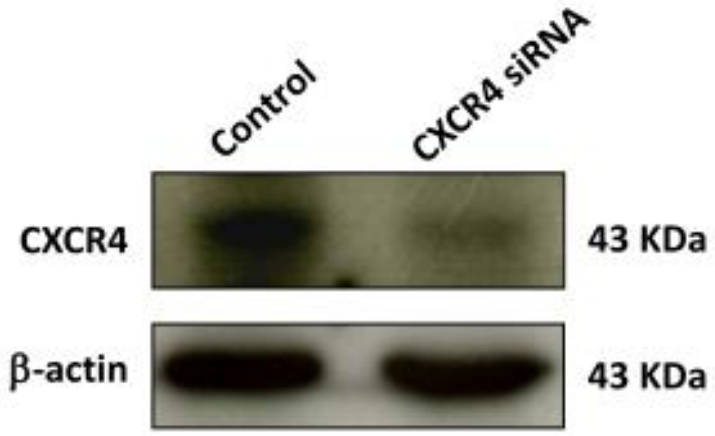
Control
CXCR4 siRNA
CXCR4
43 KDa
β-actin
43 KDa

(B)

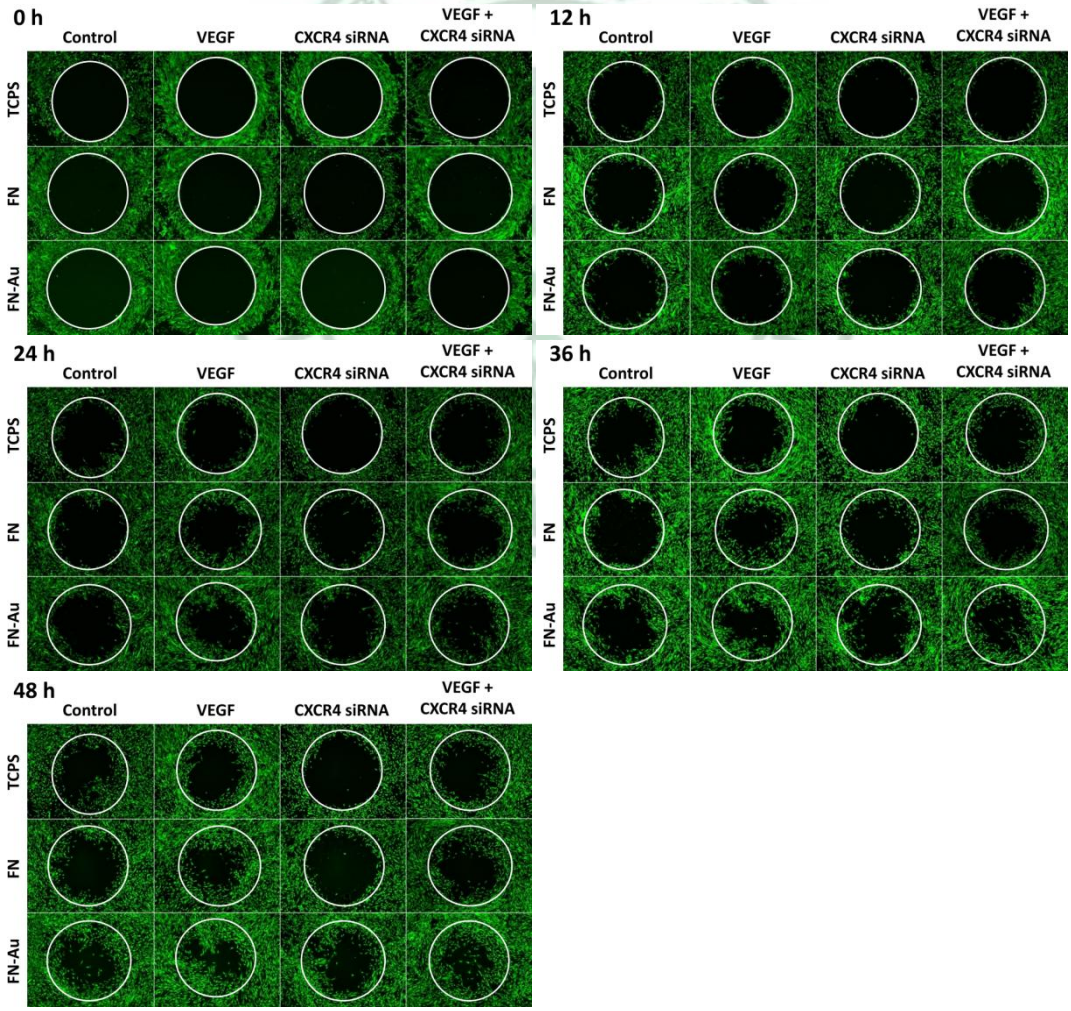
0 h
12 h
24 h
36 h
48 h
Control
VEGF
CXCR4 siRNA
VEGF + CXCR4 siRNA
TCPS
FN
FN-Au

(C)

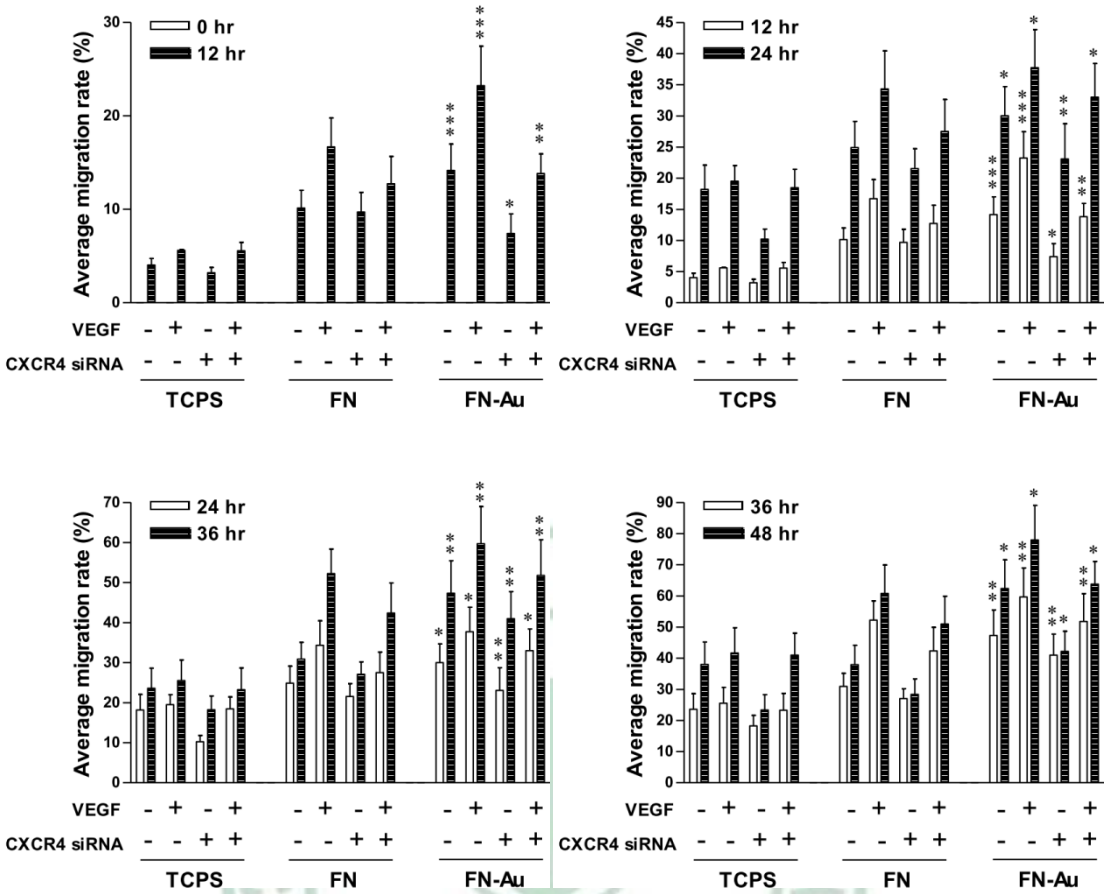

Figure 10: VEGF stimulated migration of WJCs on FN-Au through CXCR4. (A) Western Blot analysis of CXCR4 expression in WJCs by transfected with CXCR4 siRNA. (B) The migration rate of WJCs transfected with CXCR4 siRNA and stimulated without or with VEGF (50 ng/mL) at 0, 12, 24, 36 and 48 hrs were taken by fluorescence microscopy. (C) Columns, mean of three separate experiments. Data are mean ± SD. * $p < 0.05$, * * $p < 0.01$, * * *$p < 0.001$: greater than TCPS (with same treated).

Figure 11

(A)

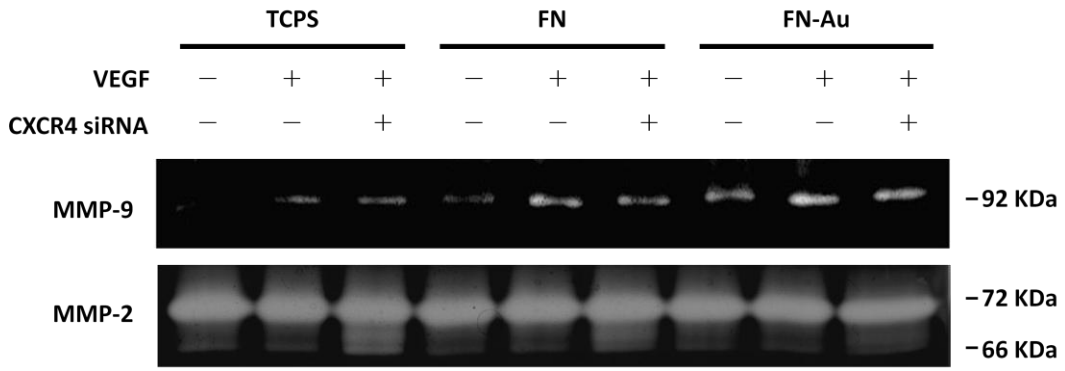

(B)

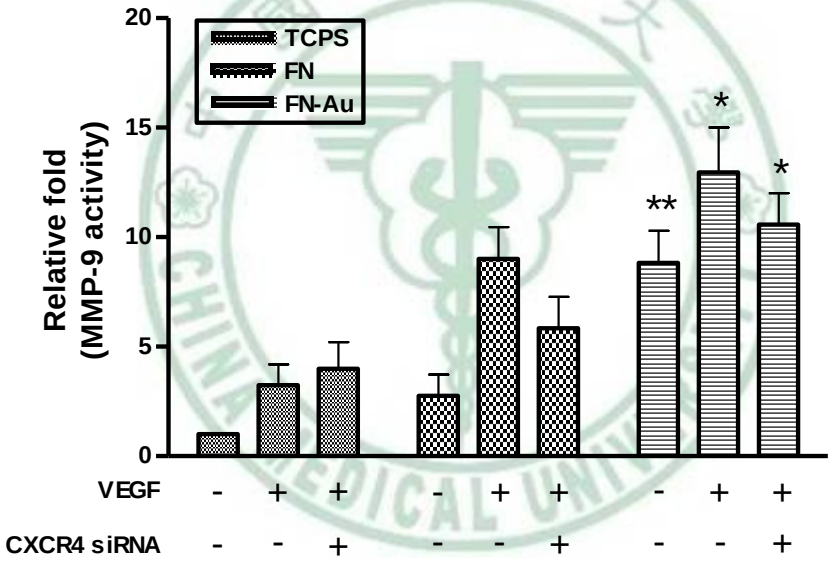

Figure 11: VEGF activated MMP-9 activity of WJCs on FN-Au through CXCR4. (A) The MMP-2 and MMP-9 activity of WJCs transfected with CXCR4 siRNA and stimulated without or with VEGF (50 ng/mL) for 48 hrs were detected by Gelatin zymography analysis. (B) Columns, mean of three separate experiments. Data are mean ± SD. * $p < 0.05$, * * $p < 0.01$: greater than FN (with same treated).

Figure 12

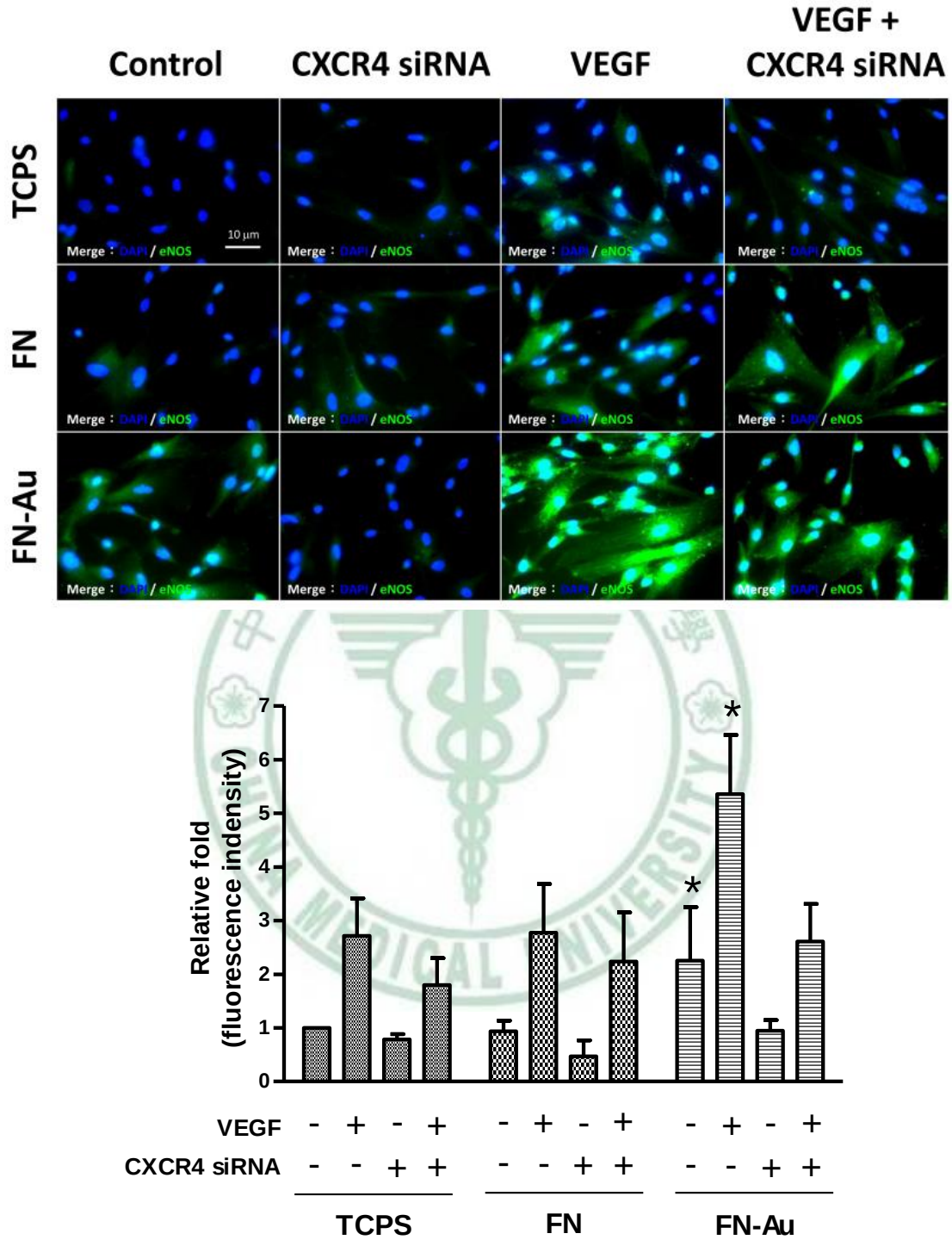

Figure 12: VEGF stimulated eNOS expression of WJCs on FN-Au through CXCR4. The eNOS expression of WJCs transfected with CXCR4 siRNA and stimulated without or with VEGF were taken by fluorescence microscopy. Columns, mean of three separate experiments. Data are mean ± SD. * $p < 0.05$: greater than TCPS (with same treated).

Figure 13

(A)

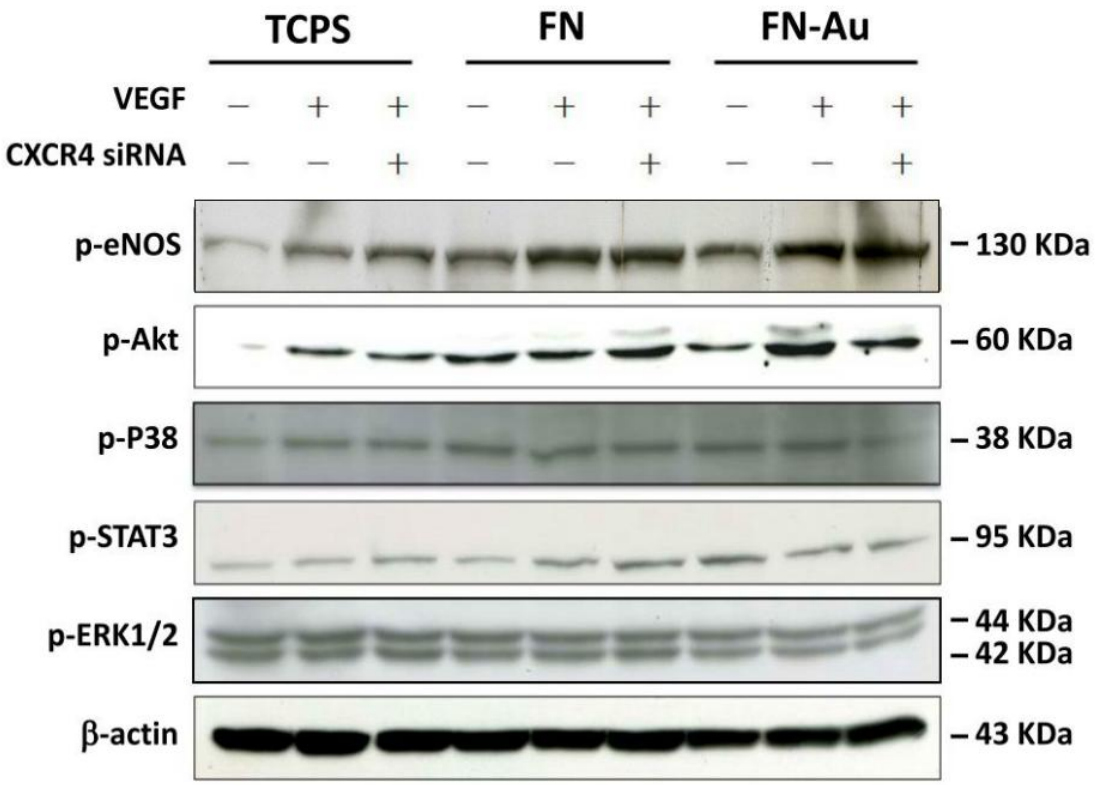

(B)

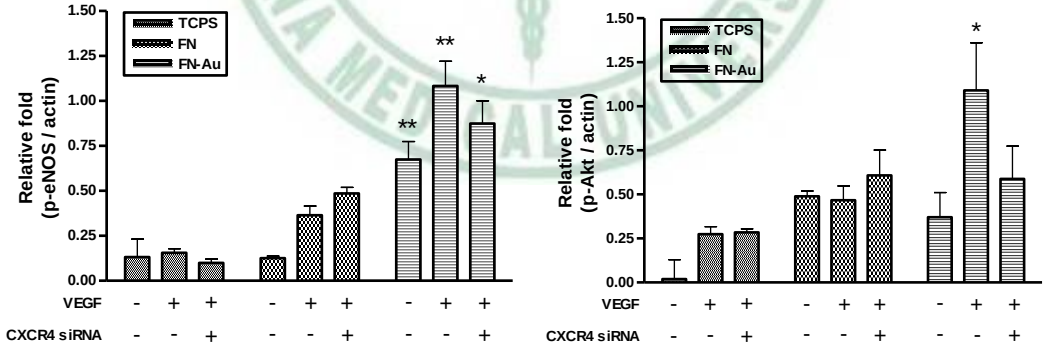

Figure 13: VEGF modulated Akt/eNOS phosphorylation of WJCs on FN-Au through CXCR4. WJCs were transfected with CXCR4 siRNA and stimulated without or with VEGF (50 ng/mL) for 48 hrs. Cells were lysed and the extracts were electrophoresed. (A) The p-eNOS, p-Akt, p-P38, p-STAT3 and p-ERK1/2 protein expressions were detected by Western Blot. β-actin was used as a loading control. (B) Columns, mean of three

separate experiments. Data are mean ± SD. * $p < 0.05$, * * $p < 0.01$: greater than FN (with same treated).

Appendix

Appendix 1.

(A)

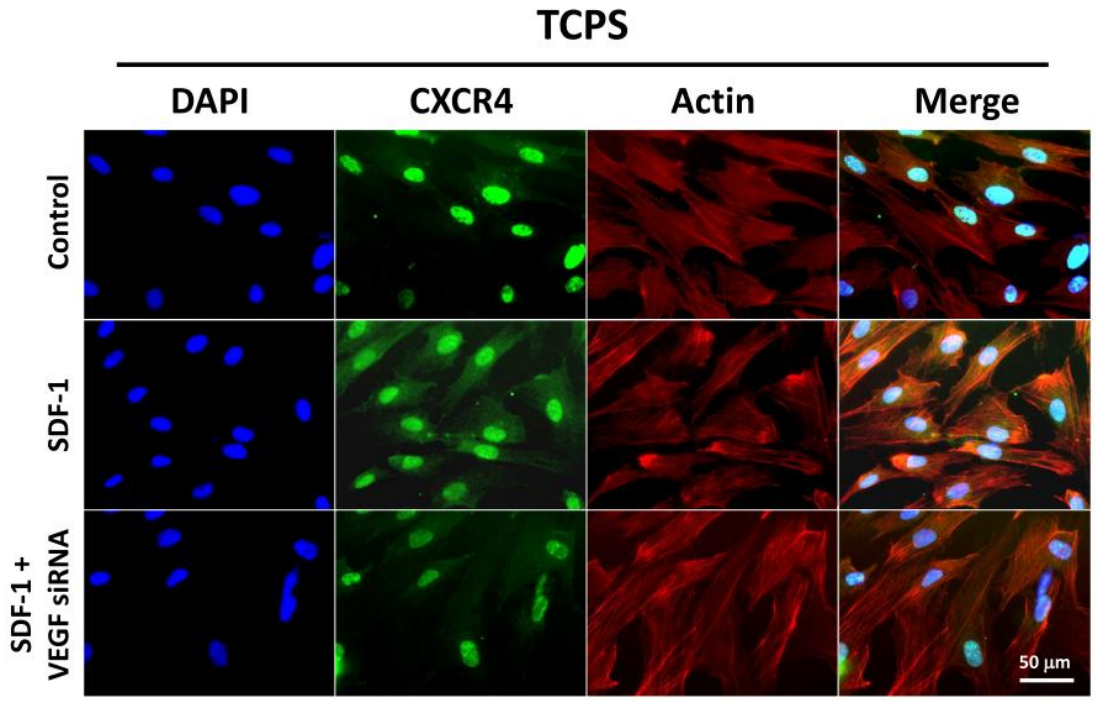

(B)

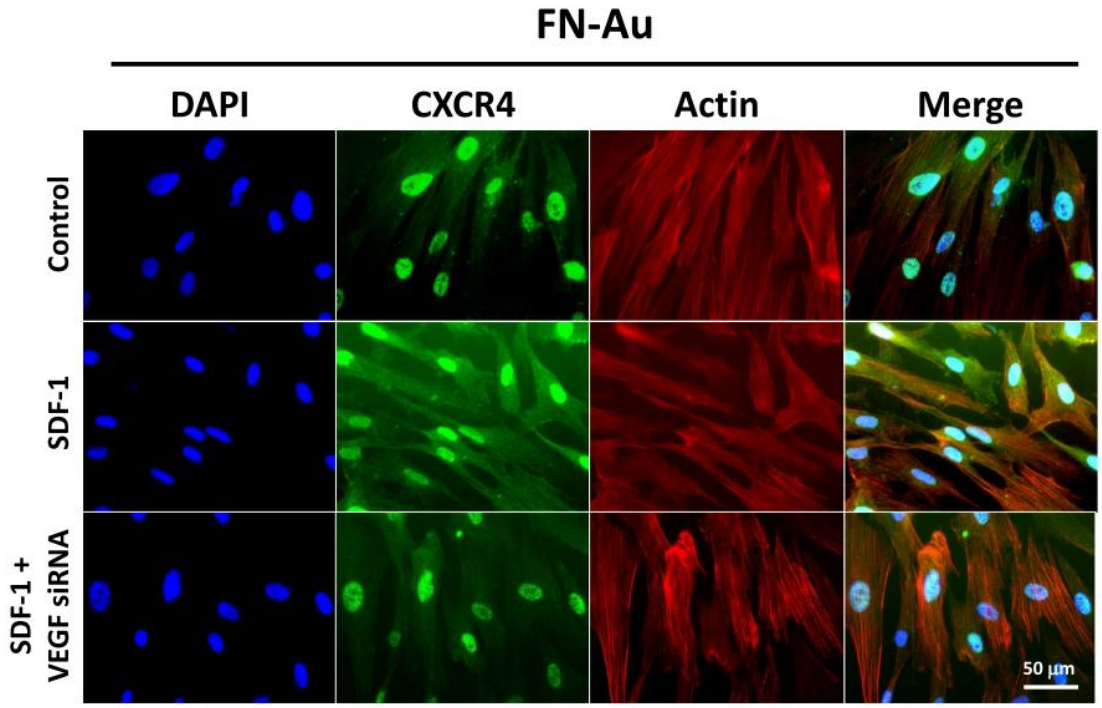

Appendix 1. SDF-1 induced CXCR4 expression by VEGF in WJCs. The CXCR4 expression of WJCs transfected with VEGF siRNA and

stimulated without or with SDF-1 (50 ng/mL) on TCPS (A) or FN-Au (B) were taken by fluorescence microscopy. This result showed that FN-Au was promoted CXCR4 expression compared to TCPS. Indeed, VEGF was mediated through SDF-1 to activate the CXCR4 expression in WJCs.

Appendix 2.

1. Reagents

A. Cell culture and growth factors

Fetal bovine serum (FBS)	Invitrogen, USA
Hight glucose Dulbecco's Modified Eagle Medium (H-DMEM)	Invitrogen, USA
Penicillin-streptomycin	Invitrogen, USA
Sodium pyruvate	Invitrogen, USA
Sodium bicarbonate	Sigma, USA
Trypsin-EDTA	Invitrogen, USA
Human Stromal Cell-Derived Factor-1 alpha (SDF-1)	Prospec, USA
Recombinant Human Vascular Endothelial Growth Factor (VEGF)	Prospec, USA

B. Nanocomposites

Au nanoparticle solution	Global Nano Tech, Taiwan

Acetic acid	島久藥品株式會社, Japan
Fibronectin	BD, NJ, USA

C. Electrophoresis and Western blot

Acrylamide-Bis (29:1)	SERVA, Germany
Ammonium persulfate (APS)	J.T.Baker, USA
Glycine	J.T.Baker, USA
Methanol	J.T.Baker, USA
N,N,N,N-Tetramethyl ethylene diamine (TEMED)	Sigma, USA
Phosphatase	Roche, Switzerland
Protease Inhibitor	Roche, Switzerland
Protein assay kits	Bio-Rad, USA
SDS-PAGE molecular weight standard Prestained marker	Fermentas, Canada

Sodium dodecylsulfate (SDS)	J.T.Baker, USA
Tris-base	J.T.Baker, USA
Tween 20	J.T.Baker, USA
Western Blot detection reagent (ECL kit)	perkinElmer, USA
Coomassie brilliant blue R-250 staining	Bio-Rad, USA
Gelatin	Invitrogen, USA
$CaCl_2$	Invitrogen, USA

Antibody

Actin mouse monoclonal antibody	Cell Signaling, USA
Phospho-Akt antibody	Cell Signaling, USA
Phospho-FAK antibody	Cell Signaling, USA
Phospho-eNOS antibody	Abcam, USA
Phospho-ERK antibody	Cell Signaling, USA
Phospho-RhoA antibody	Santa cruz, USA

Phospho-Rac/Cdc42 antibody	Cell Signaling, USA
HRP-goat anti-mouse antibody	Abcam, USA
HRP-goat anti-rabibt antibody	Abcam, USA

D. Immunofluorescence

CD29-conjugate PE antibody	MACS, USA
CD34-conjugate PE antibody	MACS, USA
CD44-conjugate PE antibody	MACS, USA
CD73-conjugate PE antibody	MACS, USA
CD105-conjugated PE antibody	MACS, USA
CD45-conjugate FITC antibody	MACS, USA
CD90-conjugate FITC antibody	MACS, USA
Fluorescein (FITC)-conjugate AffiniPure Goat anti-rabbit IgG (H+L)	Jackson ImmunoResearch, USA
Cy^{TM}5-conjugated AffiniPure Goat anti-mouse	Jackson ImmunoResearch,

IgG (H+L)	USA
CXCR4 antibody	Santa Cruz, USA
αvβ3 antibody	Santa Cruz, USA
NOS3 antibody	Santa Cruz, USA
Flk-1(VEGF-R2) antibody	Santa Cruz, USA
4,6-Diamidion-2-phenylindole (DAPI)	Invitrogen, USA
Rhodamine phalloidin	Sigma, USA

E. others

Glutaraldehyde	Sigma, USA
2,7-dichlorofluorescin diacetate (DCFH–dA)	Sigma, USA
3-(4,5-dimethylthiazol-2-yl)-2,5-diphenyl tetrazolium bromide (MTT)	Sigma, USA
lipofectamine	Santa Cruz, USA
VEGF siRNA	Santa Cruz, USA
CXCR4 siRNA	Santa Cruz, USA

Scramble siRNA	Santa Cruz, USA
Calcein-AM	Invitrogen, USA
Quantum dot	Invitrogen, USA
Hematoxylin-enosin (H&E) staining	DAKO, USA
Monoclonal Mouse Anti-Human CD31	DAKO, USA
Mounting gel	Invitrogen, USA

2. Instruments

UV/Visible spectrophotometer

Laminar flow (HAG-120, Chung Fu, Taiwan)

Water bath (WB212-B2, Chung Fu, Taiwan)

Centrifuge (X-22R, Beckman, USA)

Fluorescent microscopy (ZEISS AXIO IMAGER A1, USA)

Phase contrast microscope (ZEISS AXIO Z1, USA)

Scanning electron microscopy SEM (JEOL JEM-5200, USA)

CO_2 Incubator (Thermoforma 370, bioway, USA)

Orbital shaker (Barnstead 4630, Taiwan)

Protein III (Bio-Rad, USA)

Power supply (Bio-Rad, USA)

Wet mini trans-blot cell (Bio-Rad, USA)

Flow Cytometer (LSR II, BD, USA)

Plasma treat equipment (Openair®, Steinhagen, Germany)

Intravascular Catheter (Insyte™ Autoguard™, BD, USA)